

NASA Contractor Report 3081

NASA
CR
3081
c.1

LOAN COPY: RETURN
AFWL TECHNICAL LIBRARY
KIRTLAND AFB, NM

TECH LIBRARY KAFB, NM
0051883

Wind Tunnel Force and Pressure Tests of a 21% Thick General Aviation Airfoil With 20% Aileron, 25% Slotted Flap and 10% Slot-Lip Spoiler

W. H. Wentz, Jr. and K. A. Fisco

GRANT NSG-1165
JUNE 1979

FOR EARLY DOMESTIC DISSEMINATION

Because of its significant early commercial potential, this information, which has been developed under a U.S. Government program, is being disseminated within the United States in advance of general publication. This information may be duplicated and used by the recipient with the express limitation that it not be published. Release of this information to other domestic parties by the recipient shall be made subject to these limitations.

Foreign release may be made only with prior NASA approval and appropriate export licenses. This legend shall be marked on any reproduction of this information in whole or in part.

NASA

Date for general release November 1979



0061883

NASA Contractor Report 3081

Wind Tunnel Force and Pressure
Tests of a 21% Thick General
Aviation Airfoil With 20%
Aileron, 25% Slotted Flap
and 10% Slot-Lip Spoiler

W. H. Wentz, Jr. and K. A. Fisco
Wichita State University
Wichita, Kansas

Prepared for
Langley Research Center
under Grant NSG-1165



National Aeronautics
and Space Administration

Scientific and Technical
Information Office

1979

SUMMARY

Force and surface pressure distributions have been measured for the 21% LS(1)-0421 modified airfoil fitted with 20% aileron, 25% slotted flap and 10% slot-lip spoiler. All tests were conducted in the Walter Beech Memorial Wind Tunnel at Wichita State University at a Reynolds number of 2.2×10^6 and a Mach number of 0.13. Results include lift, drag, pitching moments, control surface normal force and hinge moments, and surface pressure distributions. The basic airfoil has a $c_{l_{\max}}$ of 1.31 with nearly constant c_l beyond the stall at 2.2×10^6 Reynolds number. Incremental performance of flap and aileron are similar to that obtained on the GA(W)-2 airfoil. Spoiler control shows a slight reversal tendency at high α , low spoiler deflection angle conditions with flap nested. Flap extended spoiler control is non-linear but positive.

INTRODUCTION

As part of NASA's program for developing new airfoil sections for general aviation applications (ref. 1), Wichita State University is conducting flap and control surface research for the new airfoils. This report documents two-dimensional wind tunnel tests of the 21% thick LS(1)-0421 modified airfoil section with: (a) 20% chord aileron, (b) 25% chord slotted flap; and (c) 10% chord slot lip spoiler.

High Reynolds number tests of the LS(1)-0421 modified airfoil have been reported in reference 2. All experimental tests reported herein were conducted in the Walter Beech Memorial Wind Tunnel at Wichita State University.

SYMBOLS

The force and moment data have been referred to the .25c location on the flap-nested airfoil. Dimensional quantities are given in International (SI) Units. Measurements were made in U.S. Customary Units. Conversion factors between the various units may be found in reference 3. The symbols used in the present report are defined as follows:

- c Airfoil reference chord (flap-nested)
- c_d Airfoil section drag coefficient, section drag/
 (dynamic pressure x c)
- c_f Flap chord
- c_h Control surface hinge moment coefficient, section moment
 about hingeline/(dynamic pressure x control surface
 reference chord²)
- c_l Airfoil section lift coefficient, section lift/
 (dynamic pressure x c)
- c_m Airfoil section pitching moment coefficient with respect
 to the .25c location, section moment/(dynamic pressure
 x c²)
- c_{m_a} Airfoil forward section moment coefficient, moment about
 leading edge/(c² x dynamic pressure)

c_{mf} Flap moment coefficient, moment about leading edge/
 $(c^2 \times \text{dynamic pressure})$
 c_n Airfoil or flap normal force coefficient, section
normal force/(dynamic pressure $\times c$)
 c_{na} Airfoil forward section normal force coefficient,
normal force/($c \times \text{dynamic pressure}$)
 c_{nai} Aileron normal force coefficient, normal force/
($c \times \text{dynamic pressure}$)
 c_{nf} Flap normal force coefficient, normal force/($c \times$
dynamic pressure)
 c_p Coefficient of pressure, $(p - p_\infty)/\text{dynamic pressure}$
 Δh Spoiler projection height normal to local airfoil
surface
 p Static pressure
 x Coordinate parallel to airfoil chord
 z Coordinate normal to airfoil chord
 α Angle of attack, degrees
 Δ Increment
 δ_a Rotation of aileron from nested position, degrees
 δ_f Rotation of flap from nested position, degrees
 δ_s Rotation of spoiler from nested position, degrees

Subscripts:

a Aileron
 f Flap
 p Pivot
 s Spoiler
 ∞ Remote free-stream value

APPARATUS AND TEST METHODS

Model Description

The LS(1)-0421 modified airfoil section is a 21% maximum thickness airfoil with a design lift coefficient of 0.4, derived from the 17% thick LS(1)-0417 (formerly designated GA(W)-1) airfoil. The LS(1)-0421 modified section is the result of several iterations of testing and theoretical analysis by the NASA Langley Airfoil Research Group to develop a highly efficient 21% thick section (ref. 2). For tests in the WSU two-dimensional facility, models were sized with 91.4 cm span and 61.0 cm chord. The forward 70% of the airfoil was fabricated from laminated mahogany bonded to a 2.5 cm x 34.8 cm aluminum spar. Trailing edge sections were fabricated from solid aluminum for the aileron, flap and spoiler configurations. Geometric details are given in figure 1.

The 20% chord aileron was designed with a 0.5% leading edge clearance gap. The 25% slotted flap and 10% spoiler were designed with an airfoil forward section which terminates at 87.5% chord. The 10% spoiler was arranged in a slot-lip configuration with the 25% slotted flap. The spoiler was fitted with ball bearing hinges at three spanwise locations, and strain-gaged cantilever beam flexures at each end for hinge moment measurement.

All components were equipped with 1.07 mm inside diameter pressure taps for pressure distribution surveys. Flap and aileron positioning was provided through a set of guide rails mounted on the end plate disks, external to the test section. The model and end plates were mounted on the wind tunnel main balance system by means of pivot pins located at the airfoil 50% chord station. Foam seals around the circumference of the 1.07 m diameter end plates protected against flow leakage. These seals were carefully adjusted during static calibration to avoid interference friction forces.

The model was fitted with 2.5 mm wide transition strips of #80 carborundum grit located at 5% chord on the upper surface, and 10% chord on the lower surface.

Instrumentation

Three-component force measurements were obtained from the tunnel main balance. Spoiler hinge moment measurements were obtained directly from strain-gage flexures, and aileron hinge moments were obtained from integration of surface pressures. Pressure measurements were made with 96 pressure tubes multiplexed to 4 unbonded pressure transducers through a system of pressure switches (see fig. 2).

Resolution of the various instrumentation systems are given in Table 1:

Table 1 - Instrumentation Resolution

<u>Item</u>	<u>Resolution</u>
lift	$\pm 0.9\text{N}$ (± 0.2 lb)
drag (wake survey)	$\pm 0.06\text{N}$ (± 0.014 lb)
(force balance)	$\pm 0.2\text{N}$ (± 0.05 lb)
pitching moment	$\pm 0.1\text{N-m}$ (± 1 in-lb)
hinge moment	$\pm 0.02\text{N-m}$ (± 0.2 in-lb)
pressure transducers	$\pm 4.8\text{N/m}^2$ (± 0.1 psf)
dynamic pressure	$\pm 4.8\text{N/m}^2$ (± 0.1 psf)
angle of attack	$\pm 0.05^\circ$
flap and aileron angles	$\pm 0.5^\circ$
spoiler angle	$\pm 0.25^\circ$
flap longitudinal and vertical settings	± 0.001 c

Experimental data were obtained, stored and processed into final corrected form using the WSU wind tunnel on-line mini-computer system. This system had a 32 kilo-byte random access memory, two 110 kilo-byte cassette tape drives for program and raw data storage,

a 120 character/sec printer, and 28 cm plotter with a 0.4 mm resolution. With this system, final data which included one-component plots were available 6 seconds after data acquisition. Final three-component plots were available 3 minutes after end of run. Incremental control effectiveness and pressure integrations were obtained by off-line computer runs on the same computing system.

Test Procedure

Three-component force measurements were made using the wind tunnel main balance system. Flap-nested drag measurements were made using the wake survey method. A scanning five tube pressure probe was used for this purpose. Surveys were conducted at one chord-length downstream from the model trailing edge. The difference between force balance drag and wake survey drag is end plate tare drag, which depends upon lift coefficient as well as airfoil section. The wake survey method cannot be utilized when separation is present. For this reason it was not applied to flap extended tests. However under high drag conditions the end plate tare is a relatively small portion of total drag. This reasoning has led to the following procedure: (a) for flap-nested cases the wake survey drag is used directly, (b) for flap, aileron or spoiler extended cases the drag as measured by the force balance is corrected by subtracting the end plate tare. The end plate tare curve is extrapolated for high lift-coefficient conditions. Details of this extrapolation are given in appendix A.

Wind Tunnel

The WSU Walter Beech Tunnel is a closed return tunnel with atmospheric test section static pressure. The test section with two-dimensional inserts is 0.91 m x 2.13 m. Complete description of the insert and calibration details are given in reference 4. Special corrections for circulation effects on the test section static pressure system have been applied as described in Appendix B.

RESULTS AND DISCUSSION

Presentation of Results

Test results and comparison with theory and other experimental results are shown in the figures as listed in Table 2.

Table 2 - List of Figures

<u>Configuration</u>	<u>Type Data</u>	<u>Comparisons</u>	<u>Figure</u>
airfoil, aileron, flap and spoiler	model geometry	---	1
pressure system schematic	---	---	2
basic section	C_l, C_d, C_m	data of ref.2	3
basic section	pressures	theory	4
basic section	tufts	---	5
20% aileron	C_l, C_d, C_m	---	6
20% aileron	$\Delta C_l, \Delta C_d, \Delta C_m, C_h$	---	7
20% aileron	pressures	---	8
25% flap	optimum flap settings	---	9
25% flap	$C_{l_{max}}$ contours	---	10
25% flap	C_l, C_d, C_m	theory	11
25% flap	flap effectiveness	GA(W)-2	12
25% flap	experimental pressures	---	13
25% flap	pressures	theory	14 - 17
10% spoiler	effect of spoilers on lift for various flap settings	---	18
10% spoiler	incremental spoiler effectiveness and hinge moments	---	19

Discussion

Flap Nested: (figures 3 through 5). The force data show that the basic section has a very unusual stalling characteristic. Initial stall occurs at a $C_{l_{max}}$ of 1.31 and an angle of attack of

11.3°. This is substantially lower than the 1.54 $c_{l_{max}}$ of the 17% thick GA(W)-1 section (ref. 5). The post-stall $c_{l_{max}}$ curve for the 21% section is quite flat, dipping to about 1.26 at 18° and subsequently recovering to a higher level above 20°. The drag and pitching moment results are similar to the lift, showing progressive changes through $c_{l_{max}}$ with no indication of abrupt separation.

The NASA tests of ref. 2 show similar results for lift and moment at 2.0×10^6 Reynolds number, but abrupt stalling characteristics at higher Reynolds numbers. The drag measurements from the present tests show the same minimum drag level as the NASA tests, but somewhat higher drag levels for lift coefficients above 0.4.

The pressure distributions and tuft studies for the flap nested configuration confirm the implications of the force measurements. The separation progression is quite slow as angle of attack is increased. In fact both tuft pattern and pressure distributions indicate that even at 30° angle of attack, separation has not reached the leading edge. Pressure distributions are characterized by very modest nose suction peaks and mild gradients. Theoretical results using the method of reference 6 show relatively poor agreement with experiment for all positive angles of attack. The discrepancies become quite large for high angles of attack when massive separation is present.

20% Aileron: (figures 6 through 8). Lift characteristics with aileron show that as aileron downward deflection is increased, the stalling characteristic becomes progressively more abrupt. Aileron drag, pitching moment and incremental control effectiveness are similar to the 17% thick GA(W)-1 airfoil (ref. 8). Aileron hinge moments are similar to the GA(W)-1, but show considerable non-linearity at high angles. Pressure distributions show mild peaks and relatively slow progression of separation with angle of attack.

25% Flap: (figures 9 through 17). $c_{l_{max}}$ contours for flap deflections from 10° to 35° show that the optimum flap settings are quite similar to other airfoils (for example, ref. 9). $c_{l_{max}}$ values for all flap settings are lower than comparable data for the 13%

thick GA(W)-2 section (ref. 9). Theoretical results over-predict lift at 30° and 35° flap deflection at all angles of attack. At 10° and 20° flap settings the theory under-predicts the lift, even at low angles of attack. While the under-prediction discrepancies are not large, they are consistent with trends observed on other airfoil-flap combinations (see ref. 9). Over-prediction of lift has been attributed to boundary layer thickness exceeding theoretical values. The reasons for under-prediction of theory for low flap deflections are not understood.

The flap effectiveness plot (fig. 12) for the 25% flap indicates higher increments in $c_{l_{\max}}$ than in c_l @ $\alpha = 0^\circ$. This is a result of increased slope of the $c_l - \alpha$ curve with flap extended, and is attributed to improved boundary layer flow ahead of the flap slot due to the aspirating effect of the slot. For the 20% plain flap (aileron), the increments in $c_{l_{\max}}$ are slightly lower than the increments in c_l @ $\alpha = 0^\circ$. All flap effectiveness characteristics are very similar to the characteristics observed for the GA(W)-2 airfoil (ref. 9).

Pressure distributions with flap extended indicate attached flap flow with separation appearing initially at the airfoil trailing edge and progressing forward very slowly as angle of attack is increased. The very modest nose suction pressure peaks associated with this section are again observed. Theoretical pressure distributions show good agreement with experiment prior to separation, and poor agreement for separation locations forward of the 0.90 c station.

A refined analysis technique has been applied to the present experimental pressure data. In earlier research (refs. 9 and 10), pressure distributions were corrected for tunnel flow angularity, but not for wake blockage, (ref. 11), since wake blockage depends upon drag, and drag is not measured simultaneously with surface pressures. In order to provide more accurate accounting for this effect the present data have been corrected in the following manner: The effect of wake blockage as obtained from force runs was used to calculate an equivalent increment in angle of

attack required to produce the apparent added lift. This increment in angle of attack is applied as a correction to the experimental data. Details of this correction are given in Appendix C. The largest correction occurs at the highest $c_{l_{\max}}$ and amounts to 0.7° increment in angle of attack.

10% Slot-Lip Spoiler: (figures 18 and 19). Effects of spoiler on lift, drag and pitching moment, and spoiler control effectiveness and hinge moment characteristics are generally similar to GA(W)-2 spoiler performance (ref. 9). With flap nested, however, a slight control reversal is observed at 8° angle of attack. With flap extended reversal is not present. It is believed that the reversal with flap nested is associated with a thick boundary layer development near the trailing edge. With the slotted flap extended the boundary layer is evidently thinned, and the reversal vanishes.

Control effectiveness is highly non-linear but positive for all spoiler deflections with flap extended. Hinge moments change from opening moments for small spoiler deflections to closing moments for large spoiler deflections.

CONCLUSIONS

1. Force, pressure and surface flow studies have been conducted for 20% aileron, 25% flap and 10% spoiler applied to the 21% thick (LS)-0421 modified airfoil section.

2. Flap nested high-lift performance of this section is substantially lower than the 17% thick GA(W)-1 section, but post- $c_{l_{\max}}$ behavior shows nearly constant c_l extending to very high angles.

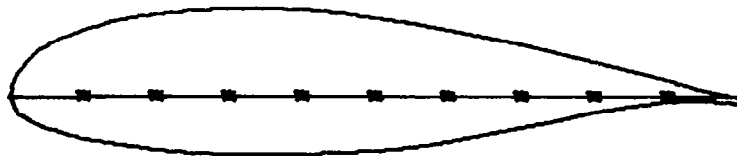
3. Incremental performance of flaps applied to this section is comparable to similar flaps applied to the GA(W)-2 airfoil.

4. Aileron control effectiveness and hinge moments are similar to comparable parameters for the GA(W)-2 airfoil section.

5. At high- α conditions with flap nested the spoiler produces control reversal for small deflections. Spoiler effectiveness with flap extended is non-linear but positive for all flap and spoiler deflections. Spoiler hinge moments are similar to hinge moments for a spoiler applied to the GA(W)-2 airfoil.

REFERENCES

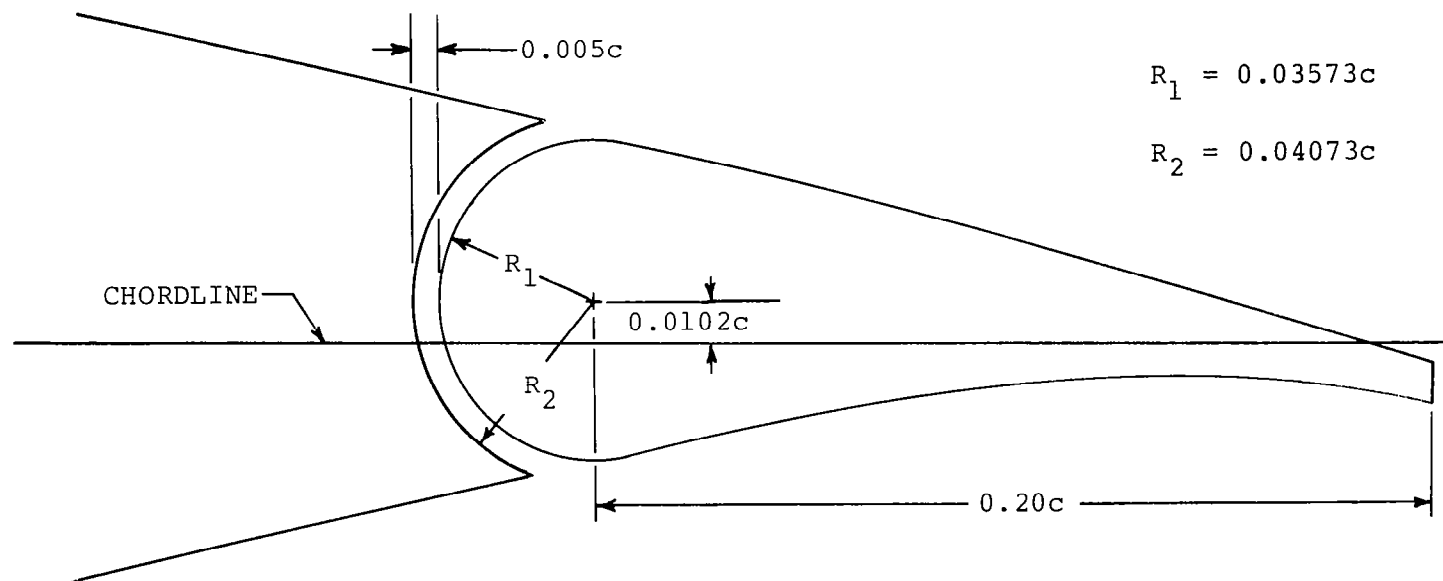
1. Pierpont, P.K.: Bringing Wings of Change. Astronautics and Aeronautics Magazine, October 1975.
2. McGhee, Robert J.; and Beasley, William D.: Wind-Tunnel Results for an Improved 21-Percent-Thick Low-Speed Airfoil Section. NASA TM 78650, 1978.
3. Mechtly, E.A.: The International System of Units--Physical Constants and Conversion Factors (Revised). NASA SP-7012, 1969.
4. Siew, R.J.: Calibration of a Two-Dimensional Insert for the WSU 7' x 10' Wind Tunnel. AR 73-2, Wichita State University, 1973.
5. Wentz, W.H., Jr.; and Seetharam, H.C.: Development of a Fowler Flap System for a High Performance General Aviation Airfoil. NASA CR-2443, 1974.
6. Smetana, Frederick O.; Summey, Delbert C.; Smith, Neill S.; and Carden, Ronald K.: Light Aircraft Lift, Drag, and Moment Prediction - A Review and Analysis. NASA CR-2523, 1975.
7. Stevens, W.A.; Goradia, S.H.; and Braden, J.A.: Mathematical Model for Two-Dimensional Multi-Component Airfoils in Viscous Flow. NASA CR-1843, July 1971.
8. Wentz, W.H., Jr.; Seetharam, H.C.; and Fisco, K.A.: Force and Pressure Tests of the GA(W)-1 Airfoil with a 20% Aileron and Pressure Tests with a 30% Fowler Flap. NASA CR-2833, 1977.
9. Wentz, W.H., Jr.: Wind Tunnel Tests of the GA(W)-2 Airfoil with 20% Aileron, 25% Slotted Flap, 30% Fowler Flap and 10% Slot-Lip Spoiler, NASA CR-145139, 1977 (date for general release, August 1978).
10. Wentz, W.H., Jr.; and Fisco, K.A.: Pressure Distributions for the GA(W)-2 Airfoil with 20% Aileron, 25% Slotted Flap, and 30% Slotted Flap. NASA CR-2948, 1978 (date for general release, February 1980).
11. Pope, A.; and Harper, J.J.: Low-Speed Wind Tunnel Testing. John Wiley and Sons, 1966.



UPPER SURFACE		LOWER SURFACE	
x/c	z/c	x/c	z/c
0.0000	0.0000	0.0000	0.0000
.0020	.0156	.0020	-.0107
.0050	.0243	.0050	-.0177
.0125	.0383	.0125	-.0265
.0250	.0540	.0250	-.0352
.0375	.0651	.0375	-.0416
.0500	.0736	.0500	-.0468
.0750	.0865	.0750	-.0550
.1000	.0960	.1000	-.0614
.1250	.1034	.1250	-.0665
.1500	.1093	.1500	-.0707
.1750	.1141	.1750	-.0741
.2000	.1179	.2000	-.0770
.2250	.1208	.2250	-.0794
.2500	.1229	.2500	-.0813
.2750	.1243	.2750	-.0828
.3000	.1250	.3000	-.0839
.3250	.1250	.3250	-.0846
.3500	.1244	.3500	-.0849
.3750	.1233	.3750	-.0849
.4000	.1217	.4000	-.0846
.4250	.1196	.4250	-.0839
.4500	.1170	.4500	-.0828
.4750	.1140	.4750	-.0813
.5000	.1106	.5000	-.0794
.5250	.1068	.5250	-.0770
.5500	.1027	.5500	-.0740
.5750	.0983	.5750	-.0705
.6000	.0936	.6000	-.0666
.6250	.0886	.6250	-.0623
.6500	.0833	.6500	-.0576
.6750	.0778	.6750	-.0525
.7000	.0721	.7000	-.0472
.7250	.0662	.7250	-.0418
.7500	.0601	.7500	-.0364
.7750	.0539	.7750	-.0310
.8000	.0476	.8000	-.0256
.8250	.0412	.8250	-.0206
.8500	.0348	.8500	-.0159
.8750	.0284	.8750	-.0118
.9000	.0220	.9000	-.0086
.9250	.0156	.9250	-.0070
.9500	.0091	.9500	-.0069
.9750	.0025	.9750	-.0088
1.0000	-.0042	1.0000	-.0132

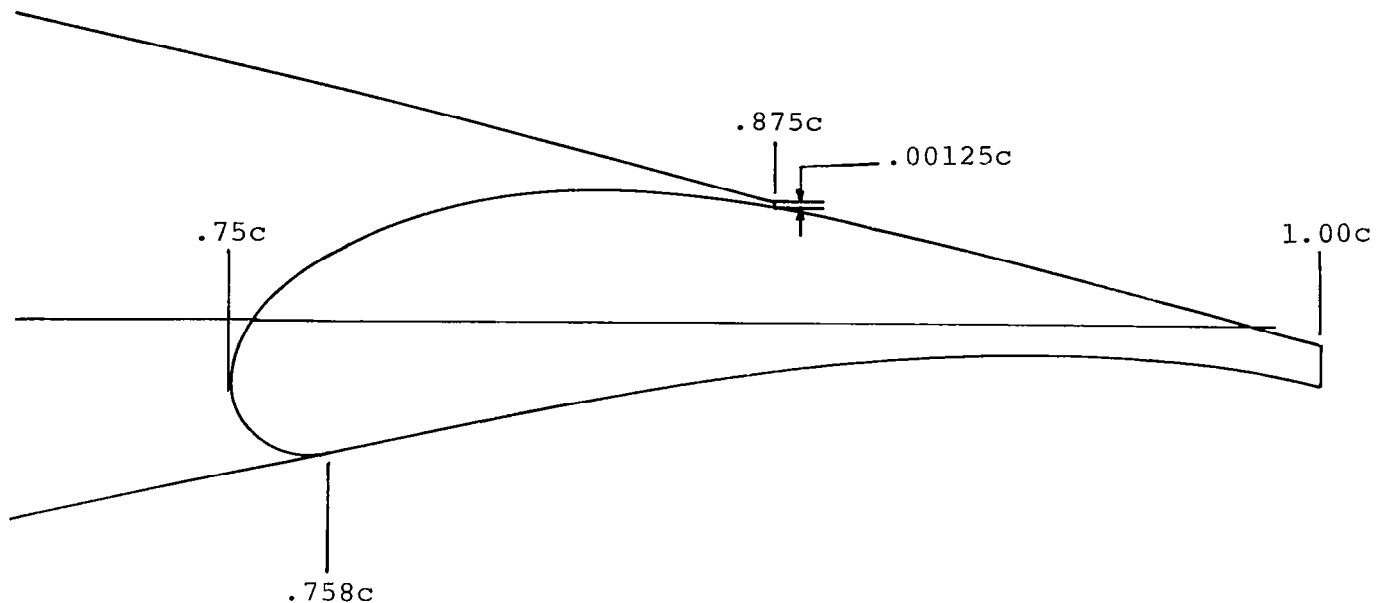
(a) Basic Airfoil

Figure 1 - Geometry.



(b) 20% Aileron.

Figure 1 - Continued.



Flap Upper Surface

x/c	z/c
0.7500	0.0139
.7531	.0038
.7562	.0009
.7625	.0073
.7687	.0124
.7750	.0165
.7850	.0228
.8000	.0268
.8250	.0308
.8500	.0307
.8750	.0271

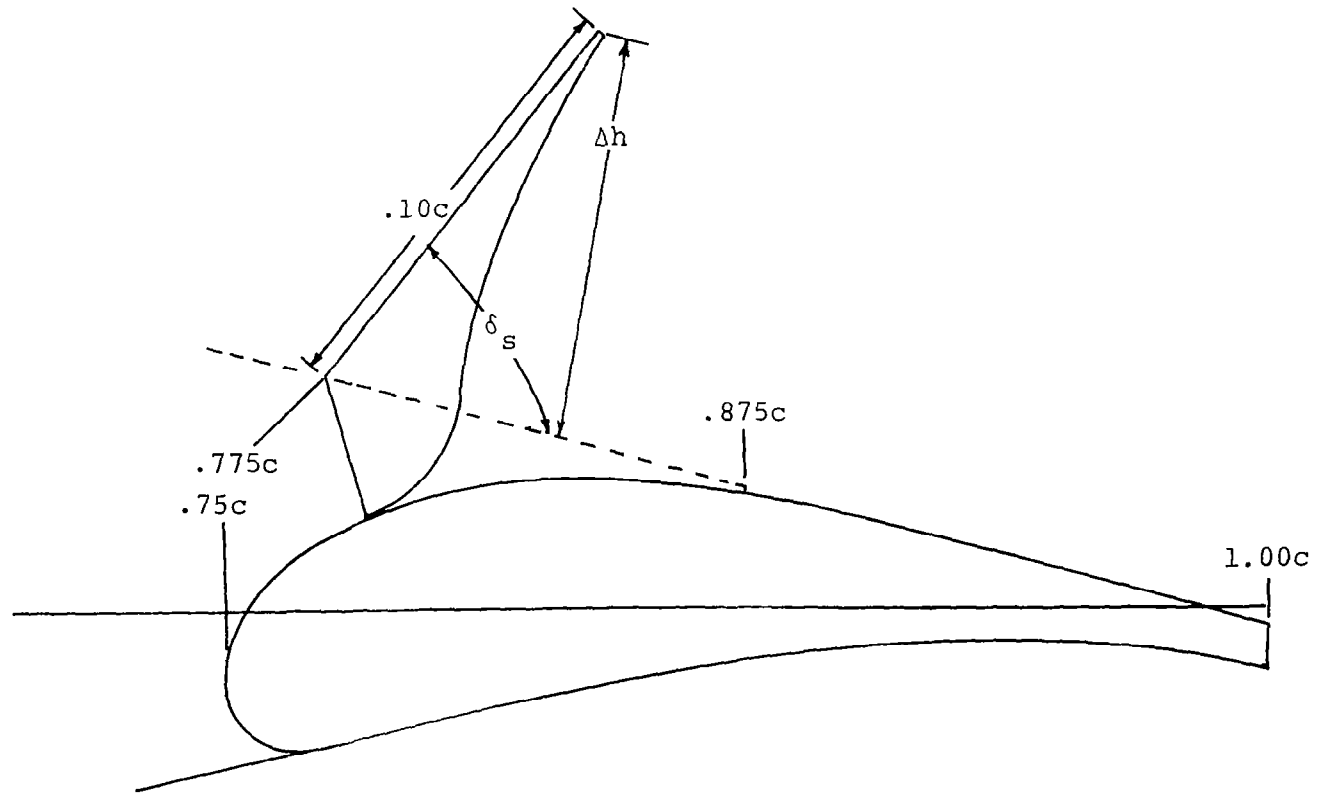
Nose Radius = $0.018c$

Nose Radius Location
 $(x/c, z/c) = (0.768, -0.014)$

Note: Remainder of flap contour
 matches basic airfoil.

(c) 25% Flap Geometry

Figure 1 - Continued.



(d) 10% Slot Lip Spoiler
Figure 1 - Concluded.

Airfoil with
Pressure Tubes

Model

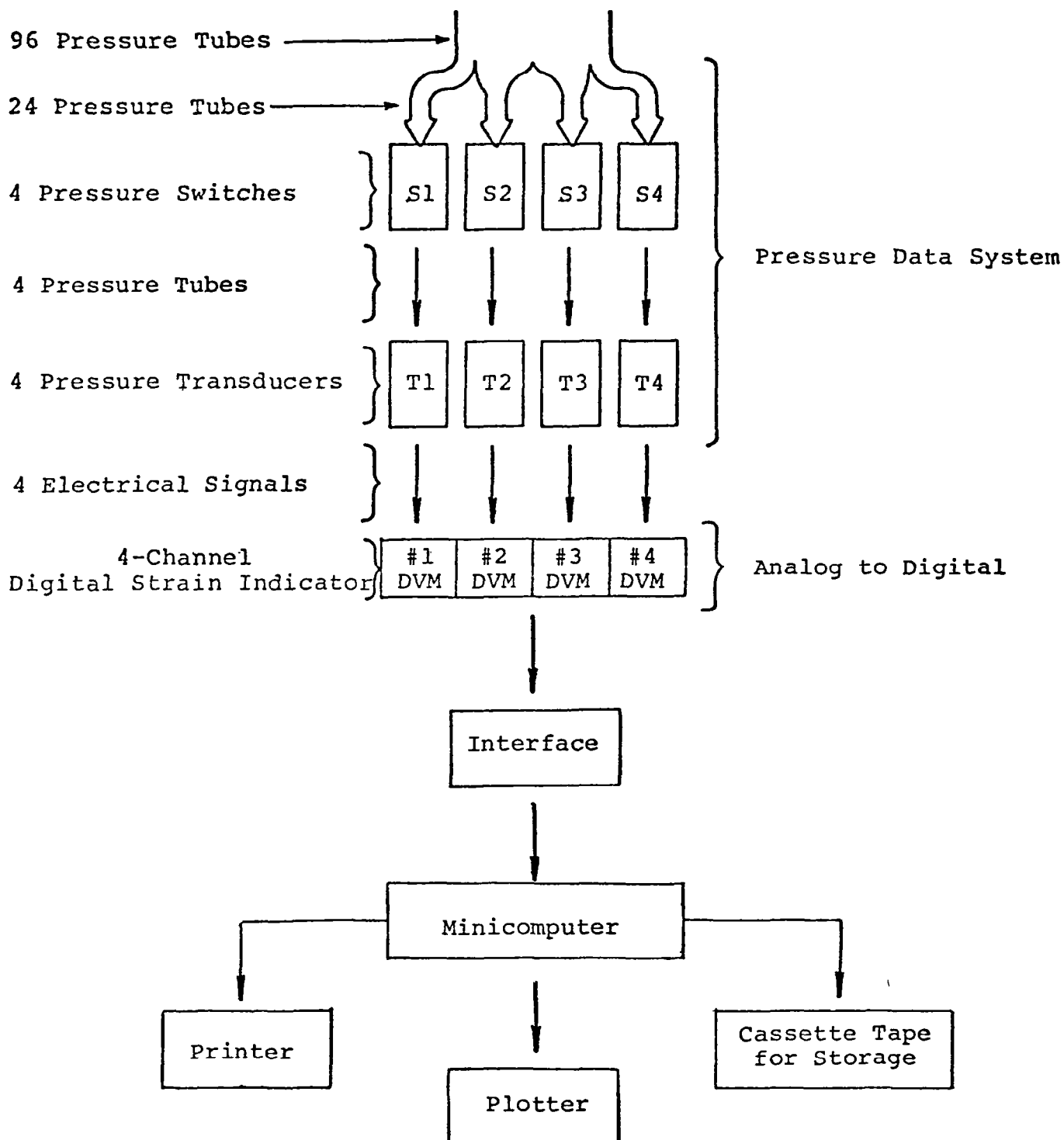


Figure 2 - Pressure Measurement and Computational System Schematic.

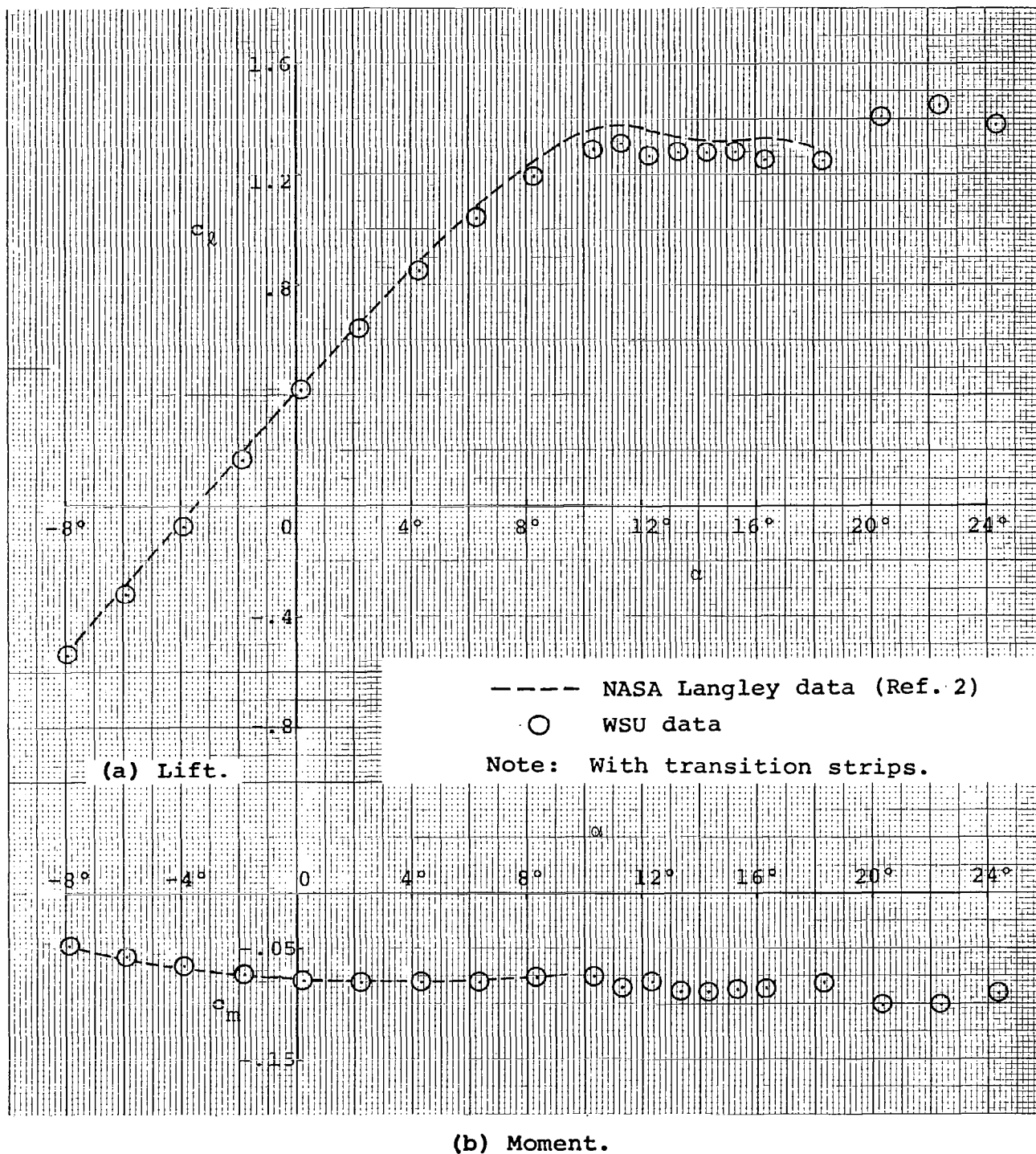
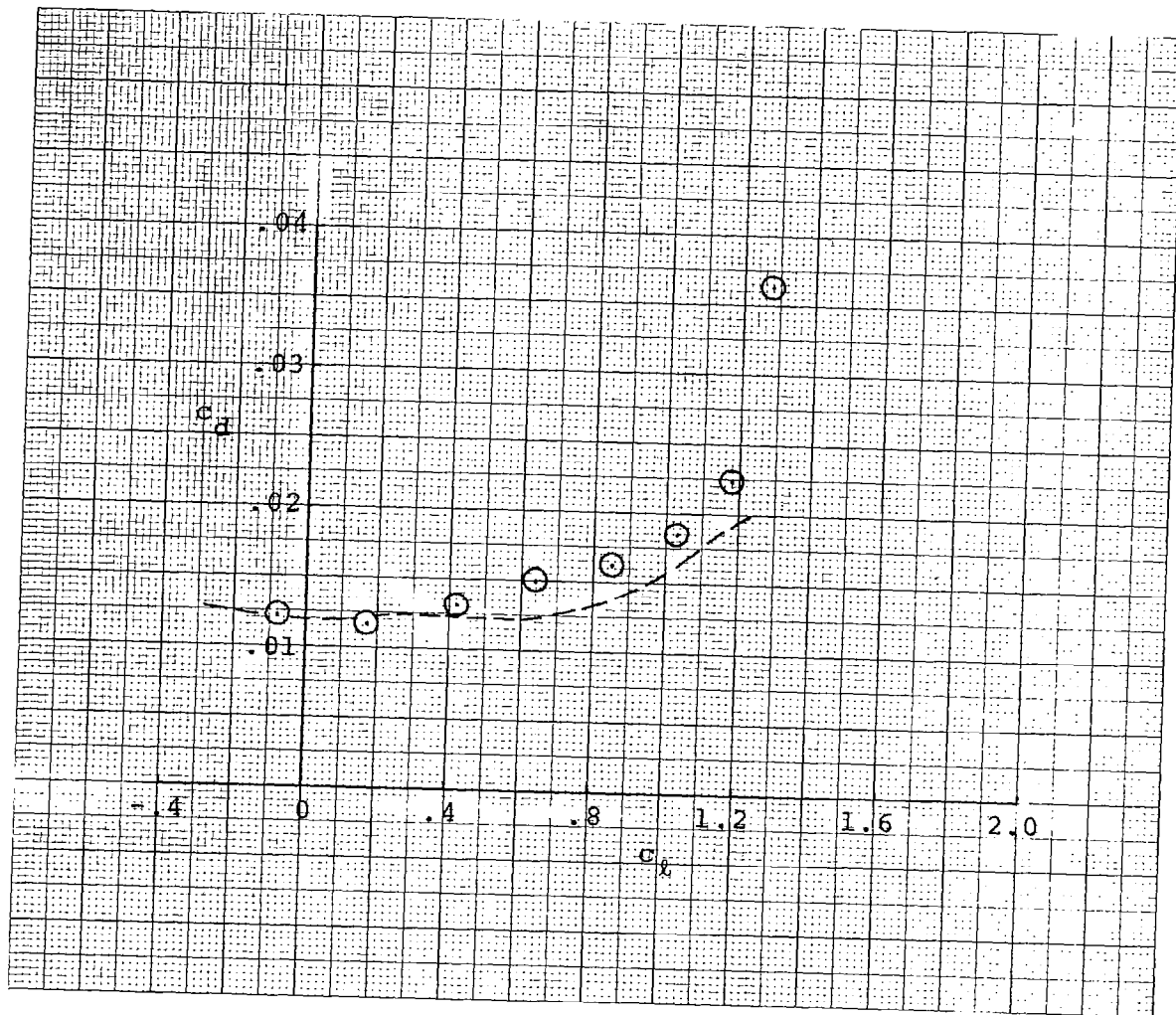


Figure 3 - Basic Airfoil Data - Comparisons with NASA Data.



----- NASA Langley data (Ref. 2)

○ WSU data

Note: With transition strips.

(c) Drag.

Figure 3 - Concluded.

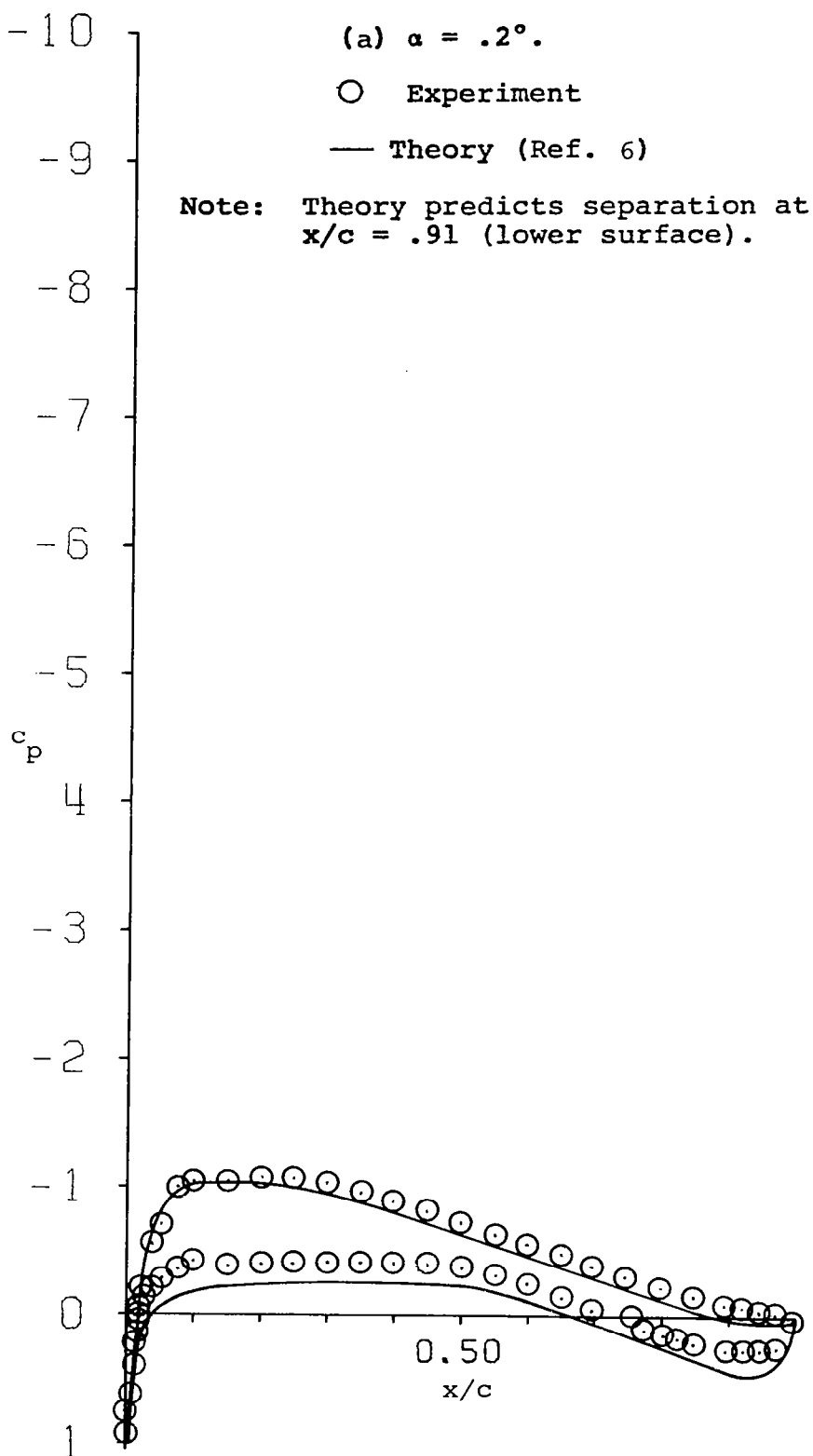


Figure 4 - Pressure Distribution for the Basic Section.

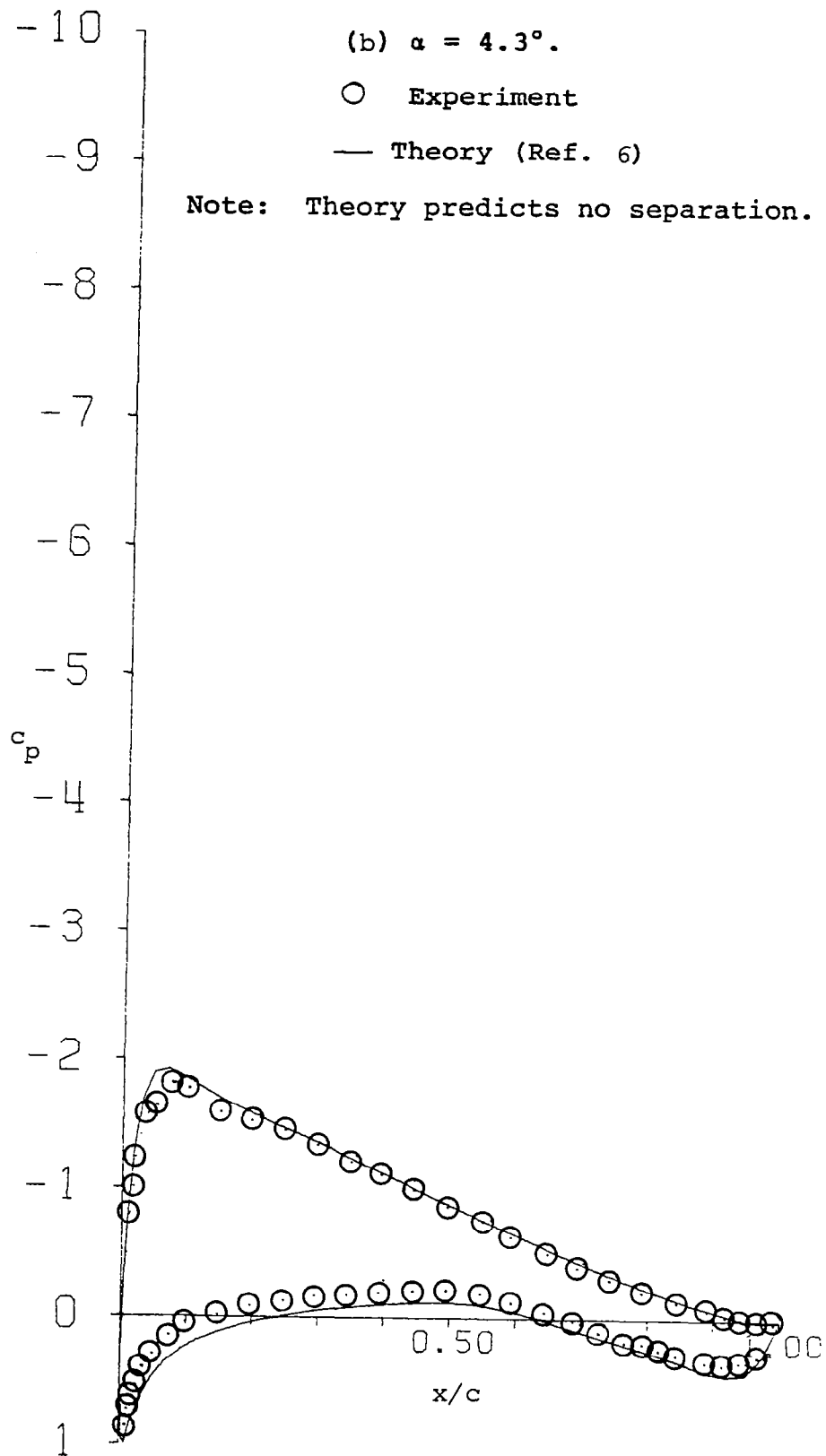


Figure 4 - Continued.

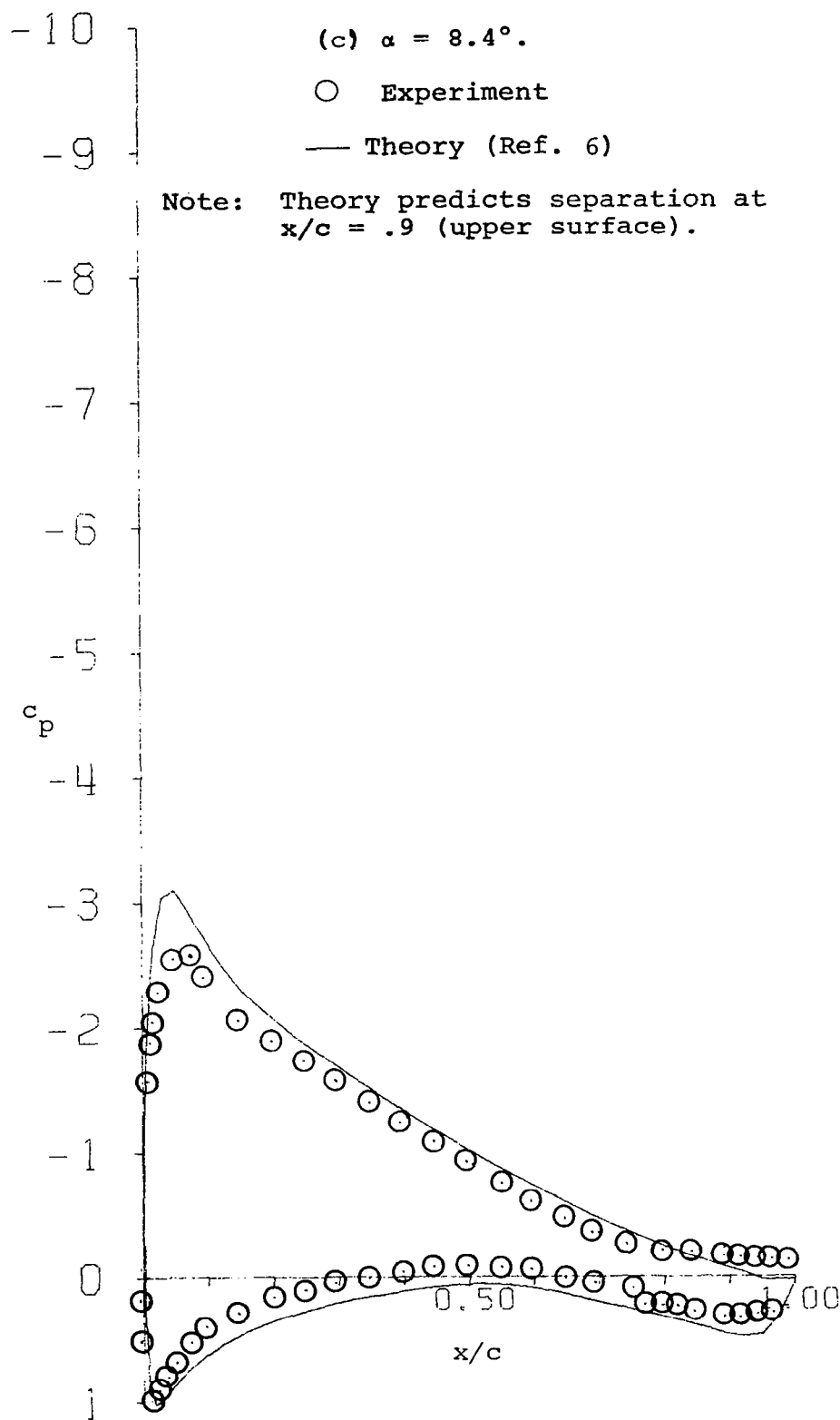


Figure 4 - Continued.

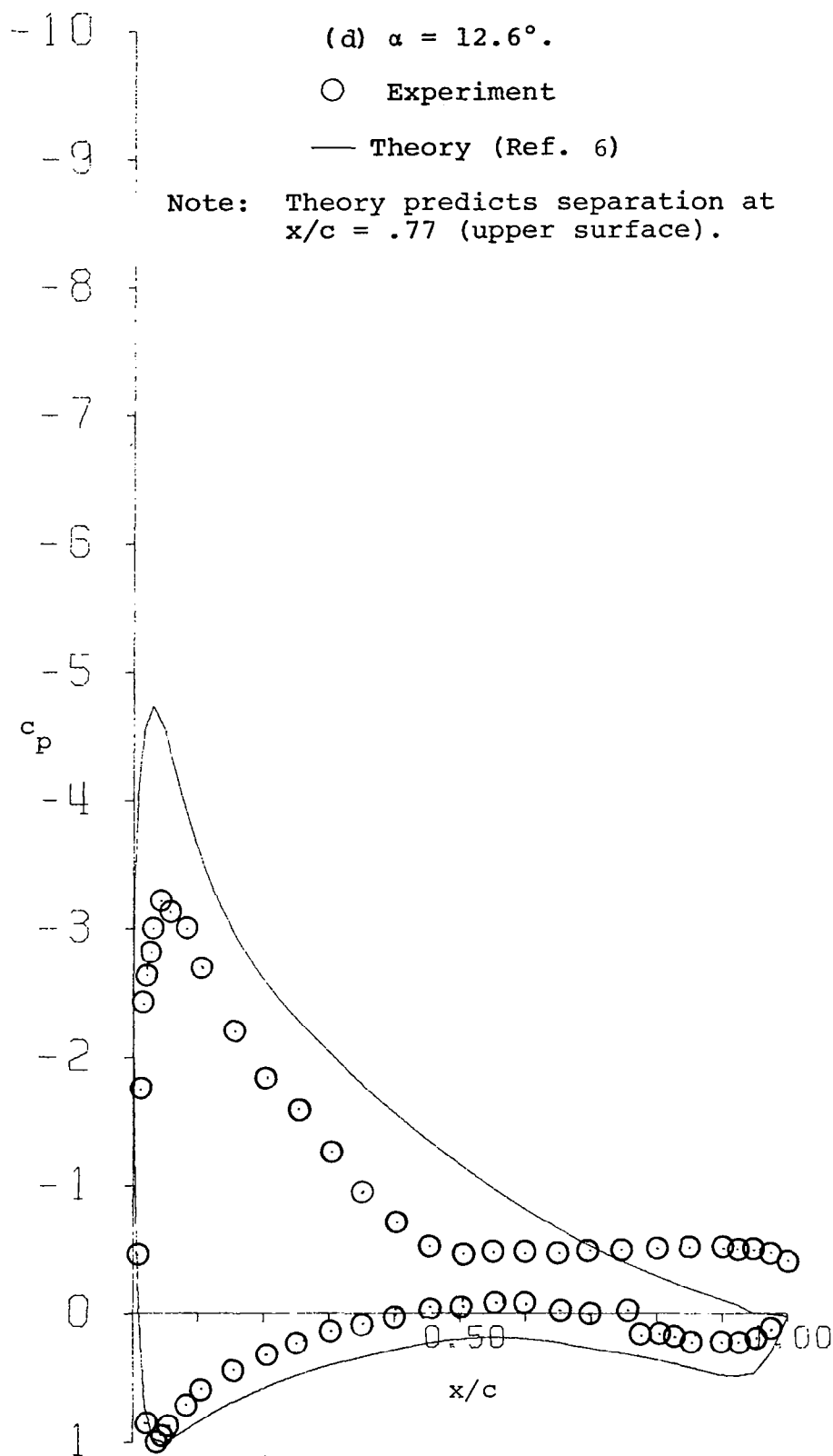


Figure 4 - Continued.

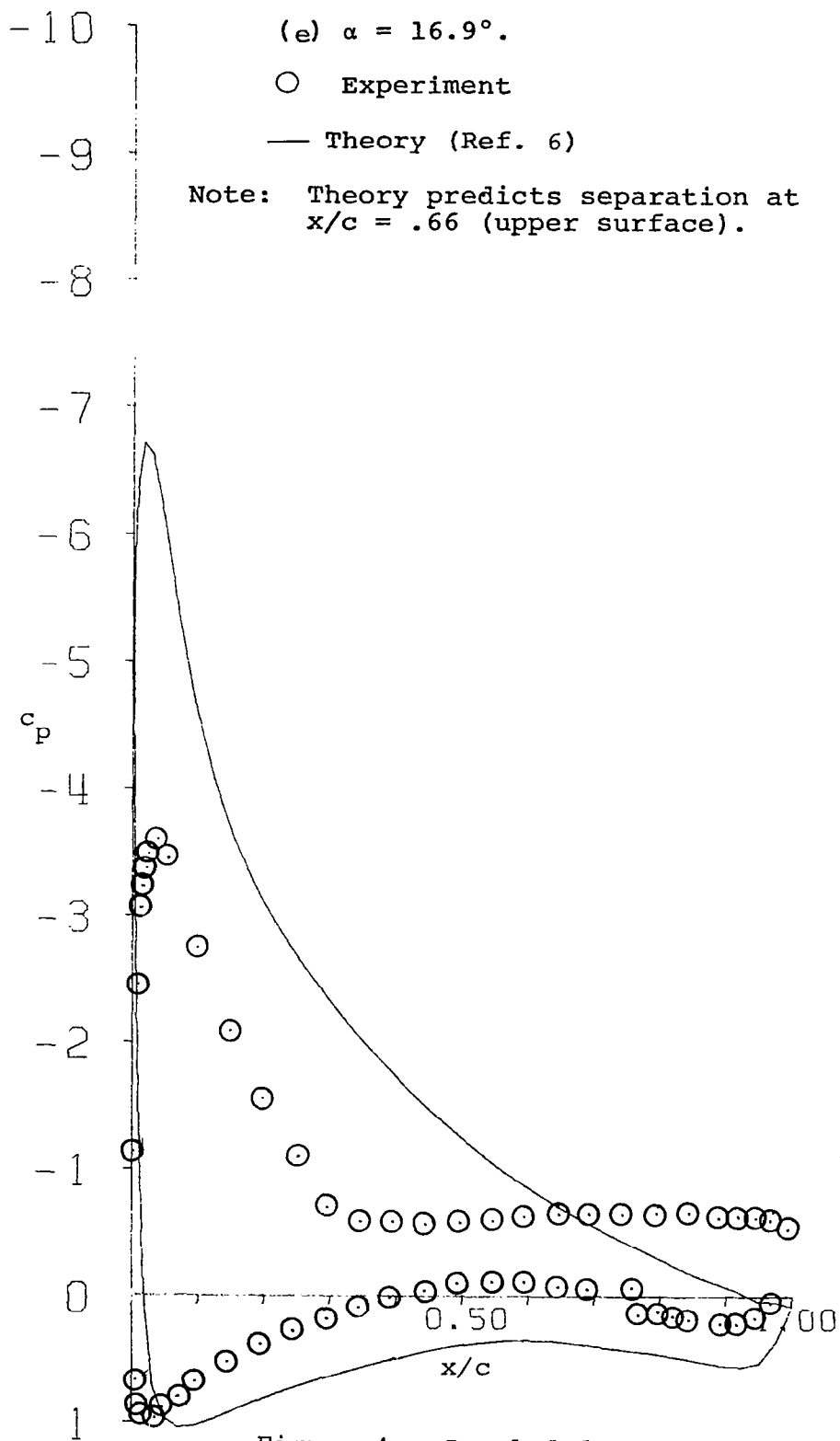
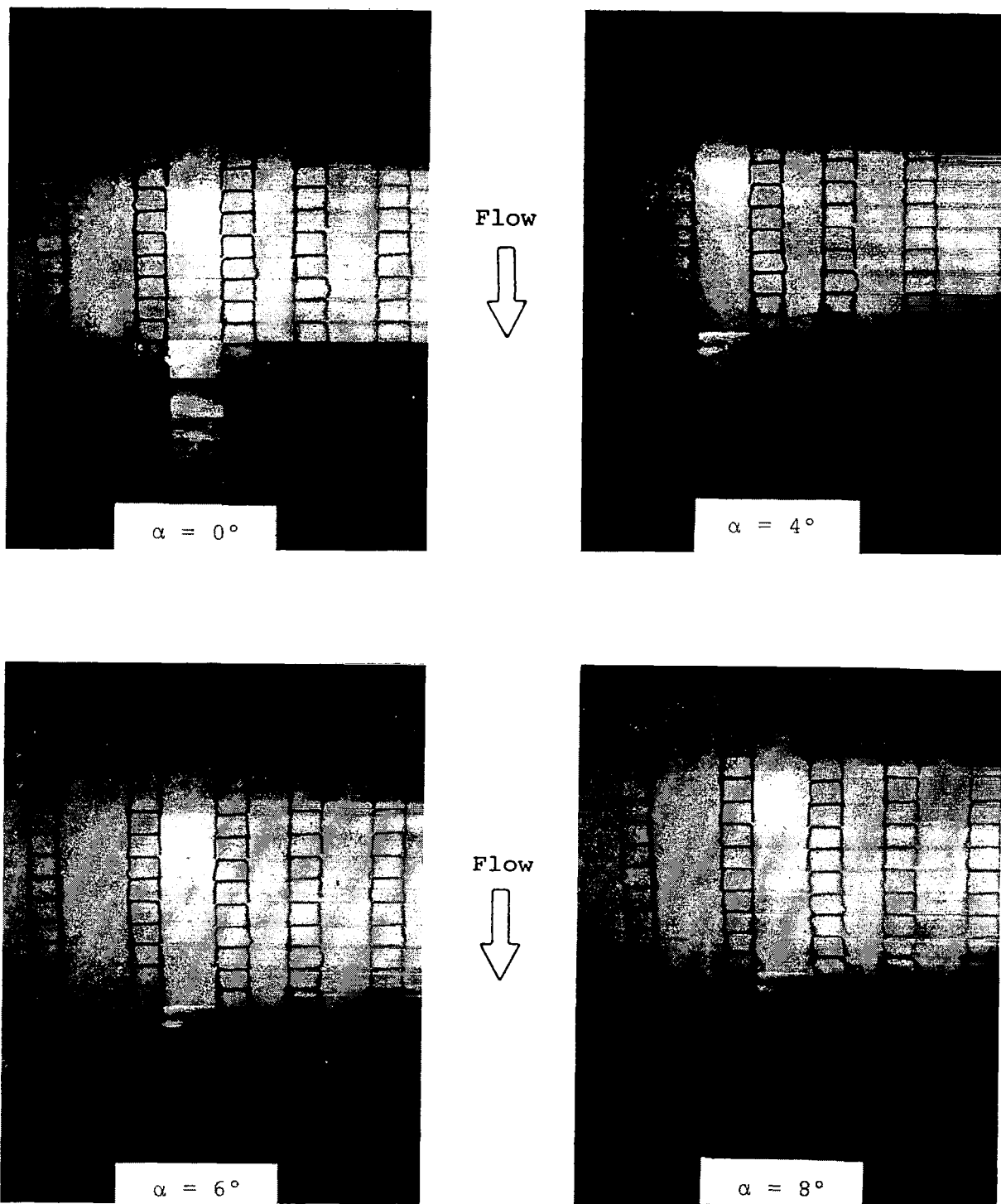
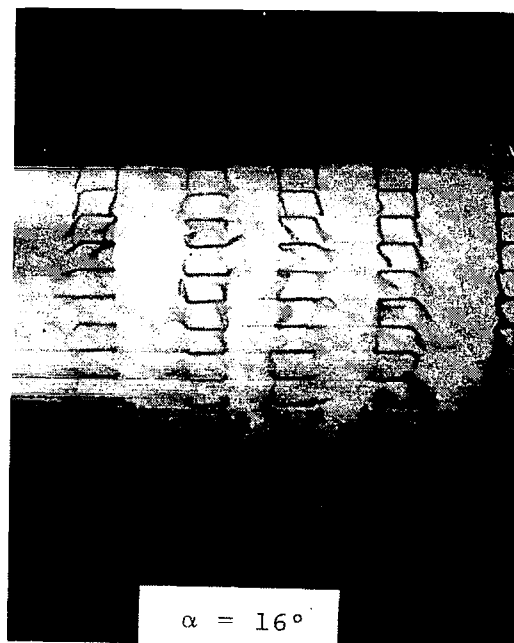
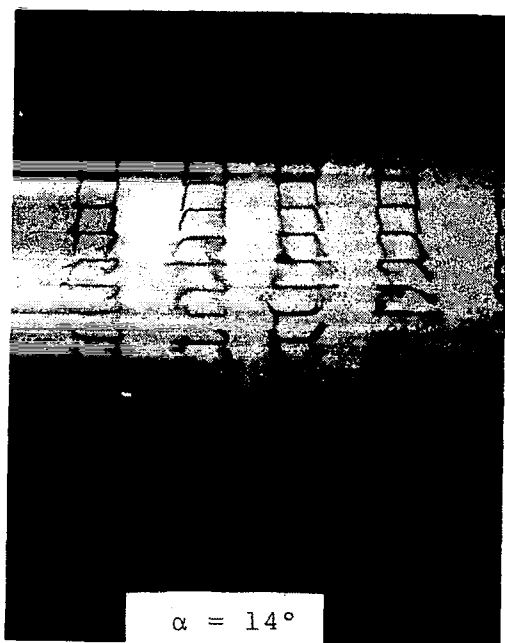
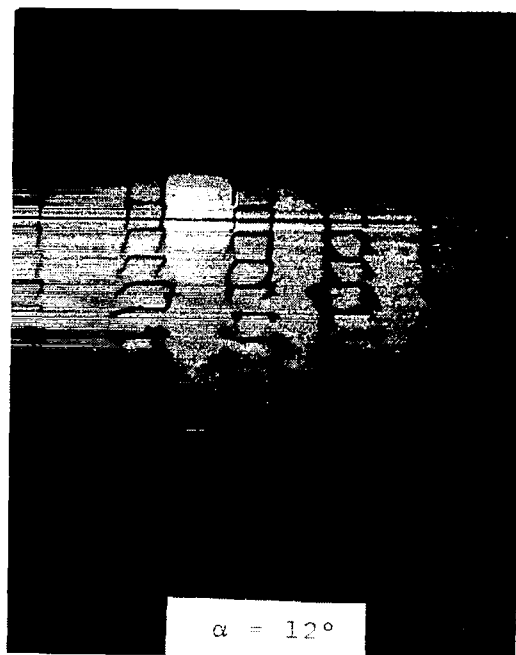
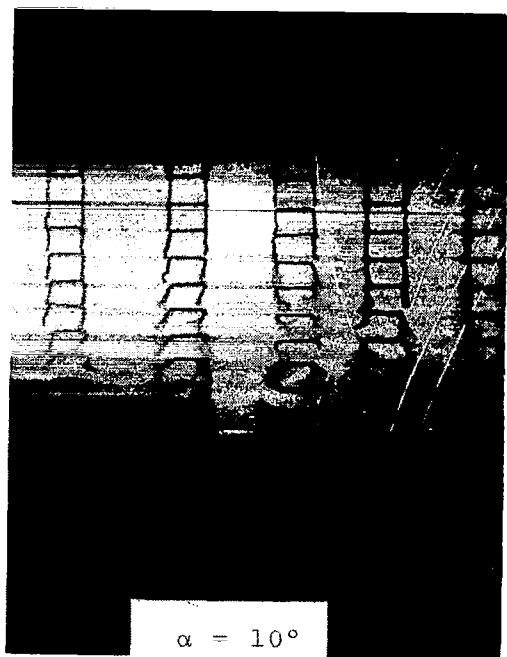


Figure 4 - Concluded.

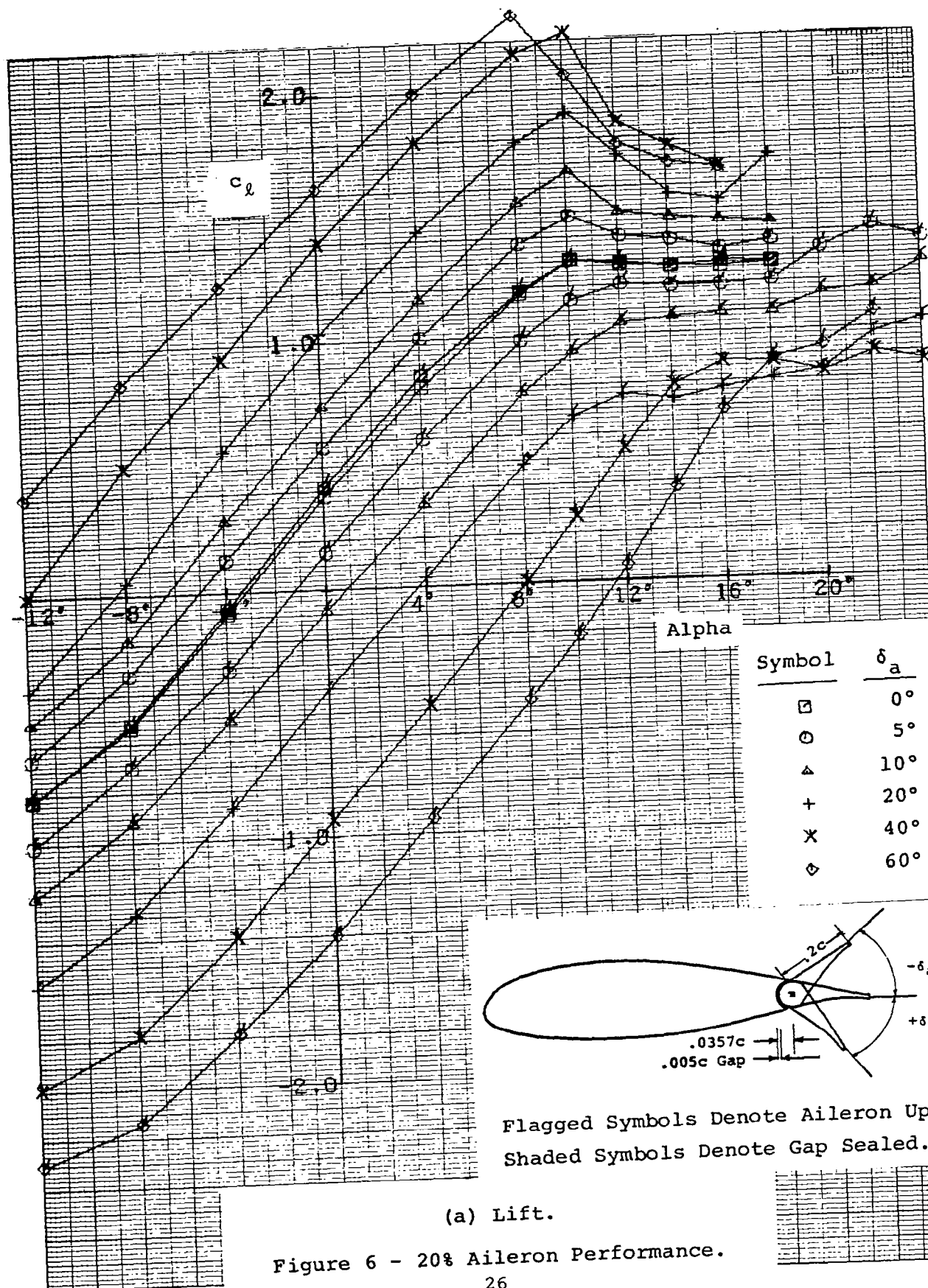


(a) Low Angles.

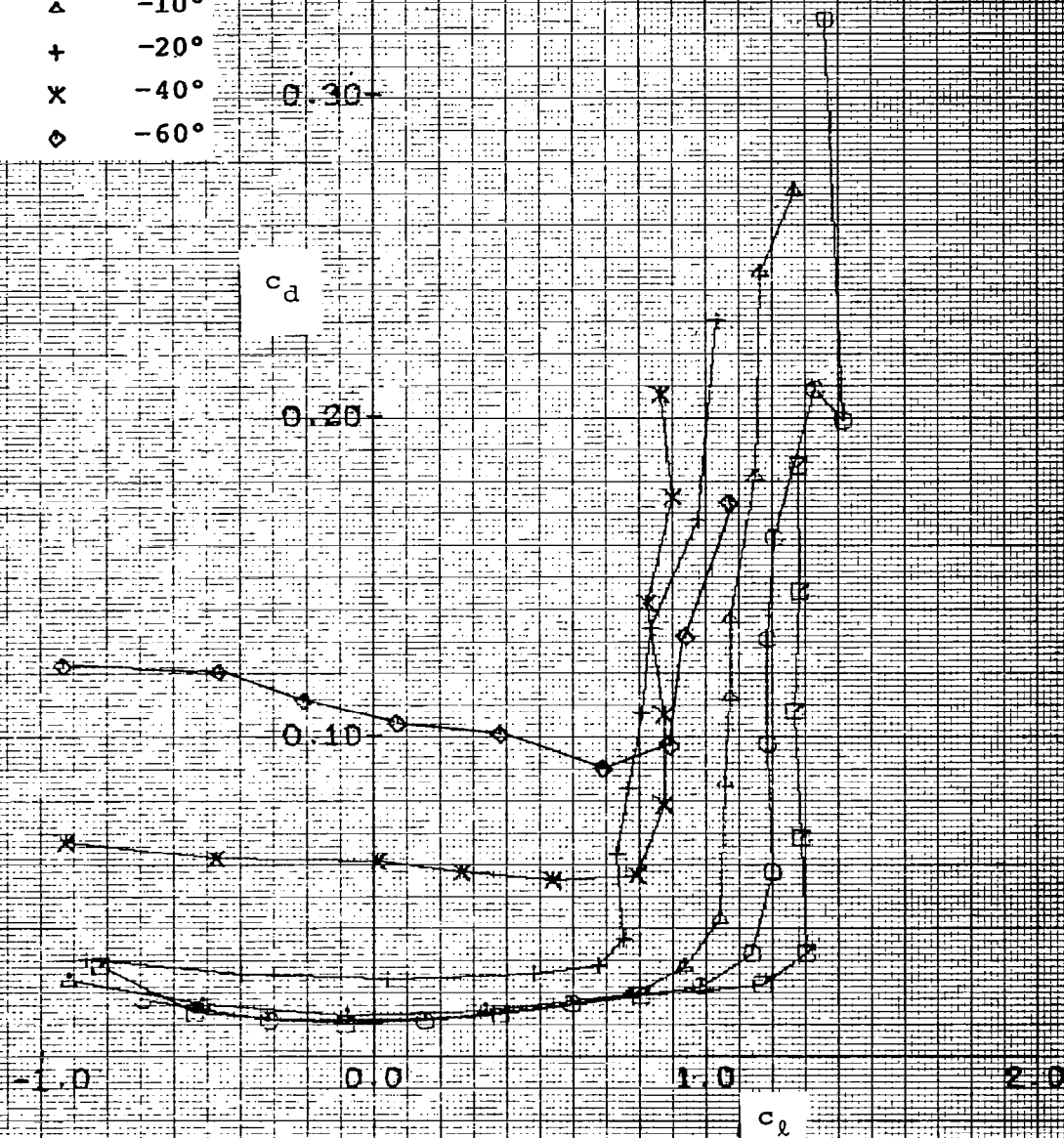
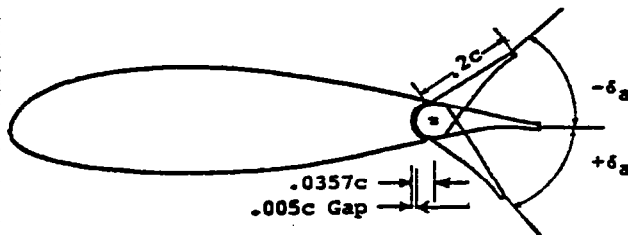
Figure 5 - Tuft Patterns With Aileron 0° , Sealed Gap.



(b) High Angles.
Figure 5 - Concluded.

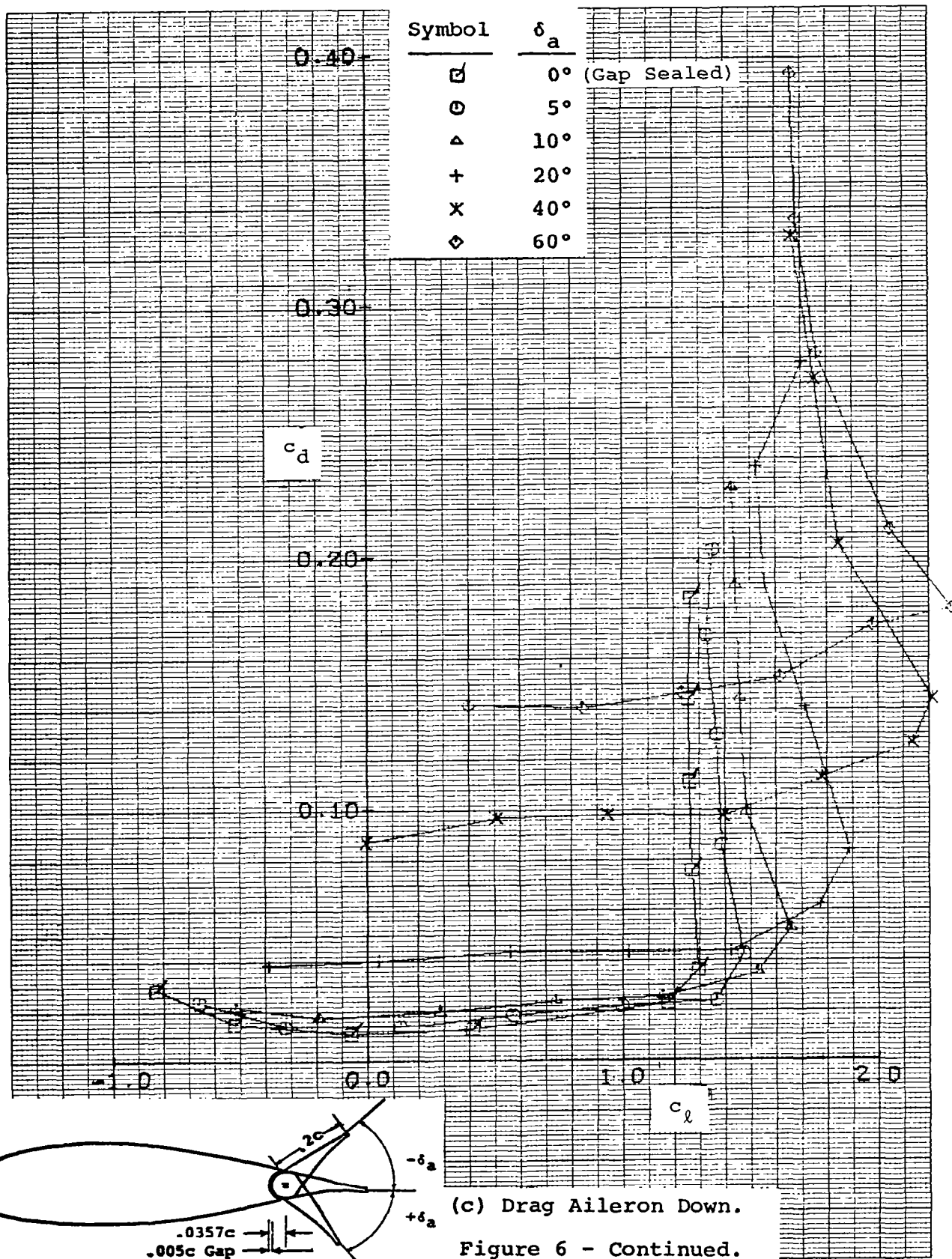


Symbol	δ_a
□	0°
○	-5°
△	-10°
+	-20°
x	-40°
◇	-60°



(b) Drag Aileron Up.

Figure 6 - Continued.



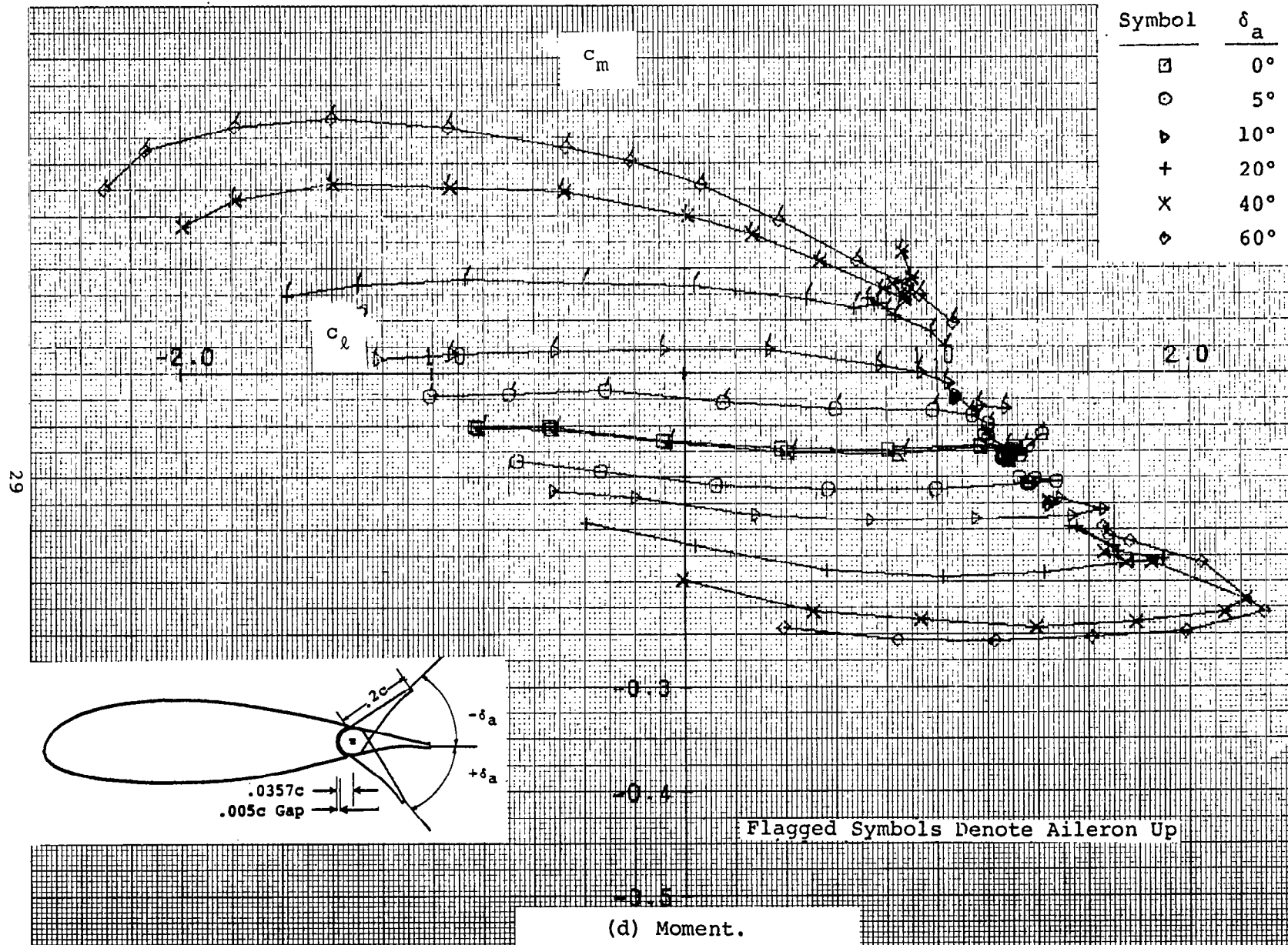


Figure 6 - Continued.

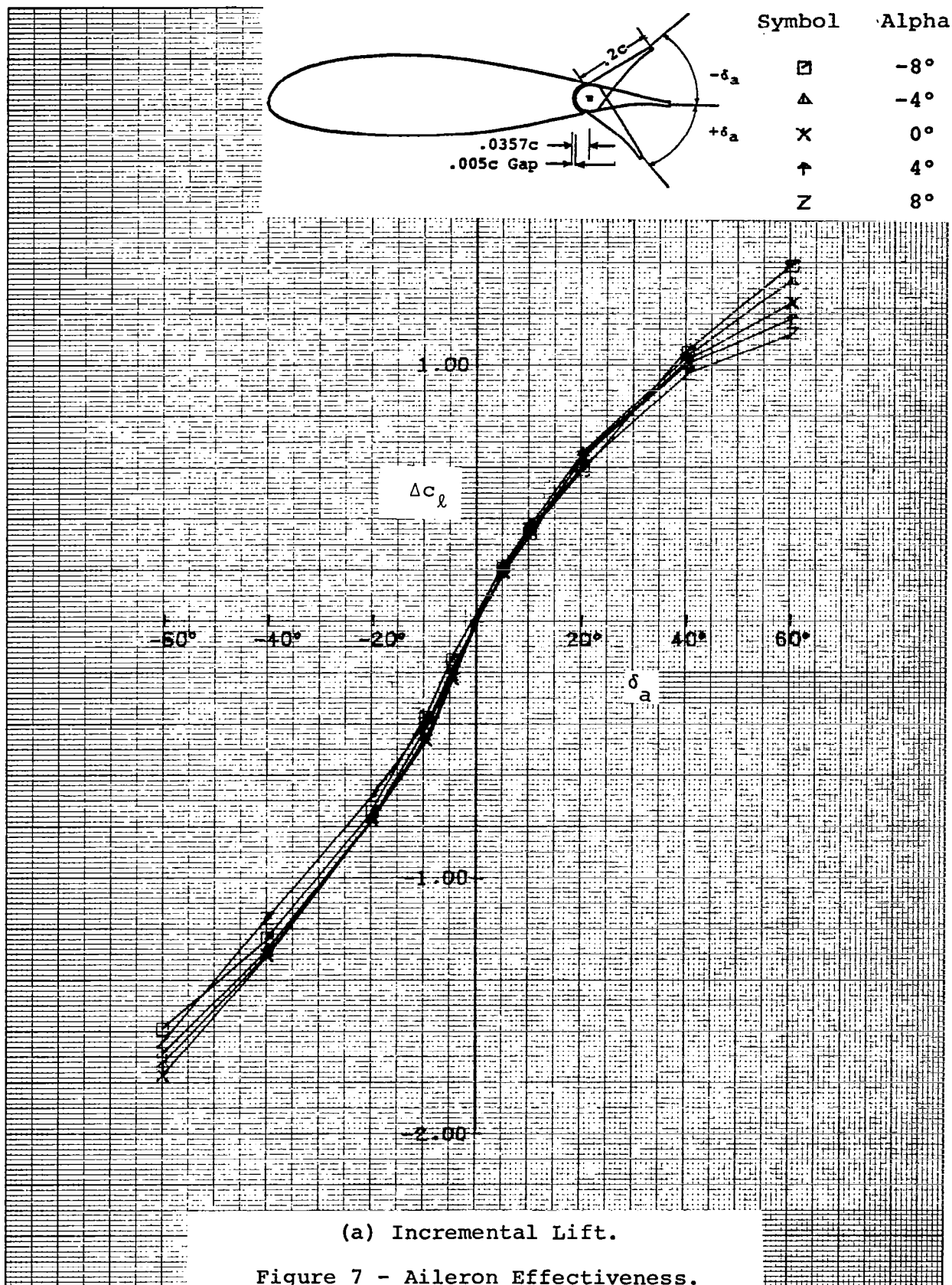
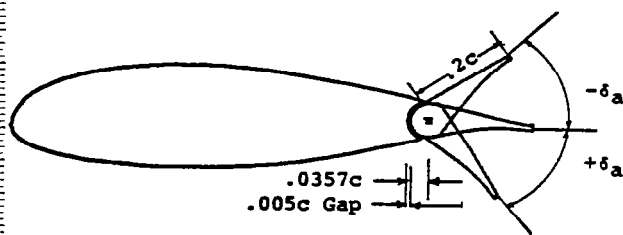
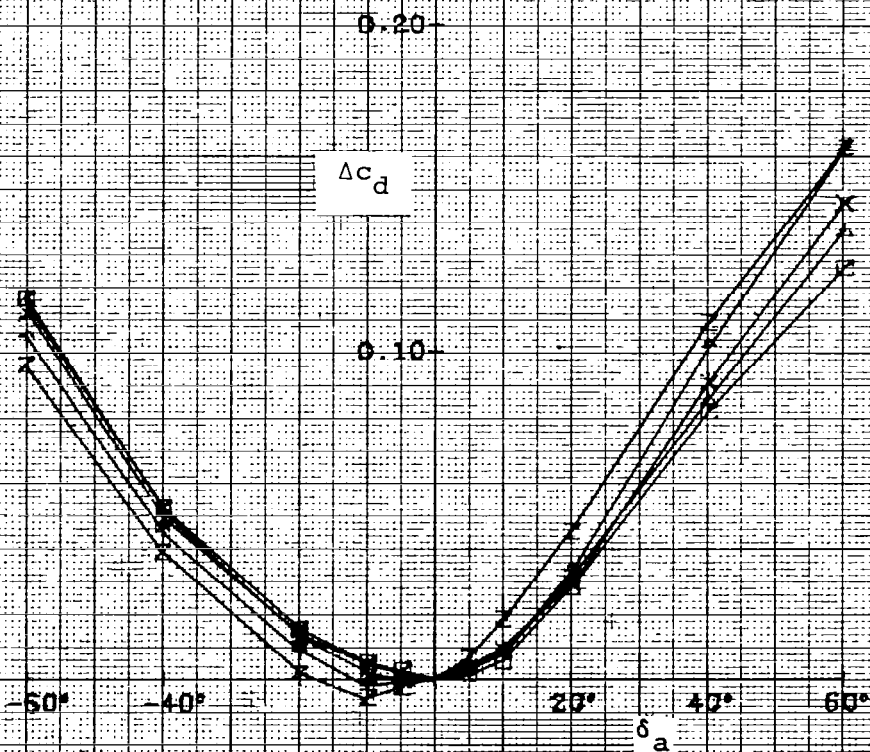


Figure 7 - Aileron Effectiveness.

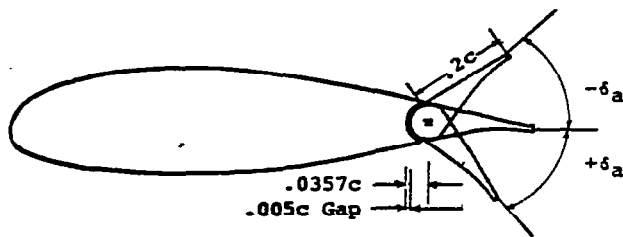


Symbol	Alpha
□	-8°
△	-4°
×	0°
+	4°
Z	8°

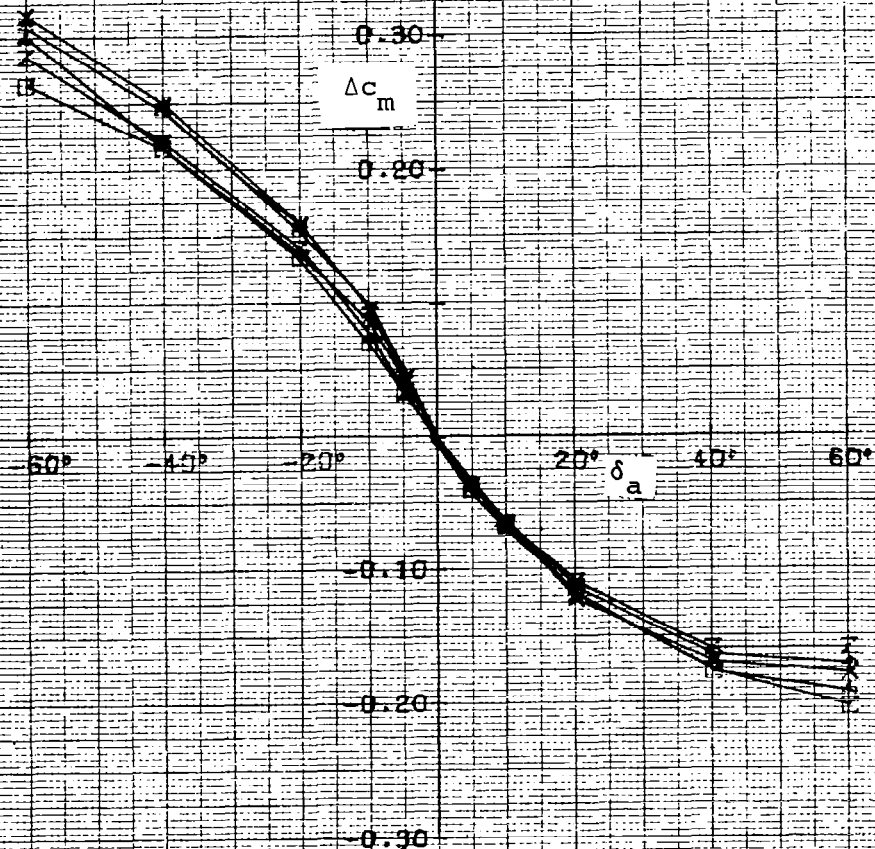


(b) Incremental Drag.

Figure 7 - Continued.

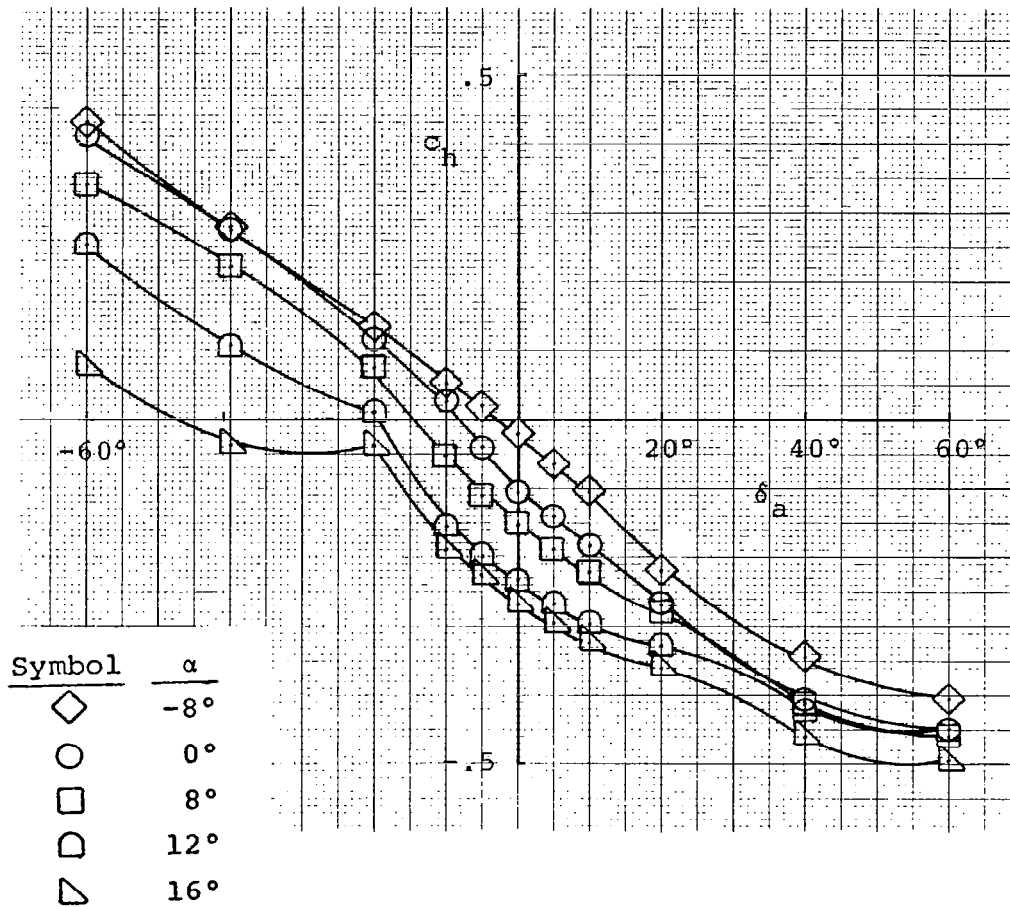
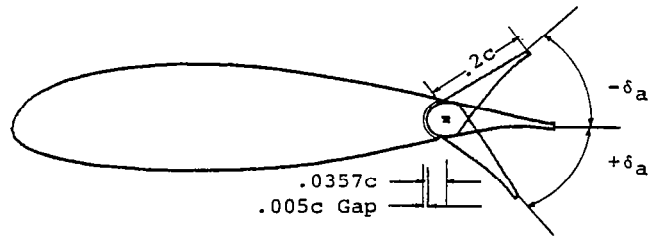


Symbol	Alpha
□	-8°
△	-4°
X	0°
↑	4°
Z	8°



(c) Incremental Moment.

Figure 7 - Continued.



(d) Hinge Moment.

Figure 7 - Concluded.

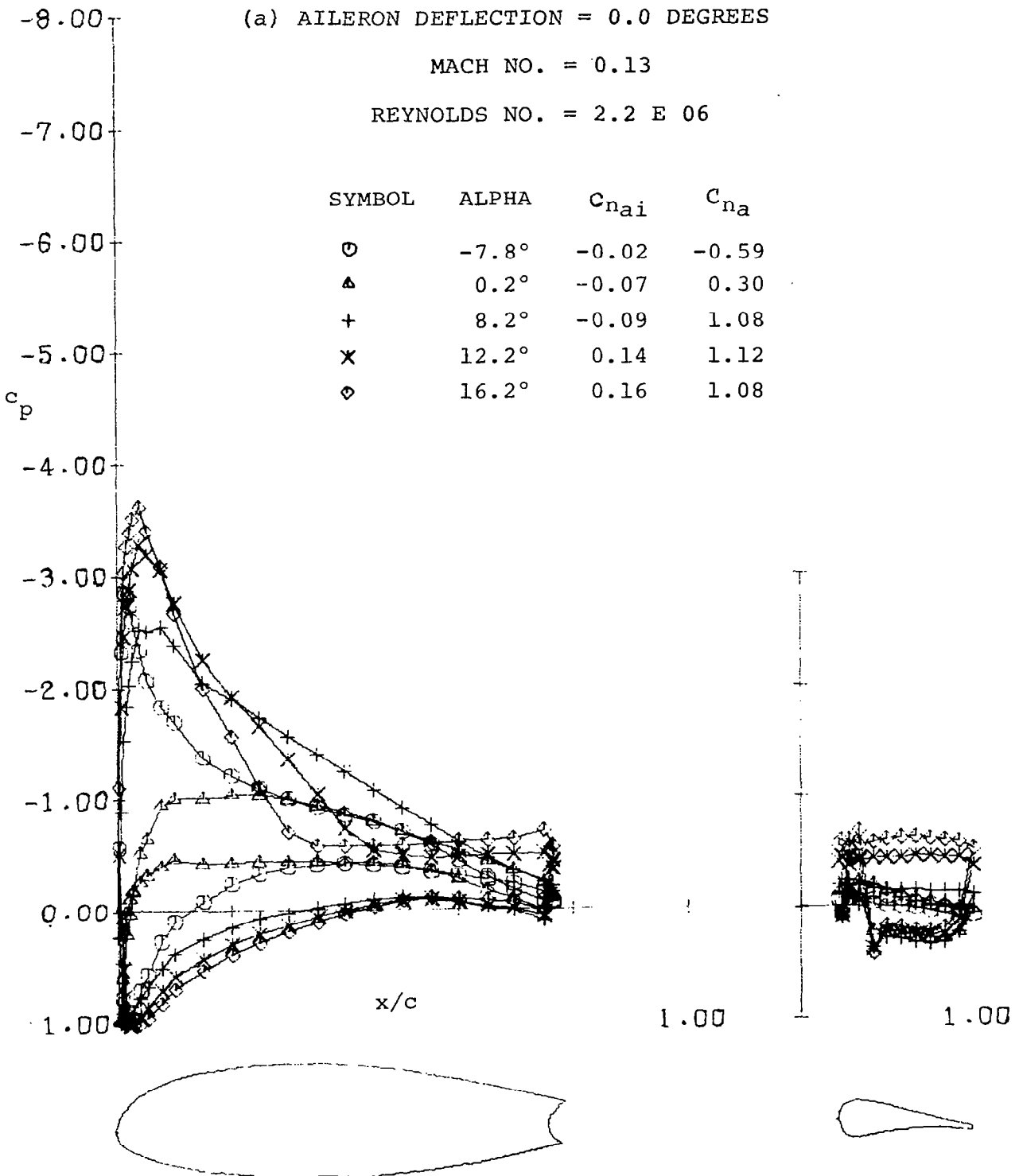


Figure 8 - Pressure Distributions with 20% Aileron.

(b) AILERON DEFLECTION = 5.0 DEGREES

MACH NO. = 0.13

REYNOLDS NO. = 2.2 E 06

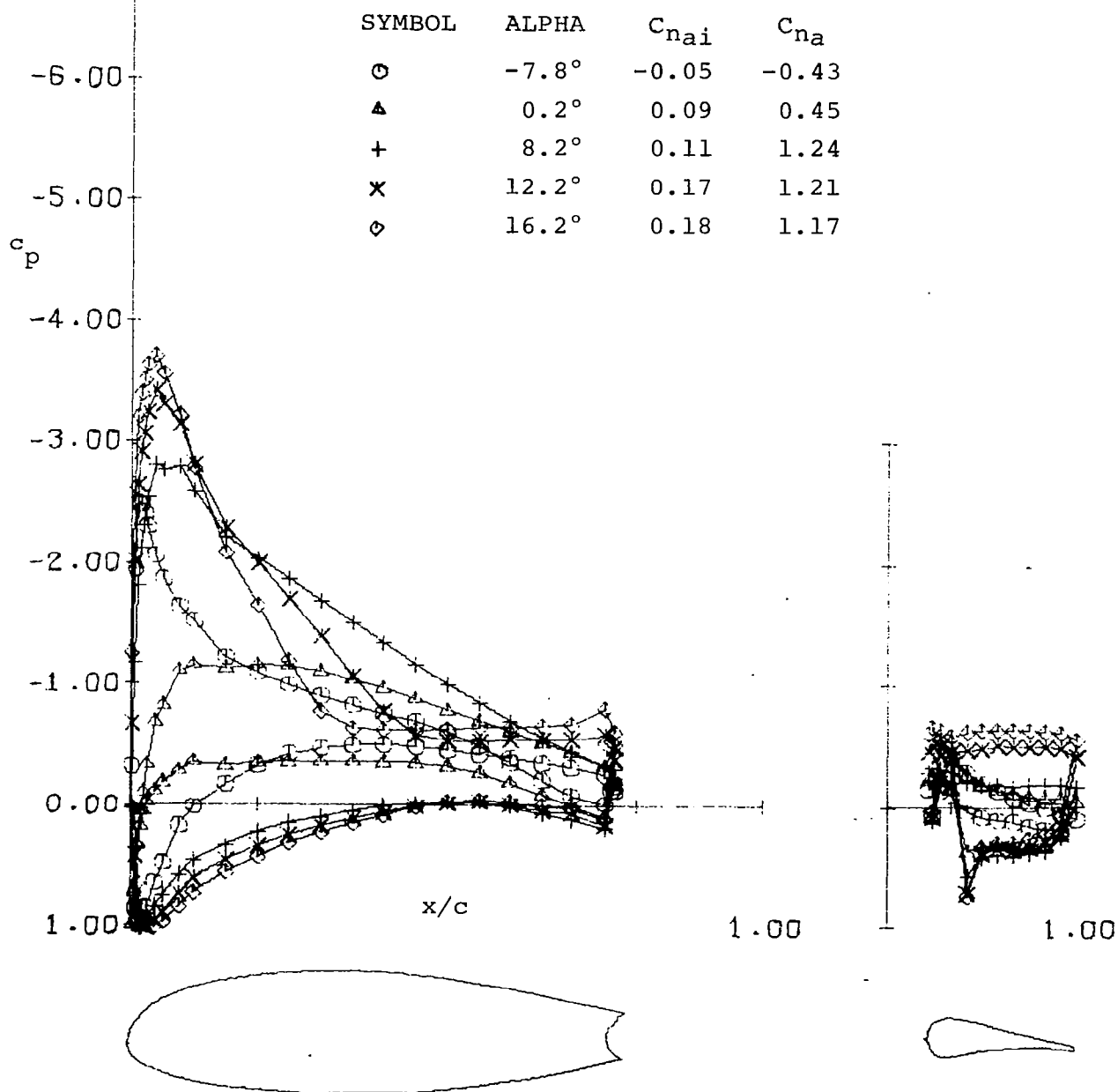


Figure 8 - Continued.

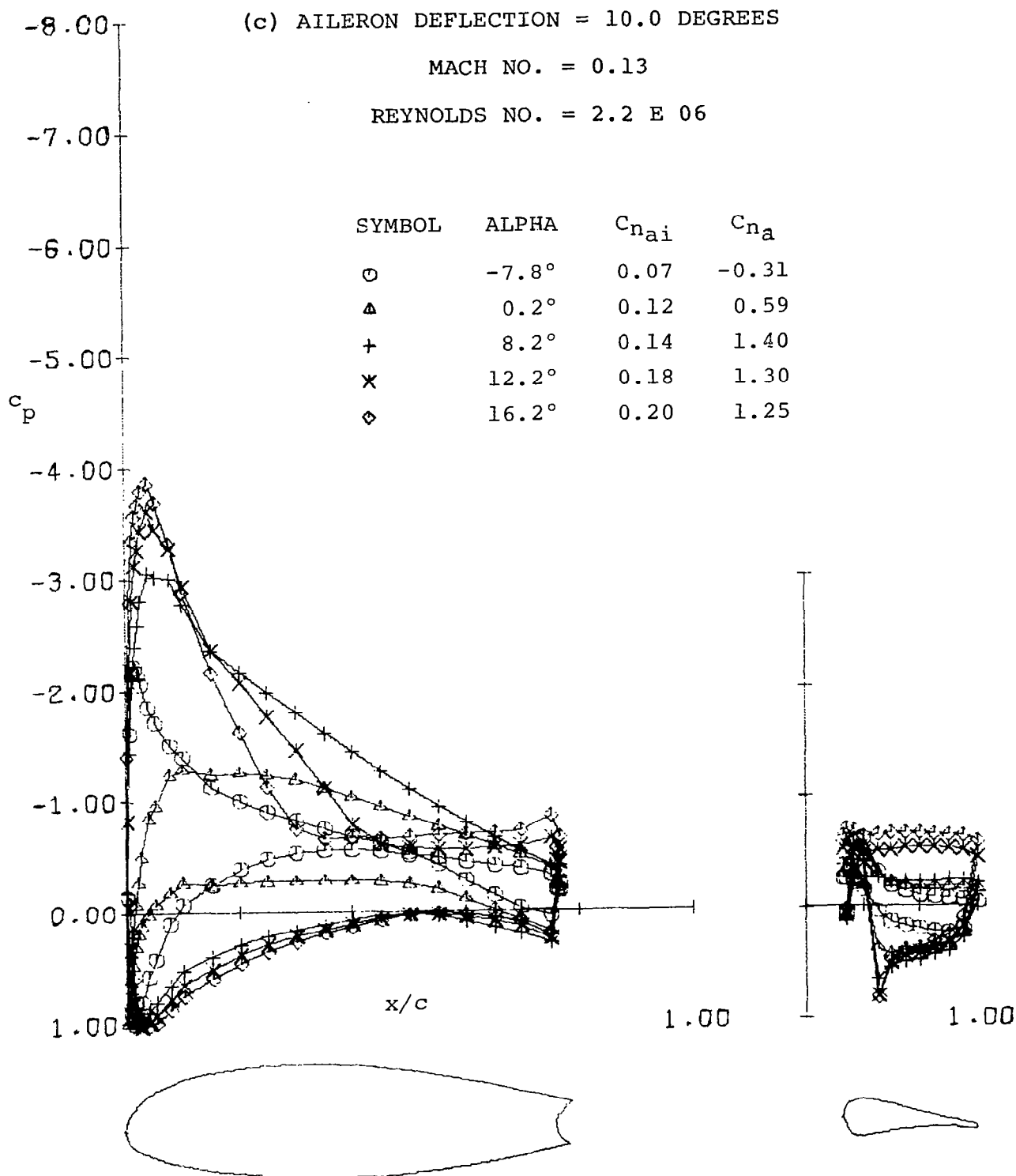


Figure 8 - Continued.

-8.00

(d) AILERON DEFLECTION = 20.0 DEGREES

MACH NO. = 0.13

REYNOLDS NO. = 2.2 E 06

-7.00

-6.00

-5.00

c_p

-4.00

-3.00

-2.00

-1.00

0.00

1.00

SYMBOL	ALPHA	$C_{n_{ai}}$	C_{n_a}
○	-7.8°	0.12	-0.11
△	0.2°	0.15	0.86
+	8.2°	0.14	0.65
×	12.2°	0.17	1.50
◇	16.2°	0.18	1.40

x/c

1.00

1.00

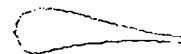
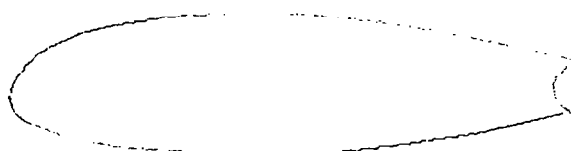


Figure 8 - Continued.

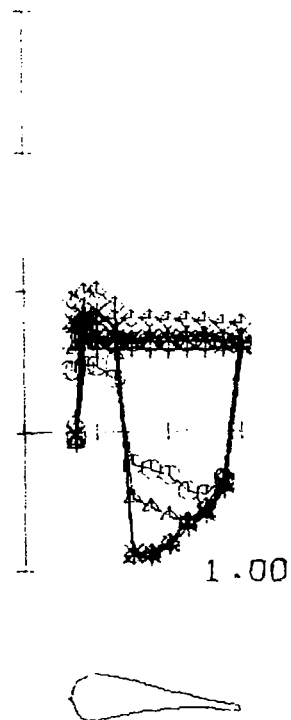
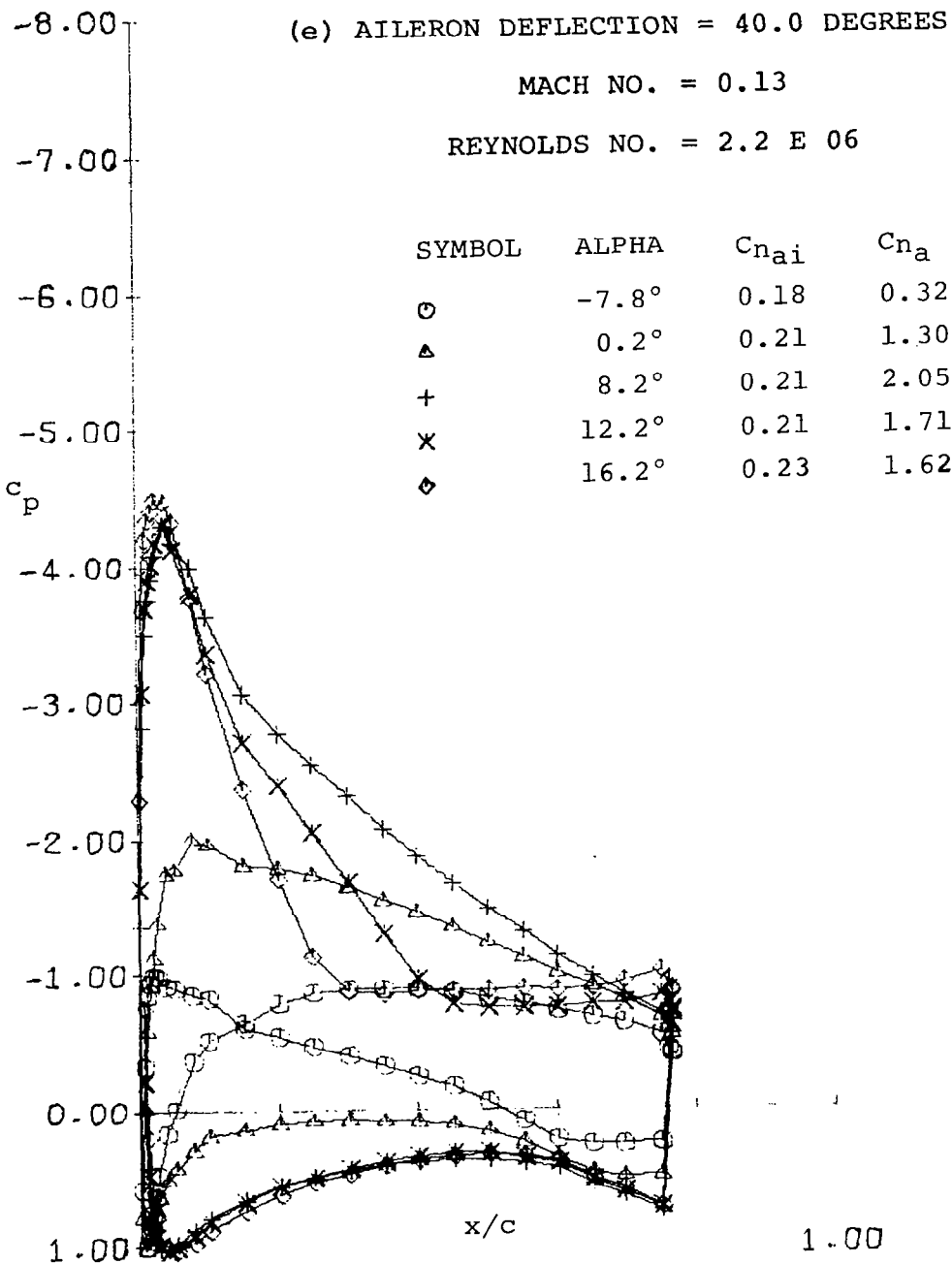


Figure 8 - Continued.

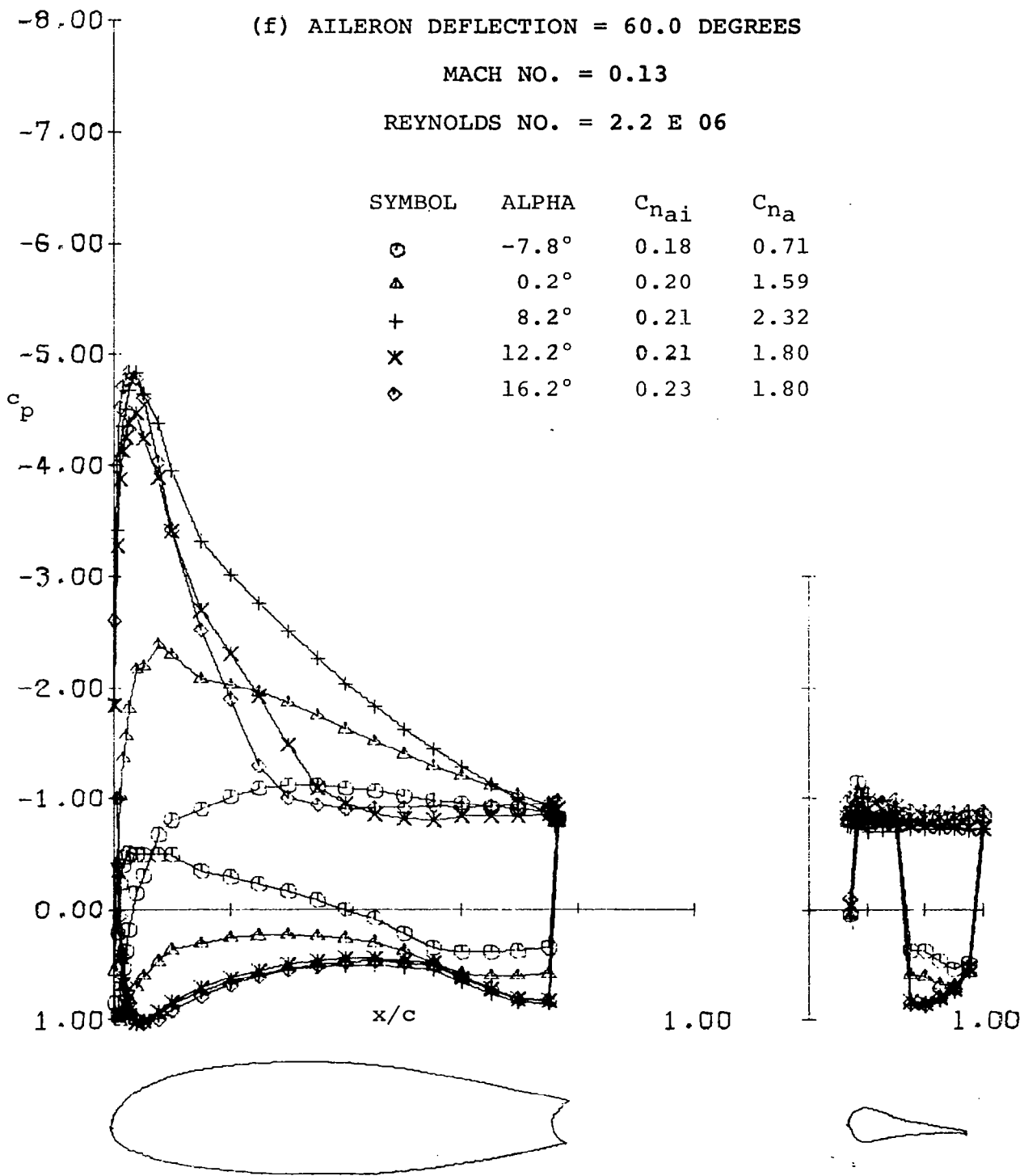


Figure 8 - Continued.

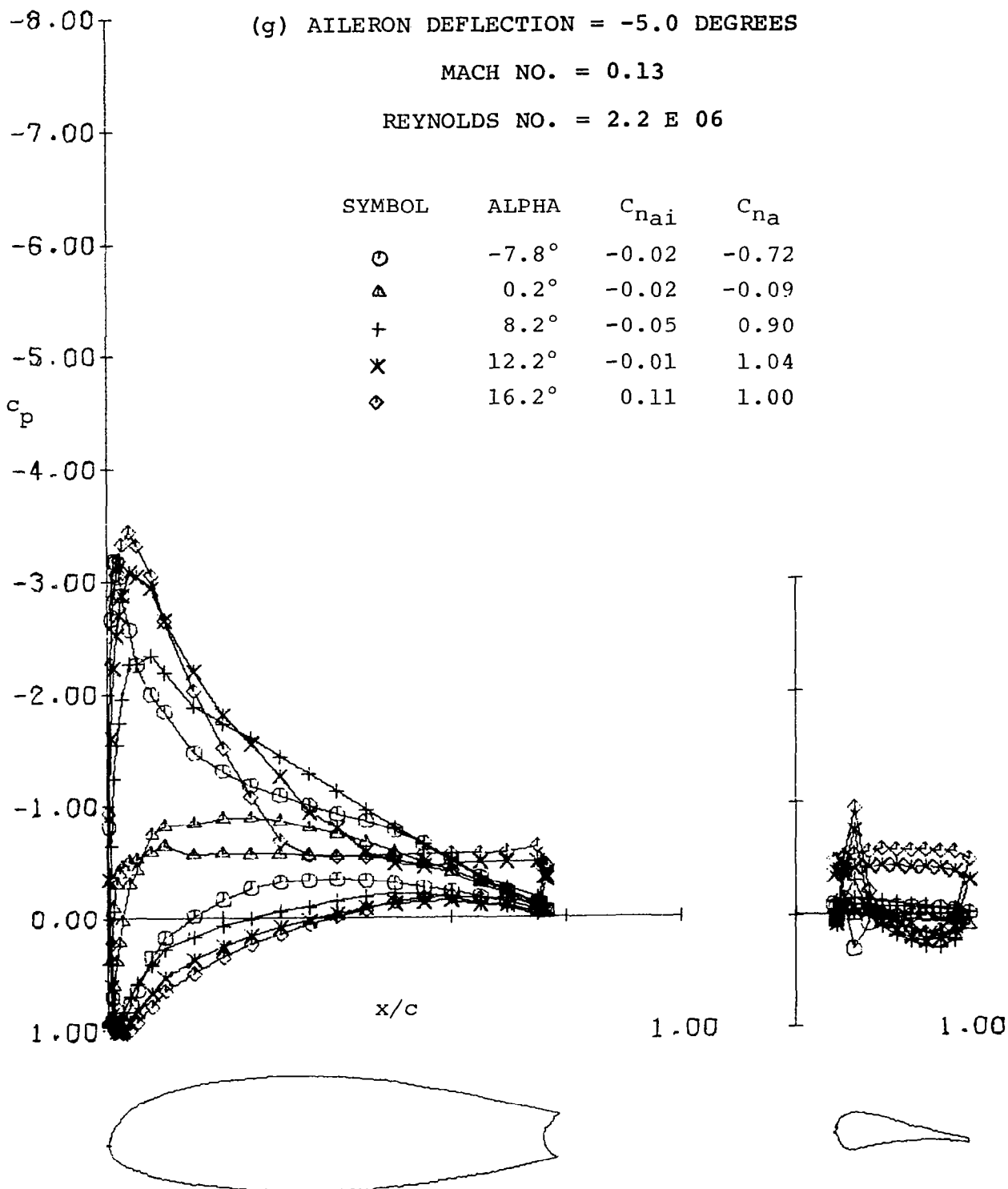


Figure 8 - Continued.

(h) AILERON DEFLECTION = -10.0 DEGREES

MACH NO. = 0.13

REYNOLDS NO. = 2.2 E 06

	SYMBOL	ALPHA	C_{nai}	C_{na}
	○	-7.8°	-0.05	-0.90
	△	0.2°	-0.03	-0.07
	+	8.2°	-0.02	0.75
	×	12.2°	-0.07	0.98
	◇	16.2°	-0.08	0.92

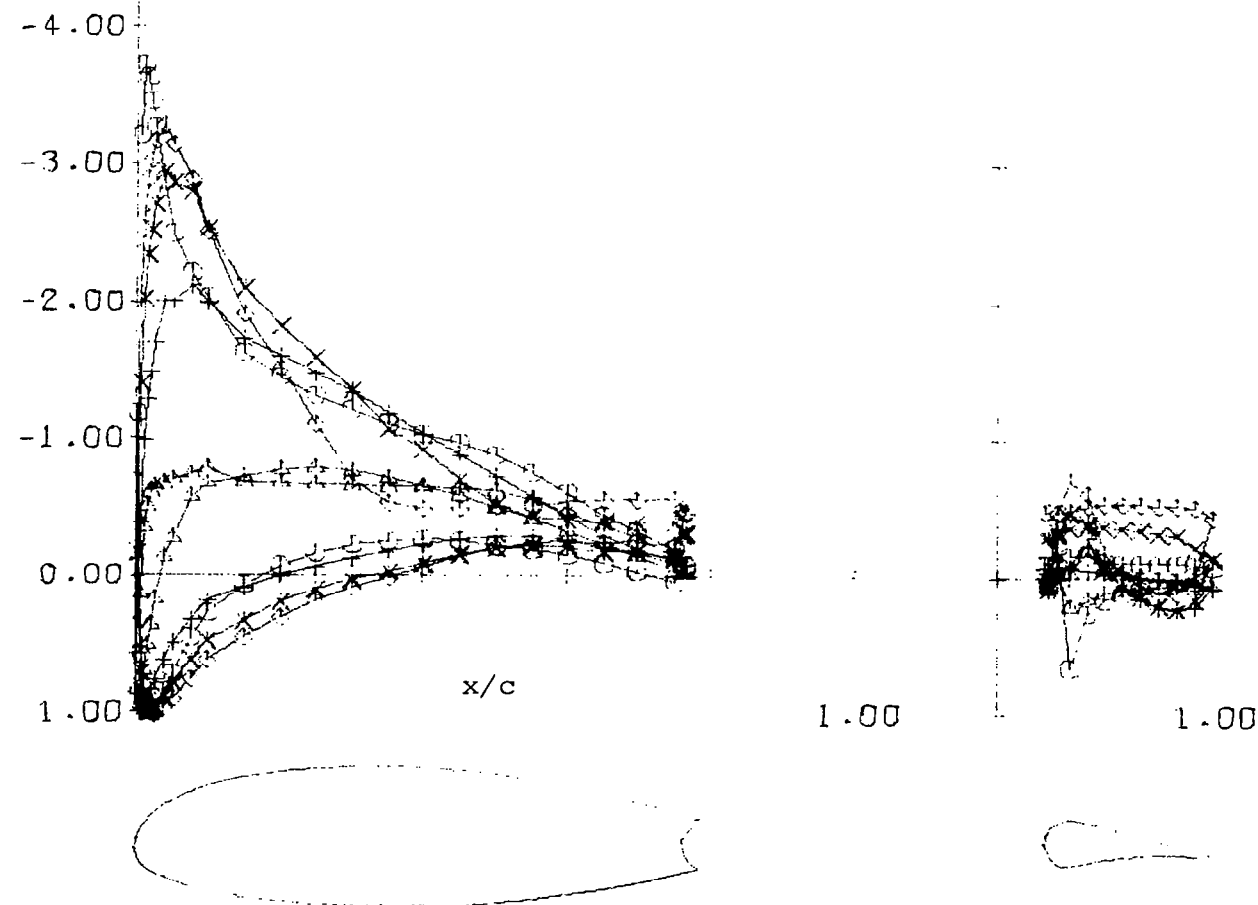


Figure 8 - Continued

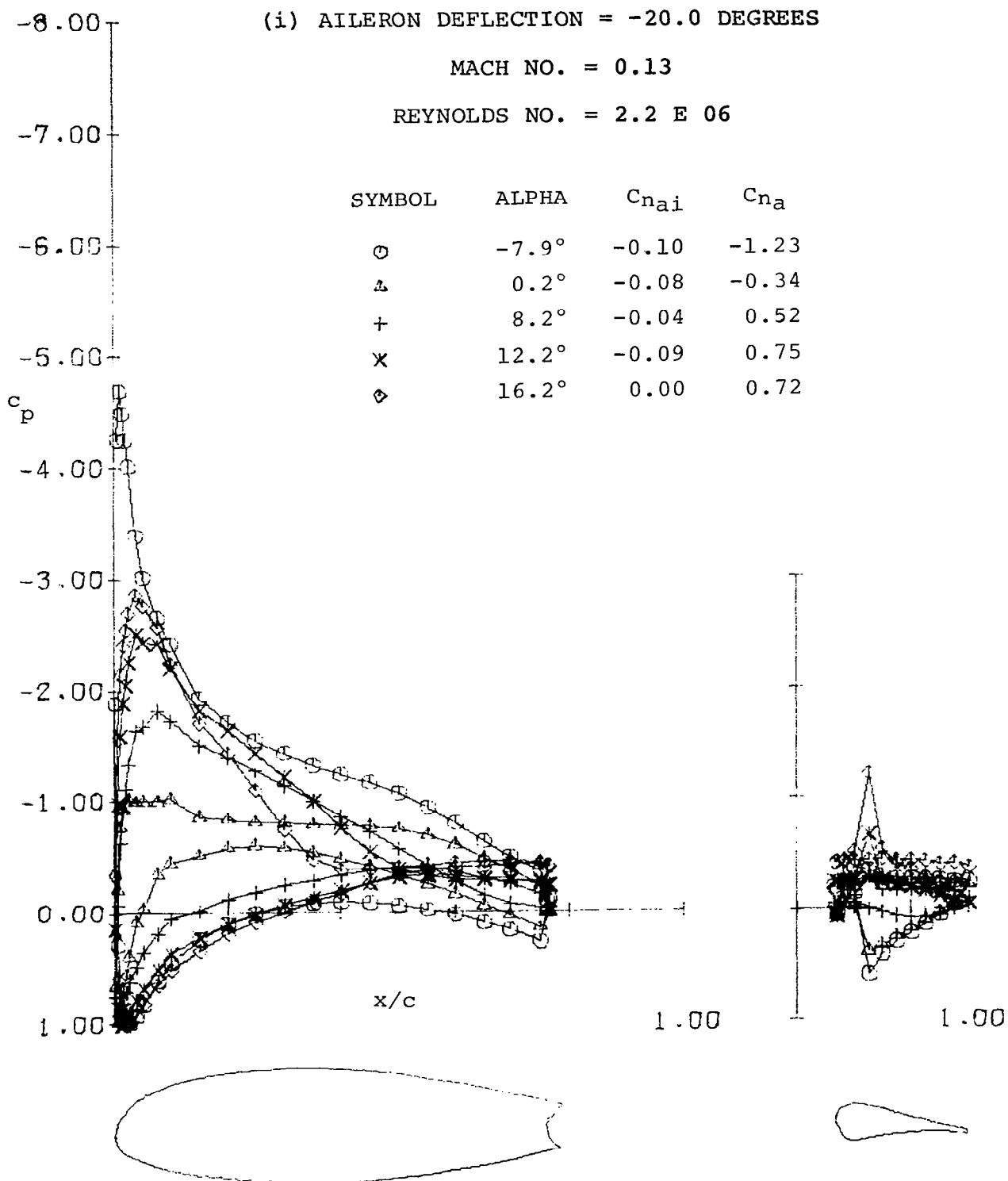


Figure 8 - Continued.

-8.00

(j) AILERON DEFLECTION = -40.0 DEGREES

MACH NO. = 0.13

REYNOLDS NO. = 2.2 E 06

-7.00

-6.00

-5.00

-4.00

-3.00

-2.00

-1.00

0.00

1.00

SYMBOL

ALPHA

C_{nai}

C_{na}

○

-7.9°

-0.18

-1.71

△

0.2°

-0.17

-0.84

+

8.2°

-0.13

0.10

x

12.2°

-0.06

0.59

◇

16.2°

-0.02

0.81

c_p

x/c

1.00

1.00

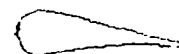


Figure 8 - Continued.

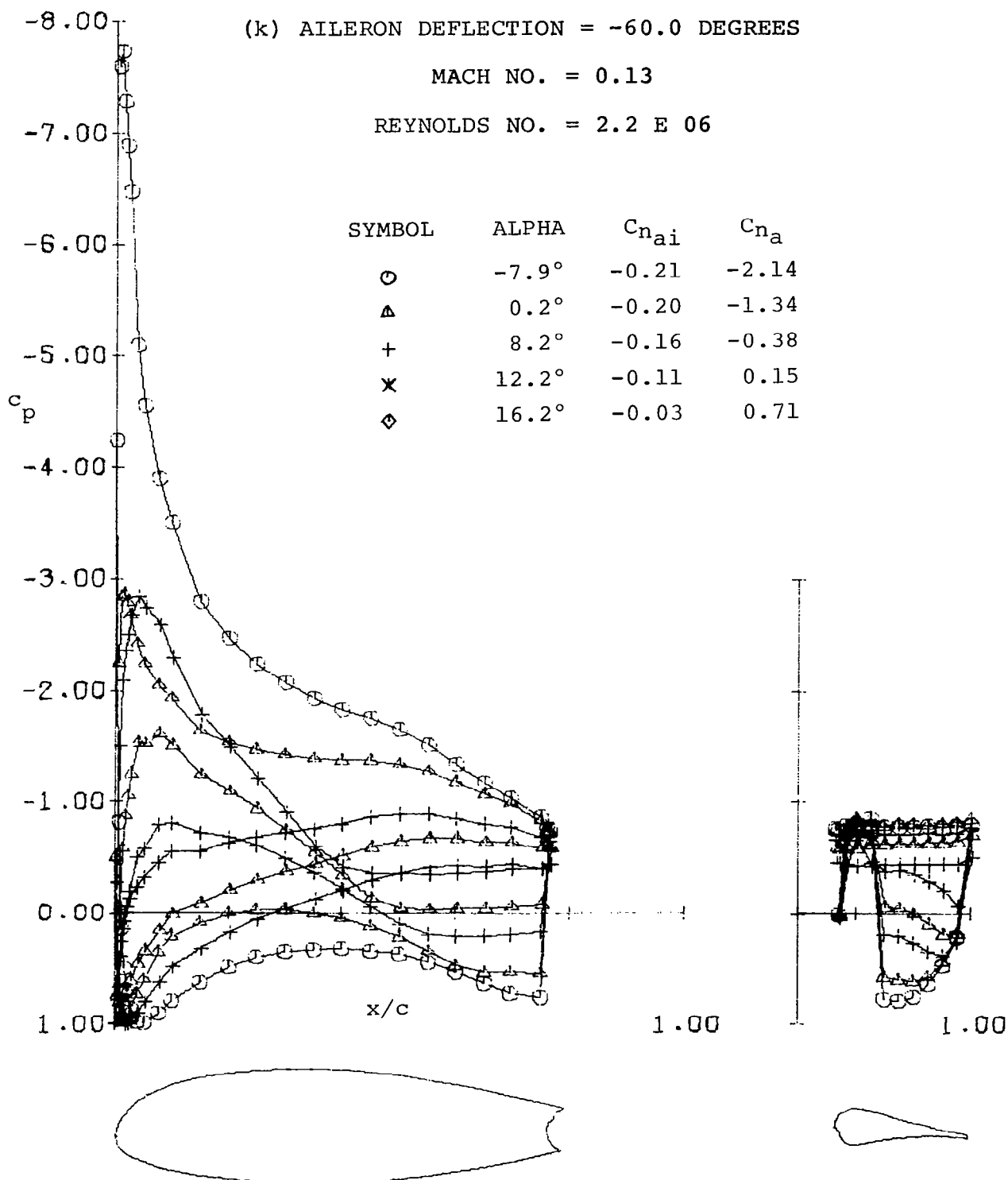
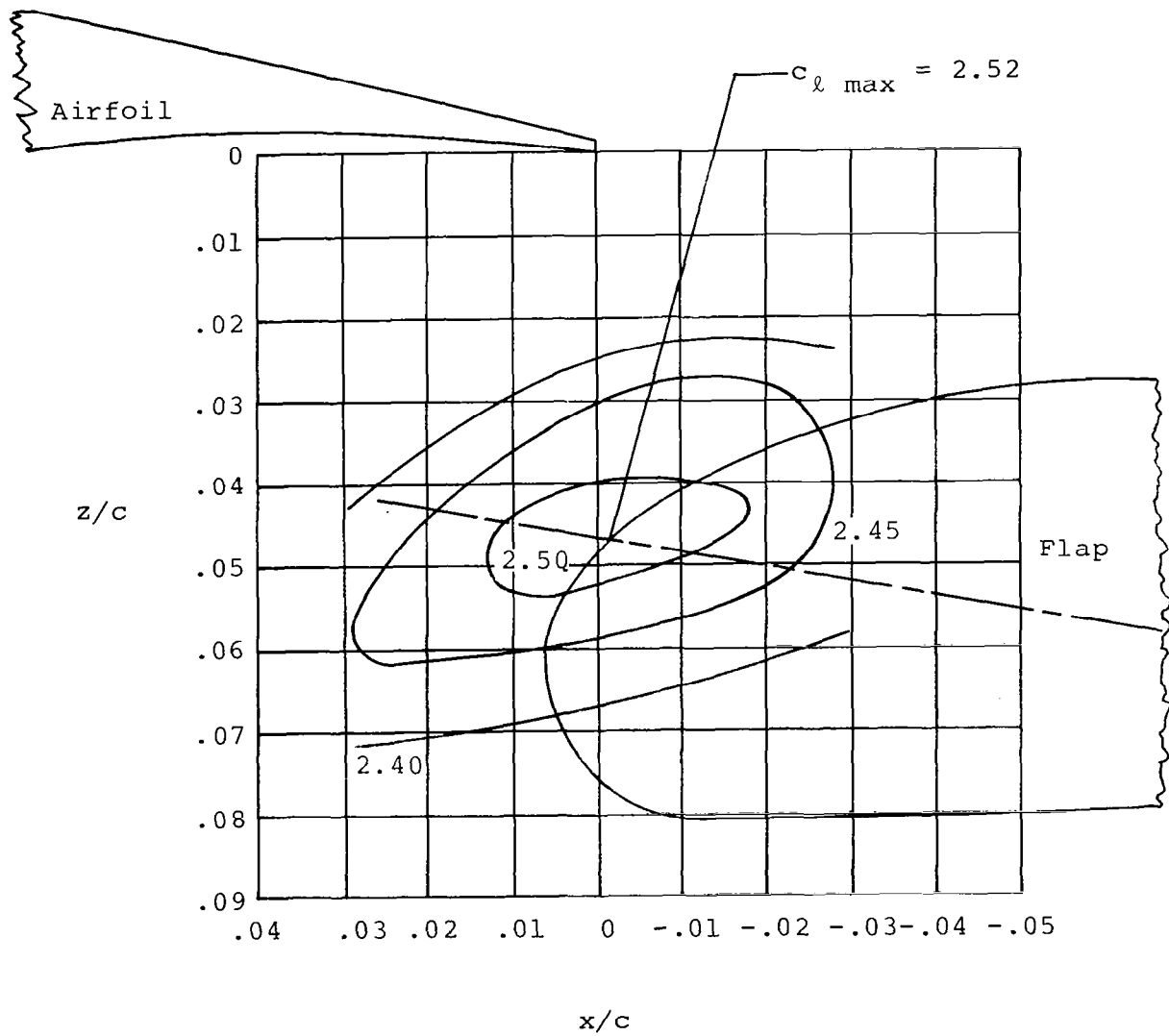


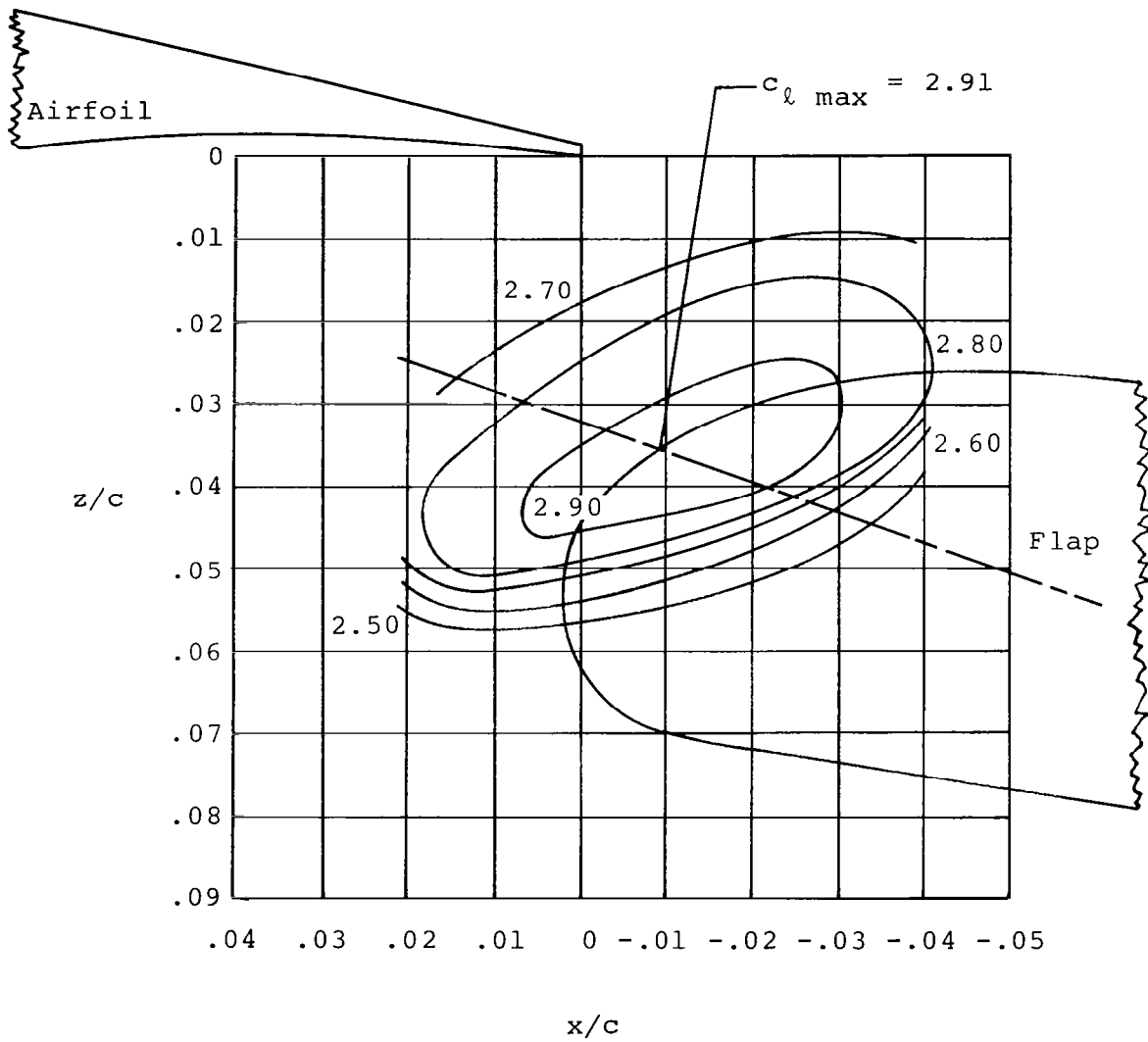
Figure 8 - Concluded.



Note: Contours are for locus of flap nose point.

(a) 10° Flap Deflection

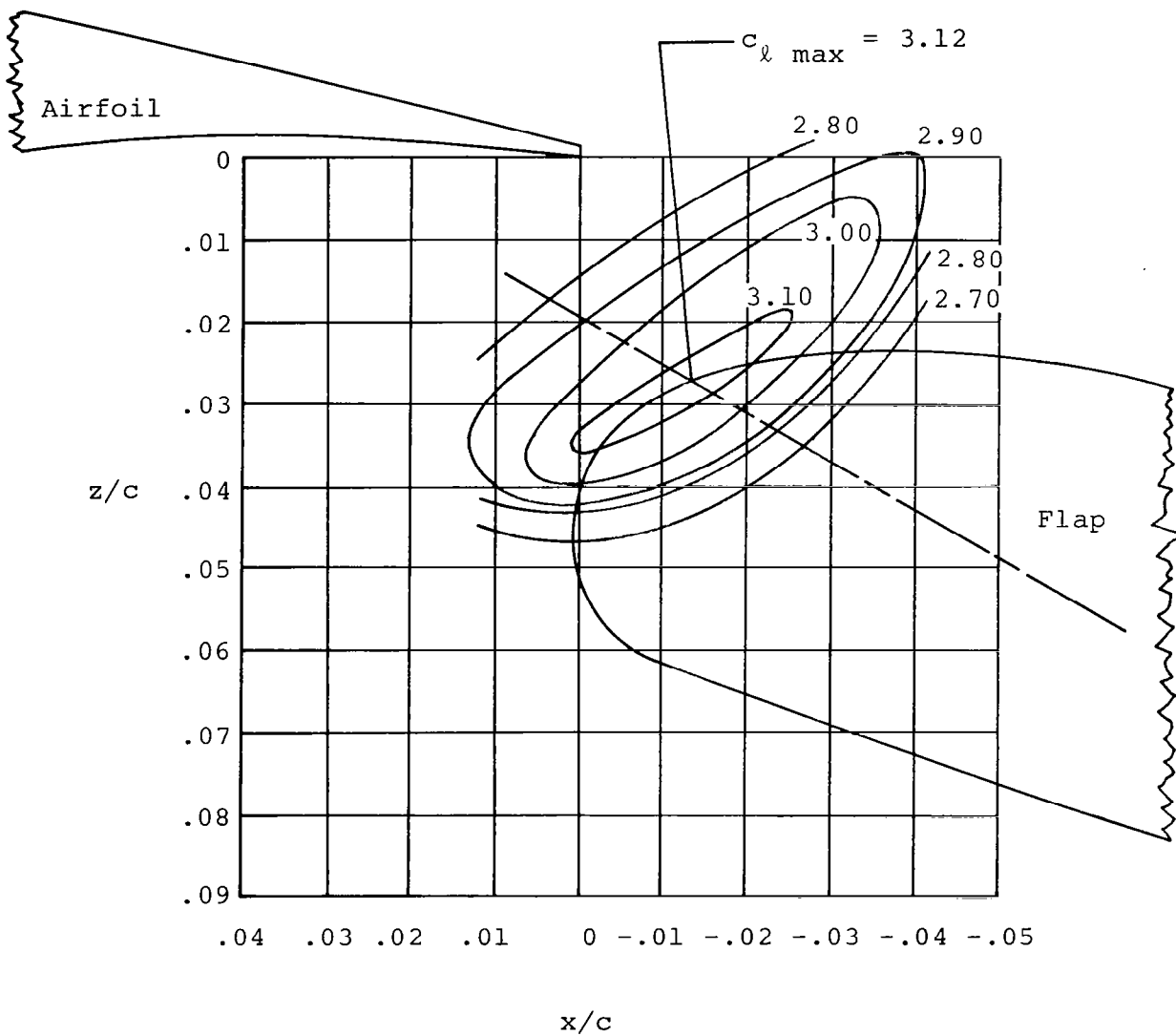
Figure 10 - $c_{l \max}$ Contours.



Note: Contours are for locus of flap nose point.

(b) 20° Flap Deflection

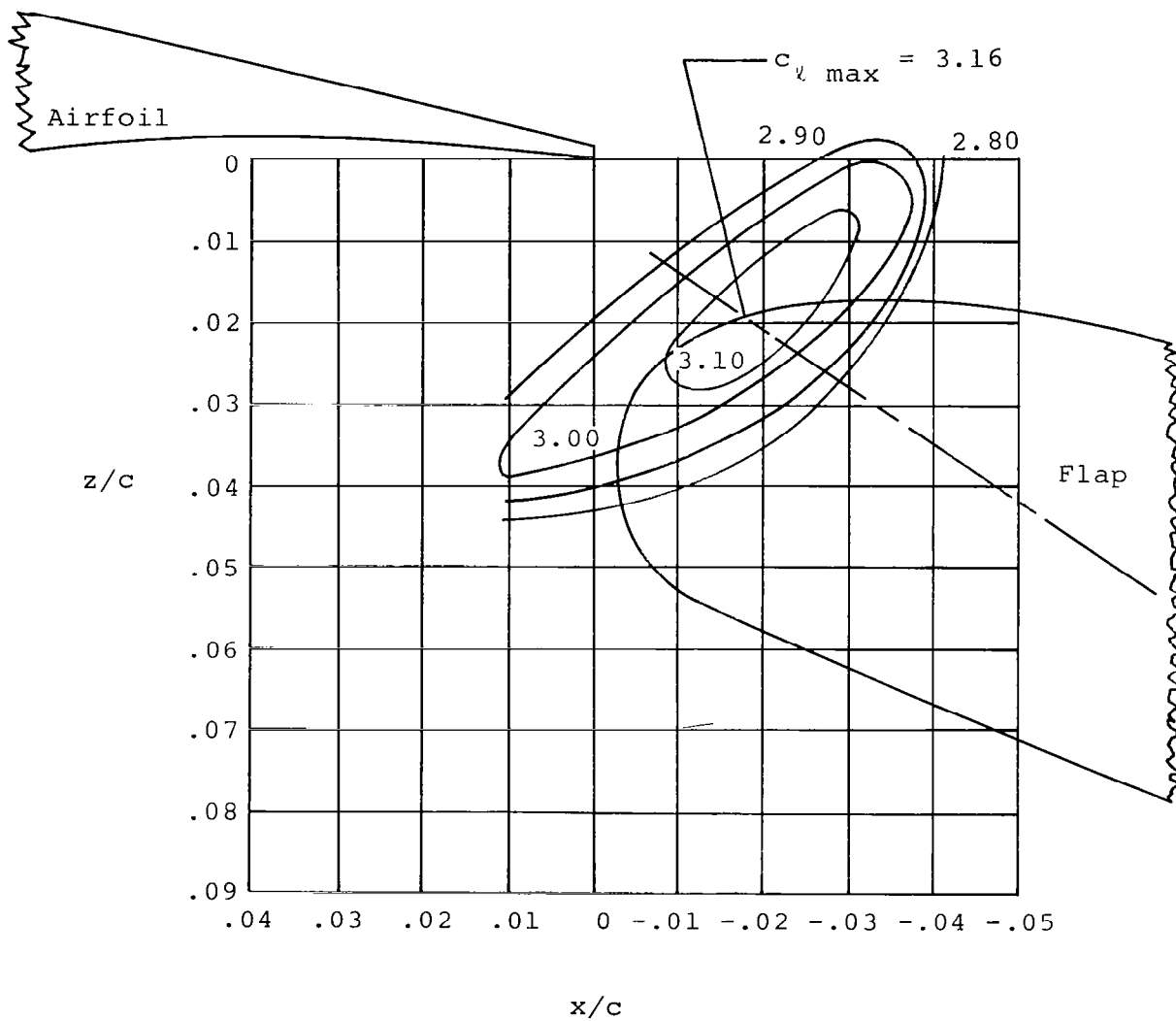
Figure 10 - Continued.



Note: Contours are for locus of flap nose point.

(c) 30° Flap Deflection

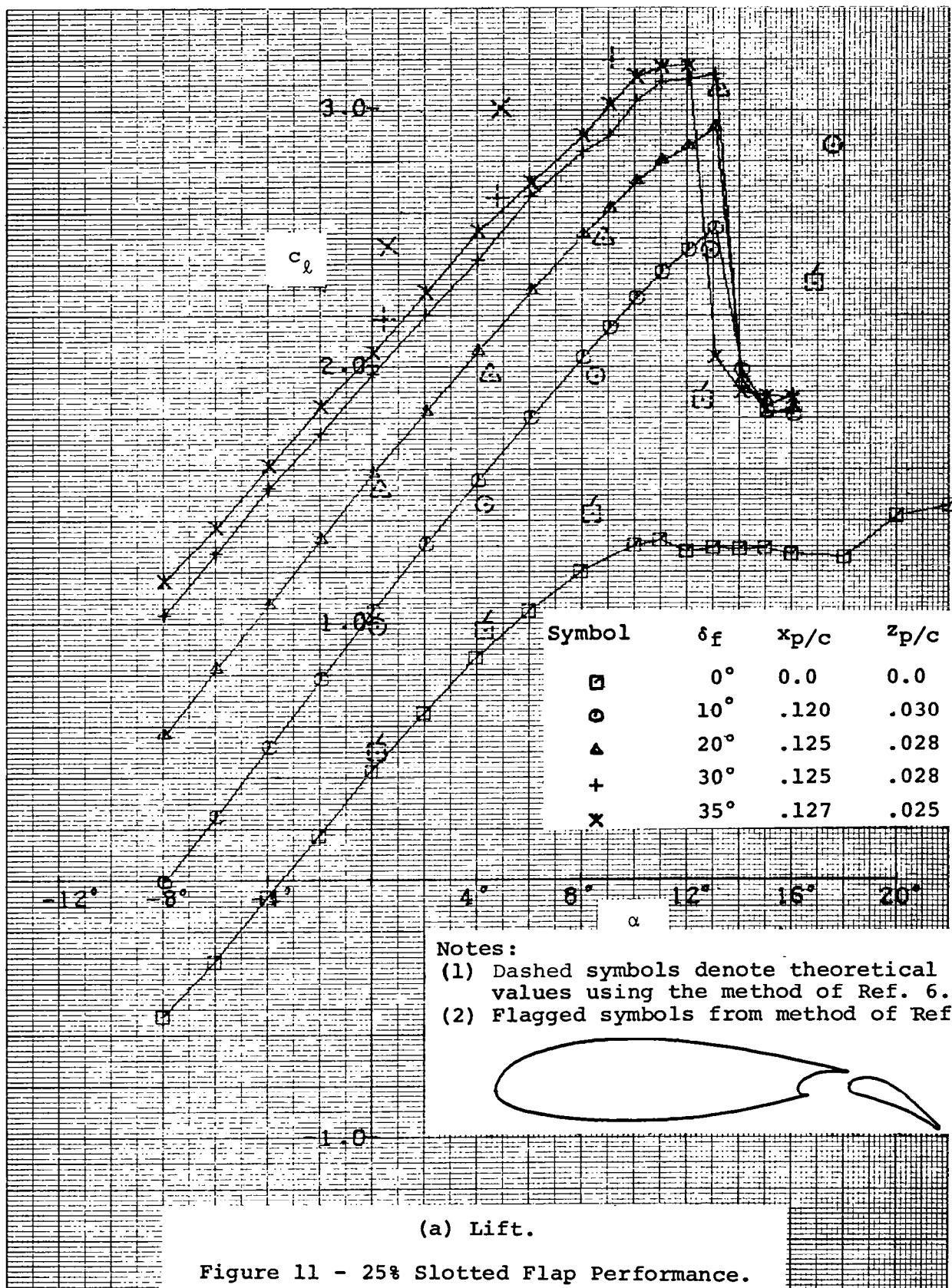
Figure 10 - Continued.



Note: Contours are for locus of flap nose point.

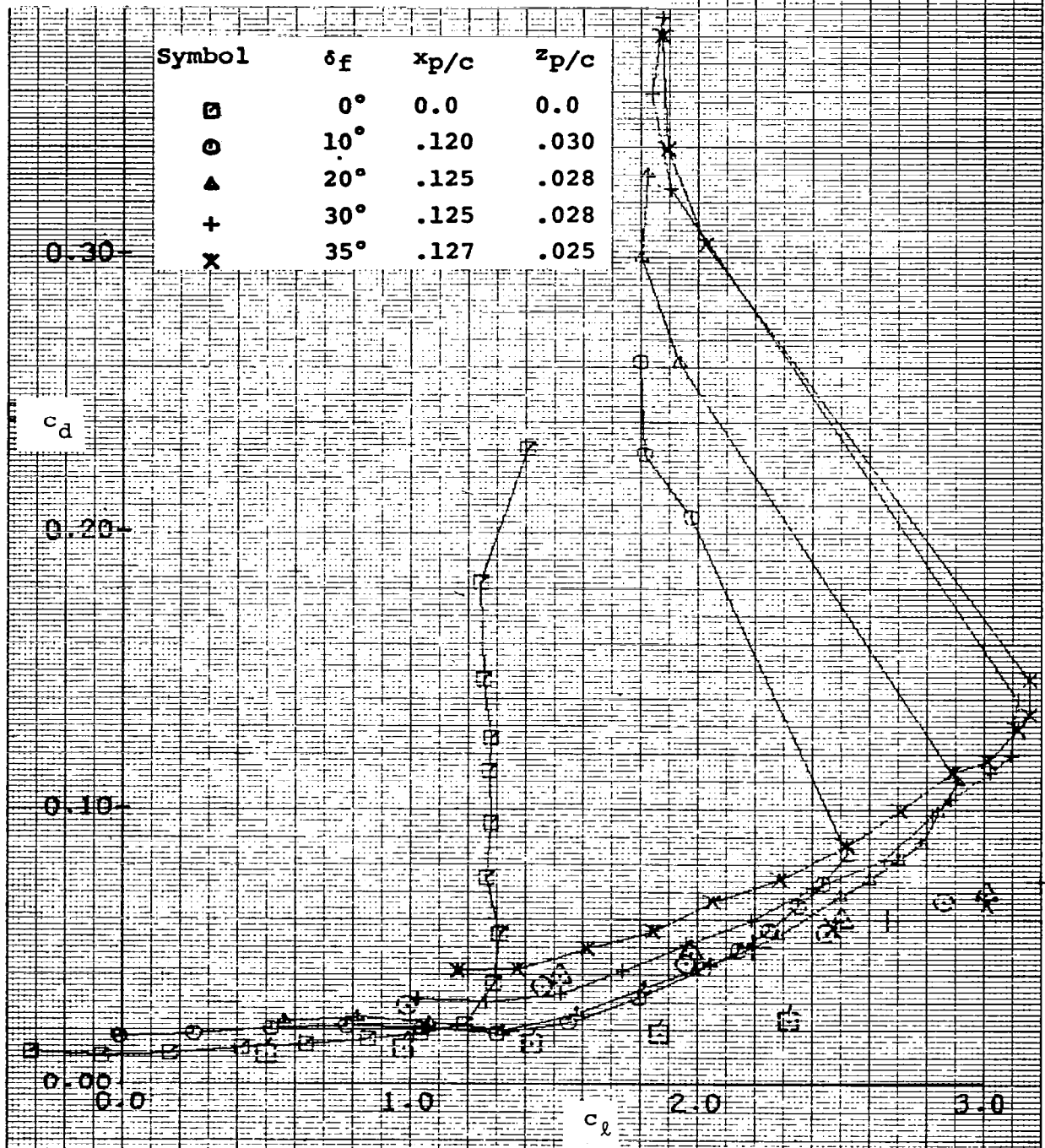
(d) 35° Flap Deflection

Figure 10 - Concluded.



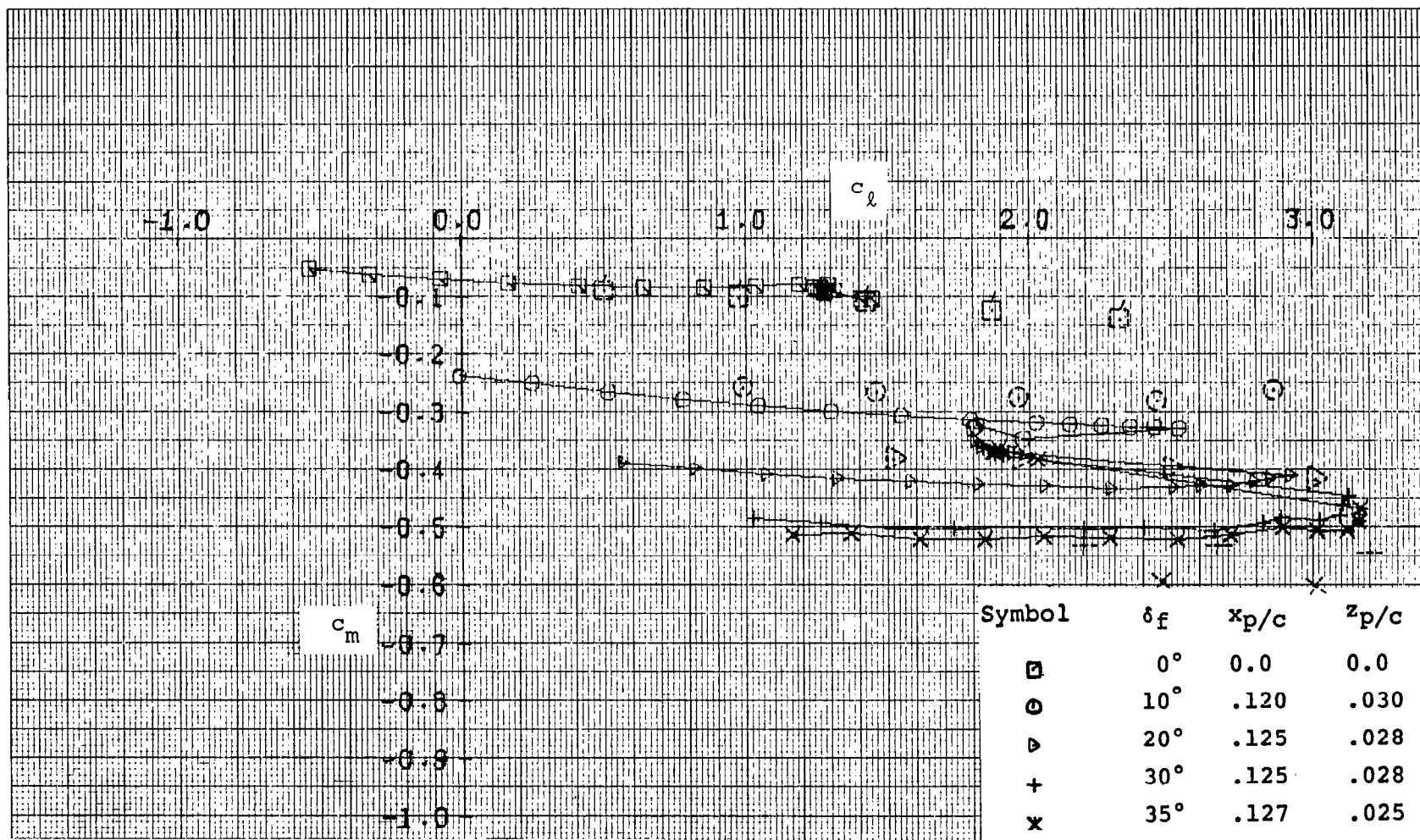
Notes:

- (1) Dashed symbols denote theoretical values using the method of Ref. 6.
- (2) Flagged symbols from method of Ref. 5.



(b) Drag.

Figure 11 - Continued.

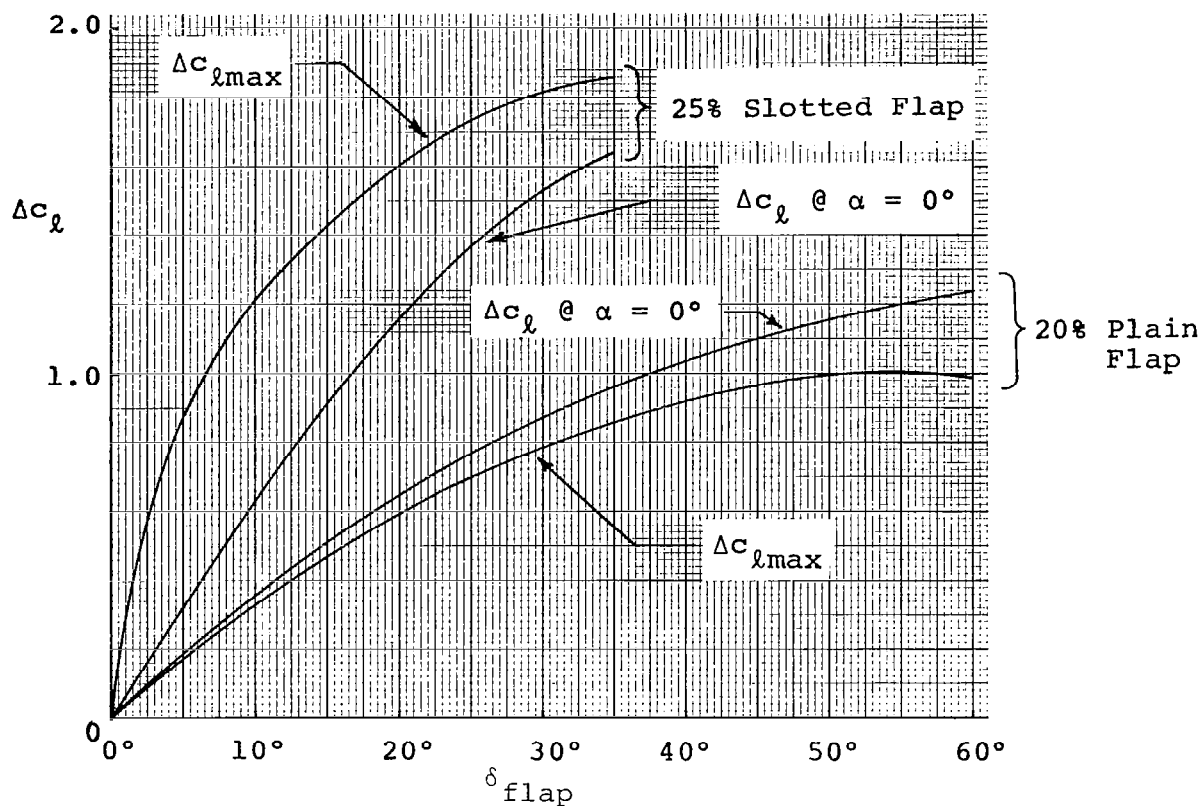


Notes:

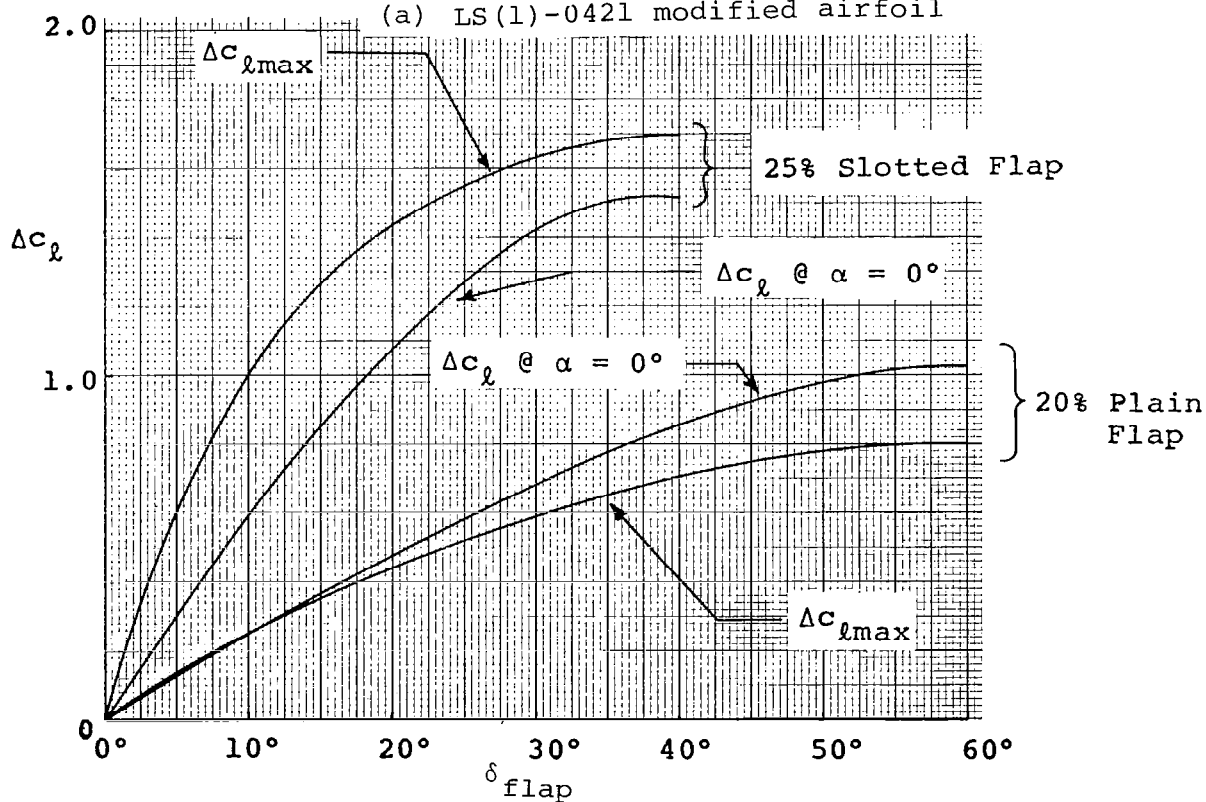
- (1) Dashed symbols denote theoretical values using the method of Ref. 6.
- (2) Flagged symbols from method of Ref. 5.

(c) Moment.

Figure 11 - Concluded.



(a) LS(1)-0421 modified airfoil



(b) GA(W)-2 Airfoil.

Figure 12 - Flap Effectiveness.

(a) FLAP DEFLECTION = 0.0 DEGREES, LOW α 'S

-8.00--

MACH NO. = 0.13

REYNOLDS NO. = 2.2 E 06

-7.00--

SYMBOL	ALPHA	C_{n_a}	C_{n_f}
O	-7.9°	-.54	.01
Δ	-3.9°	-.12	.05
+	0.2°	.36	.07
×	4.3°	.80	.08
◇	8.3°	1.12	..09

-6.00--

-5.00--

C_p

-4.00--

-3.00--

-2.00--

-1.00--

0.00--

1.00--

x/c

1.00

Figure 13 - Pressure Distributions with 25% Slotted Flap.

(b) FLAP DEFLECTION = 0.0 DEGREES, HIGH α 'S
 -8.00-

MACH NO. = 0.13

REYNOLDS NO. = 2.2 E 06

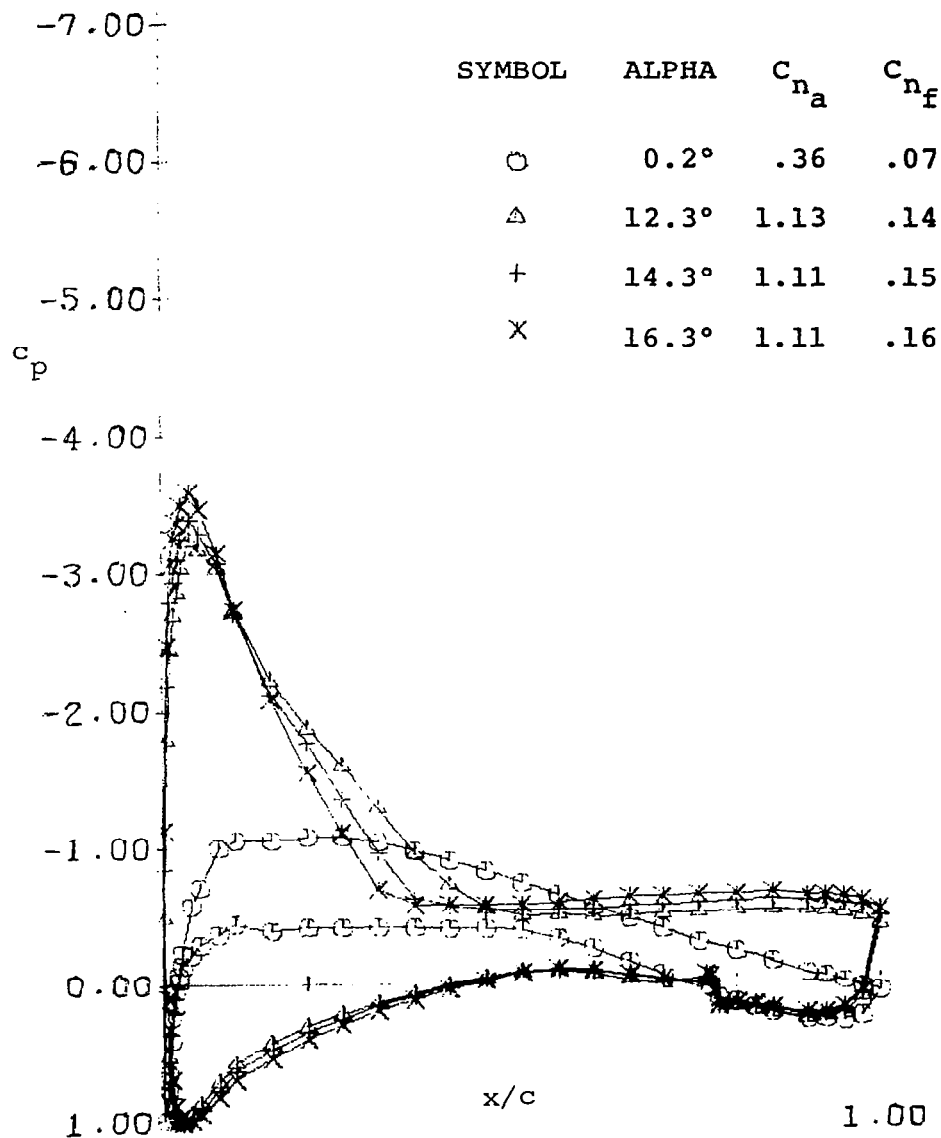


Figure 13 - Continued.

-8.00 (c) FLAP DEFLECTION = 10.0 DEGREES, LOW α 'S

MACH NO. = 0.13

REYNOLDS NO. = 2.2 E 06

-7.00

	SYMBOL	ALPHA	C_{n_a}	C_{m_a}	C_{n_f}	C_{m_f}
-6.00	○	-8.0°	-.26	.00	.25	-.17
	△	-3.9°	.23	-.12	.28	-.18
-5.00	+	0.2°	.76	-.26	.31	-.18
C_p	×	4.2°	1.27	-.40	.32	-.19
	◇	8.3°	1.76	-.53	.33	-.19

-4.00

-3.00

-2.00

-1.00

0.00

1.00

x/c

1.00

1.00

Figure 13 - Continued.

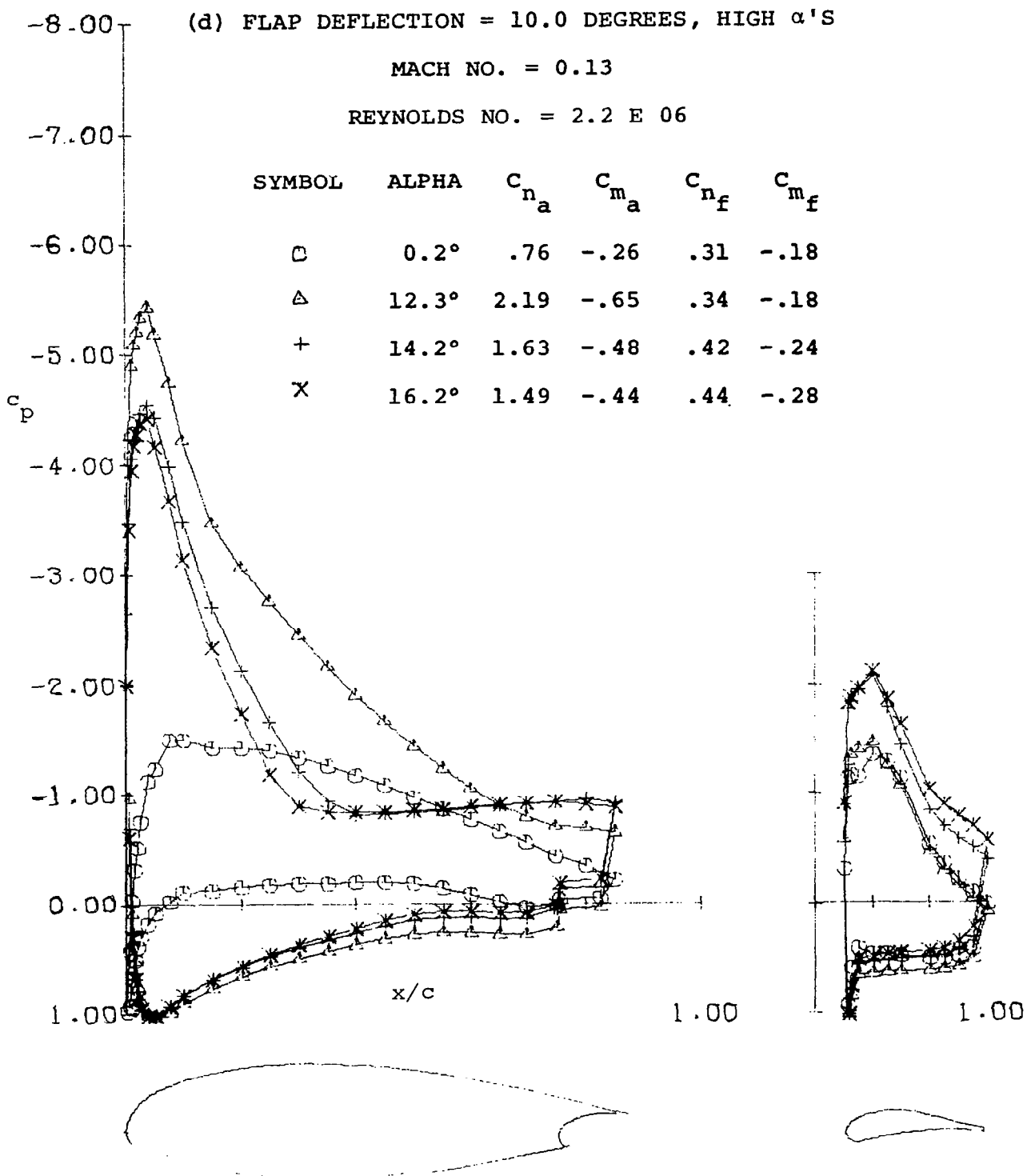


Figure 13 - Continued.

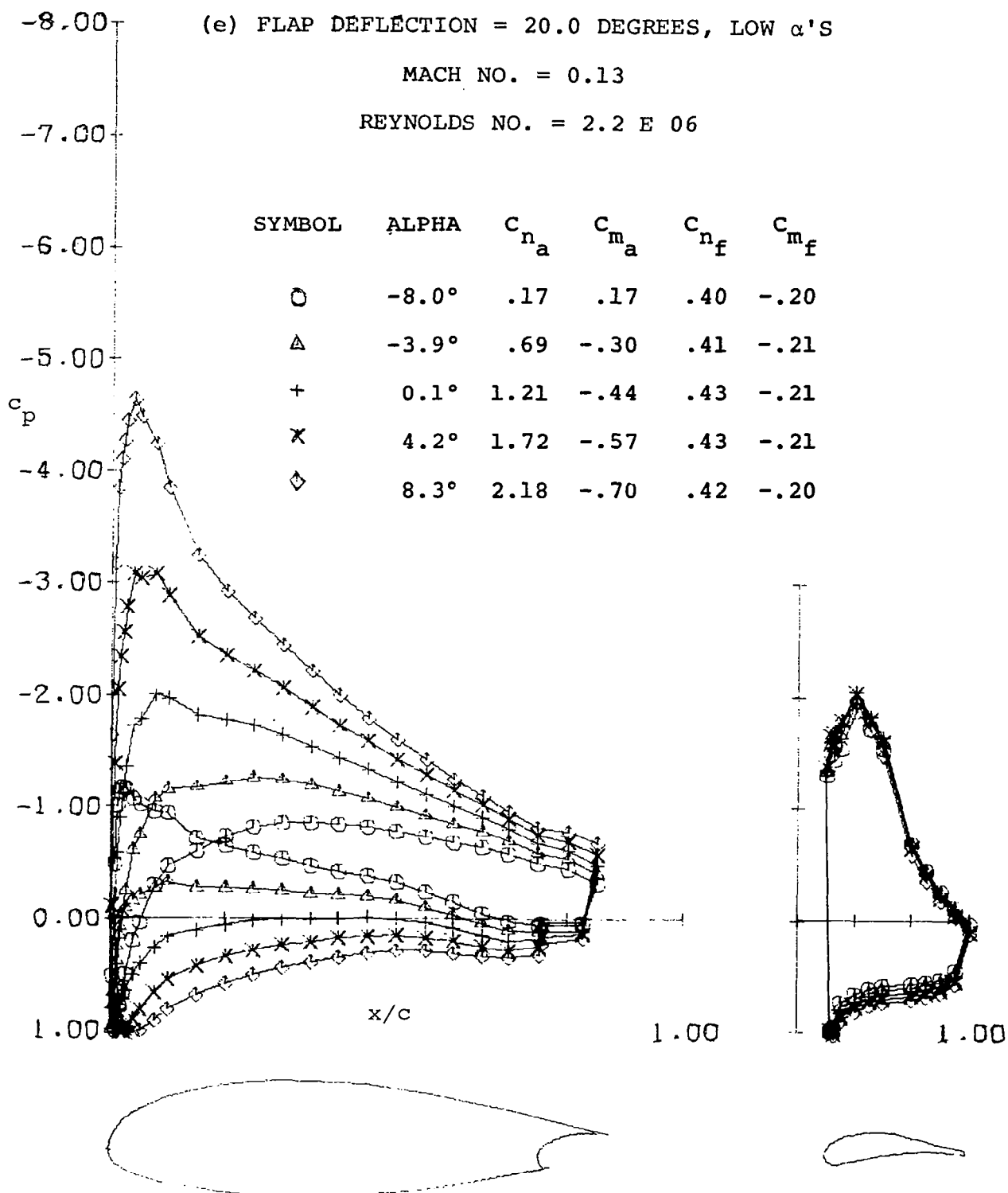


Figure 13 - Continued.

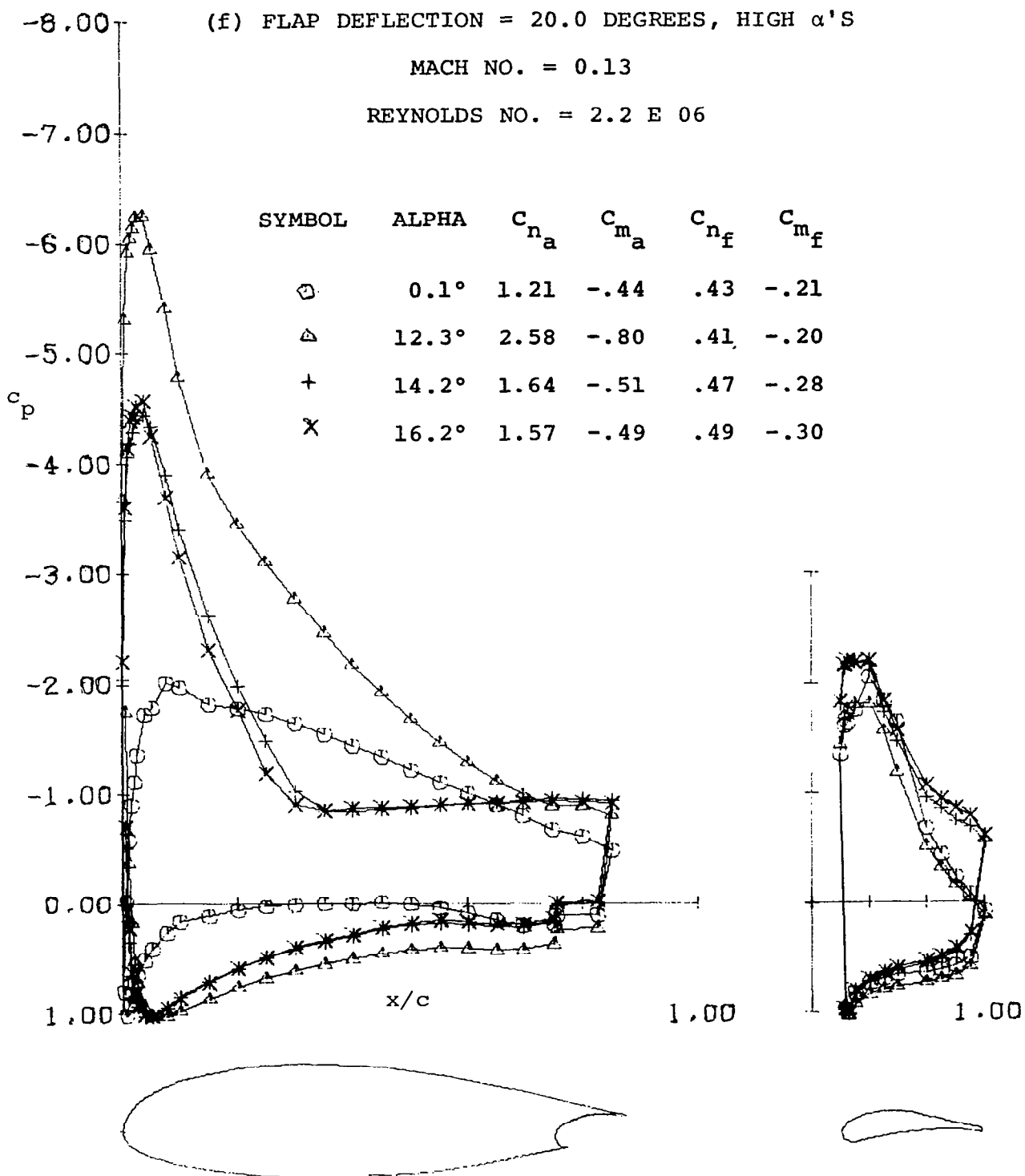


Figure 13 - Continued.

-8.00--

(g) FLAP DEFLECTION = 30.0 DEGREES, LOW α 's

MACH NO. = 0.13

REYNOLDS NO. = 2.2 E 06

-7.00--

	SYMBOL	ALPHA	C_{n_a}	C_{m_a}	C_{n_f}	C_{m_f}
-6.00--	C	-8.0°	.58	-.32	.49	-.21
	Δ	-3.9°	1.10	-.46	.49	-.21
-5.00--	+	0.2°	1.59	-.59	.46	-.21
c_p	X	4.2°	2.08	-.72	.47	-.20
-4.00--	\diamond	8.3°	2.53	-.84	.47	-.19

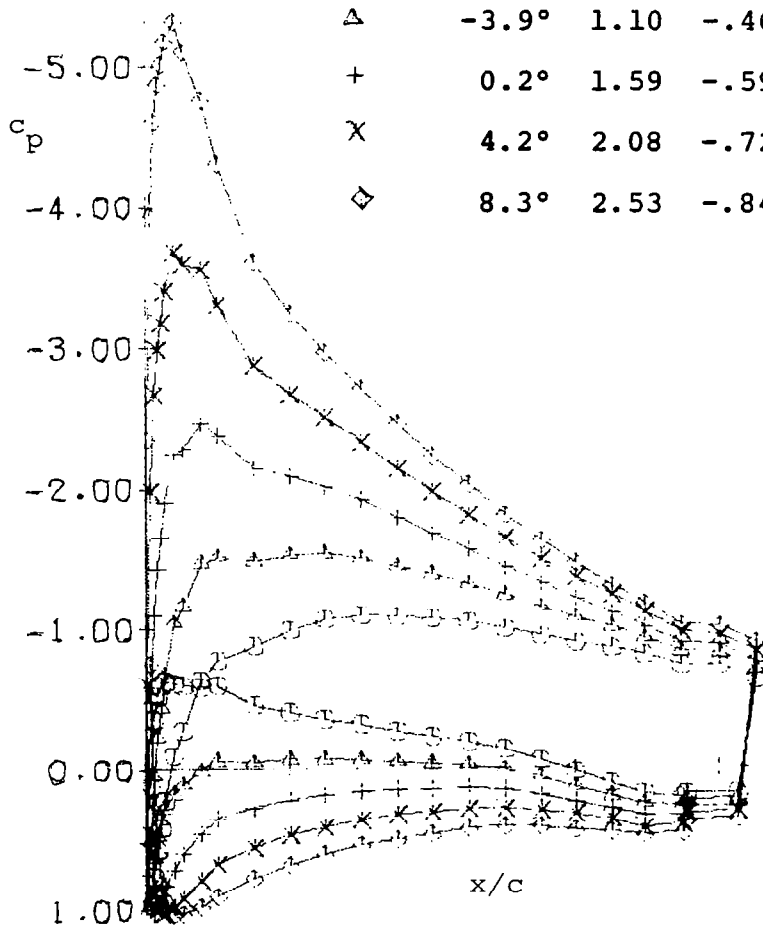


Figure 13 - Continued.

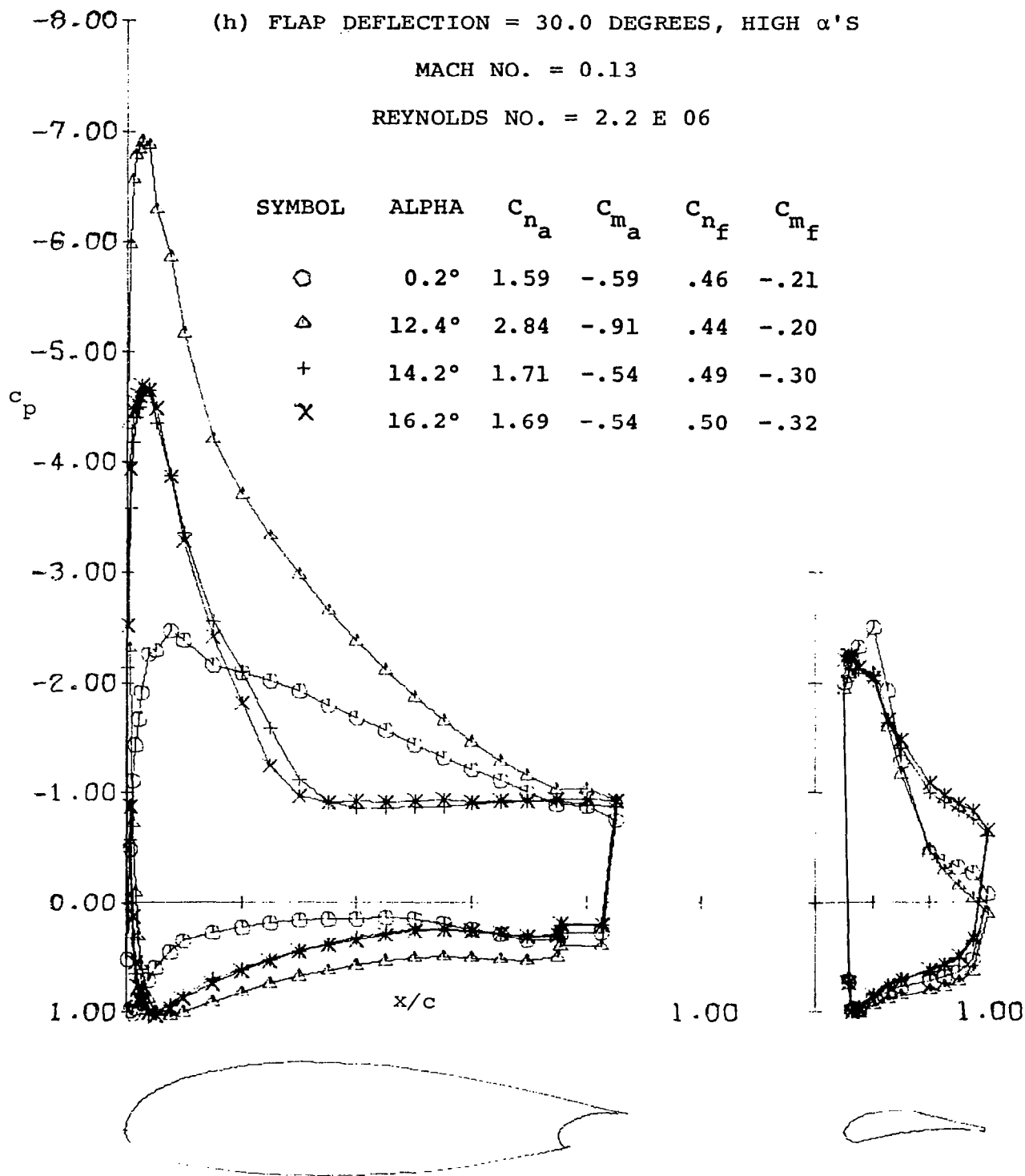


Figure 13 - Continued.

-8.00-

(i) FLAP DEFLECTION = 35.0 DEGREES, LOW α 'S

MACH NO. = 0.13

REYNOLDS NO. = 2.2 E 06

-7.00-

SYMBOL	ALPHA	C_{n_a}	C_{m_a}	C_{n_f}	C_{m_f}
○	-8.0°	.76	-.39	.47	-.22
△	-3.9°	1.25	-.52	.45	-.21
+	0.2°	1.76	-.66	.46	-.21
×	4.2°	2.23	-.78	.44	-.20
◇	8.3°	2.69	-.91	.45	-.20

-6.00-

C_p

-5.00-

-4.00-

-3.00-

-2.00-

-1.00-

0.00

1.00

x/c

1.00

1.00

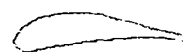


Figure 13 - Continued.

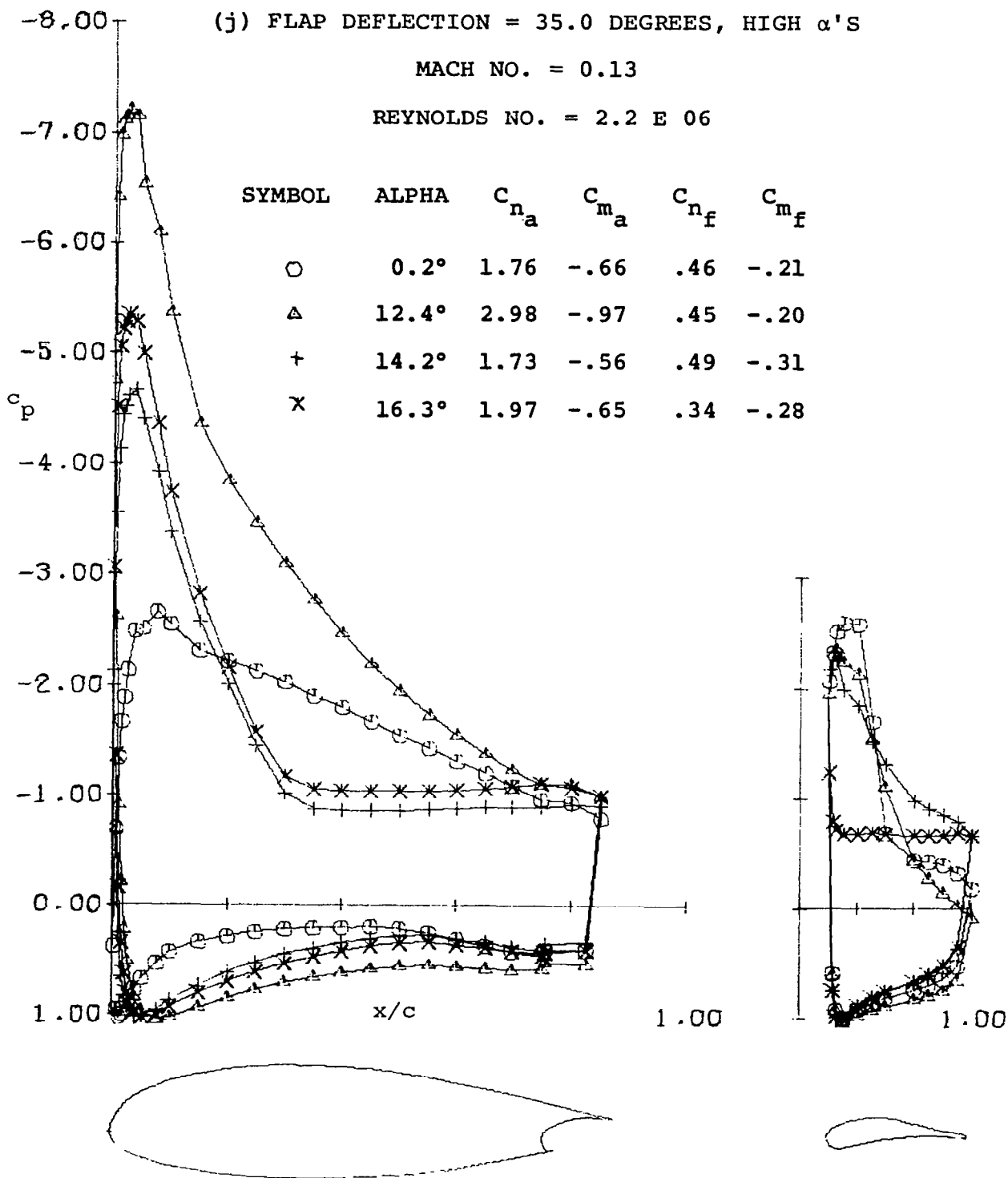


Figure 13 - Concluded.

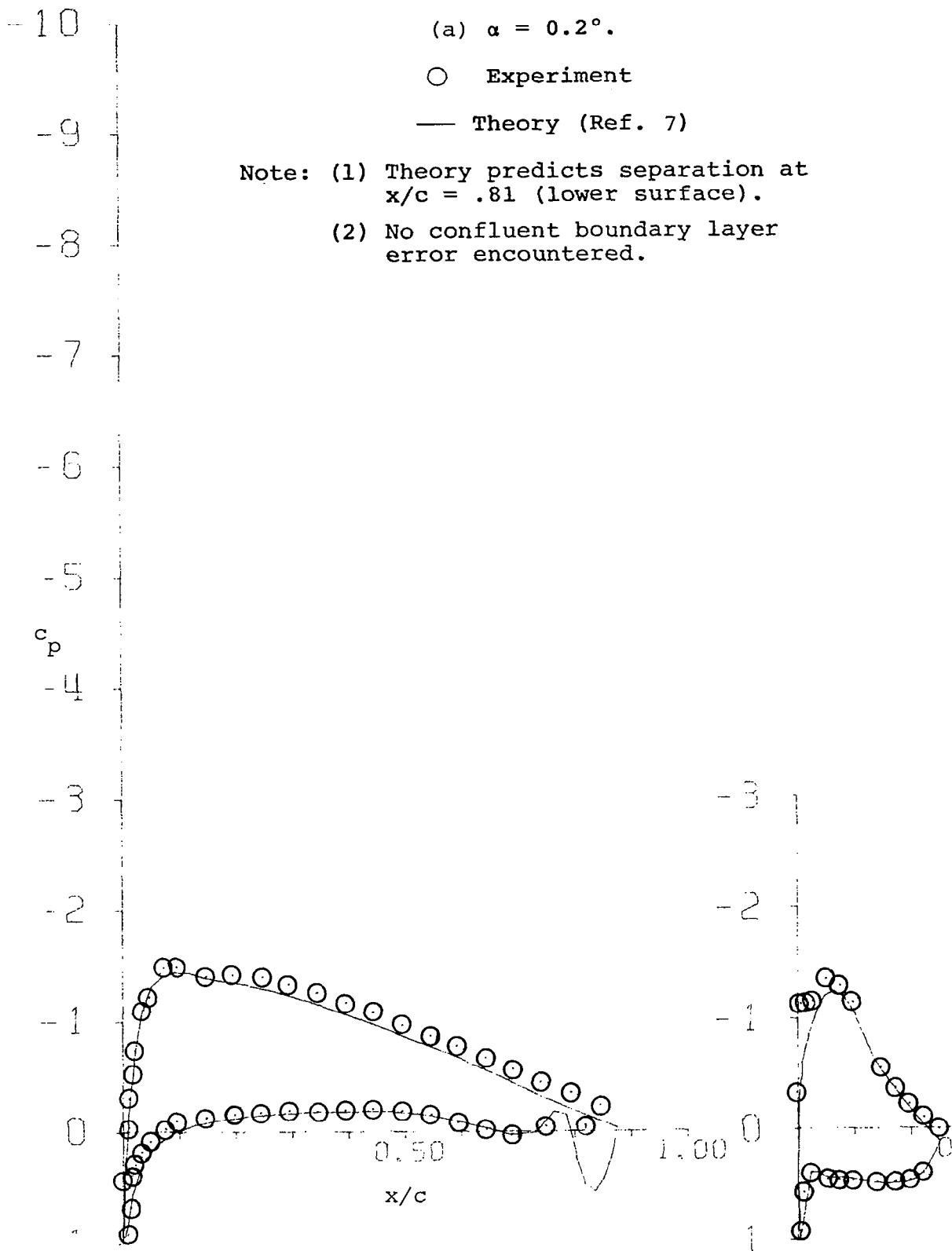


Figure 14 - Pressure Distributions with 25% Slotted Flap,
 10° Flap Deflection.

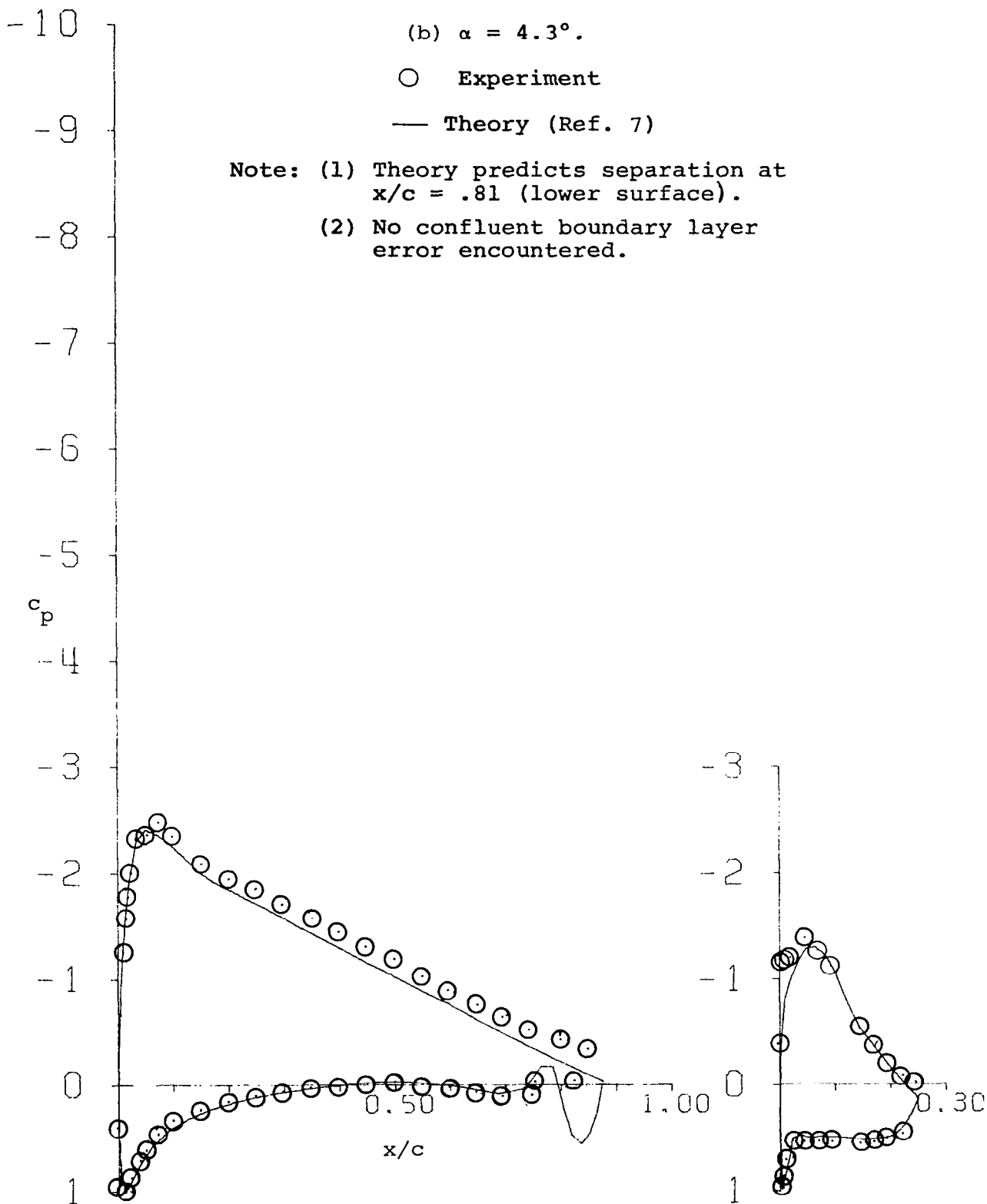


Figure 14 - Continued.

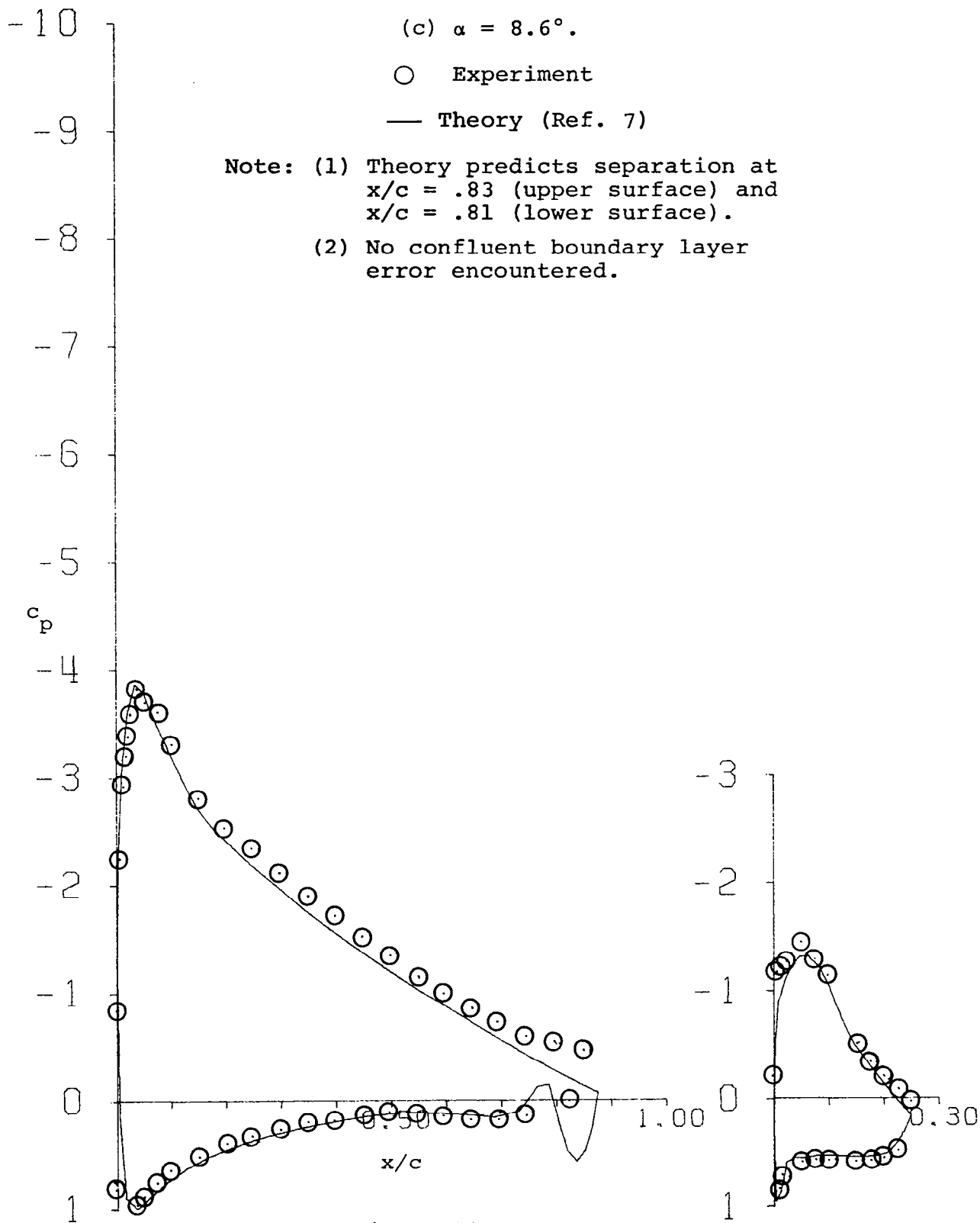


Figure 14 - Continued.

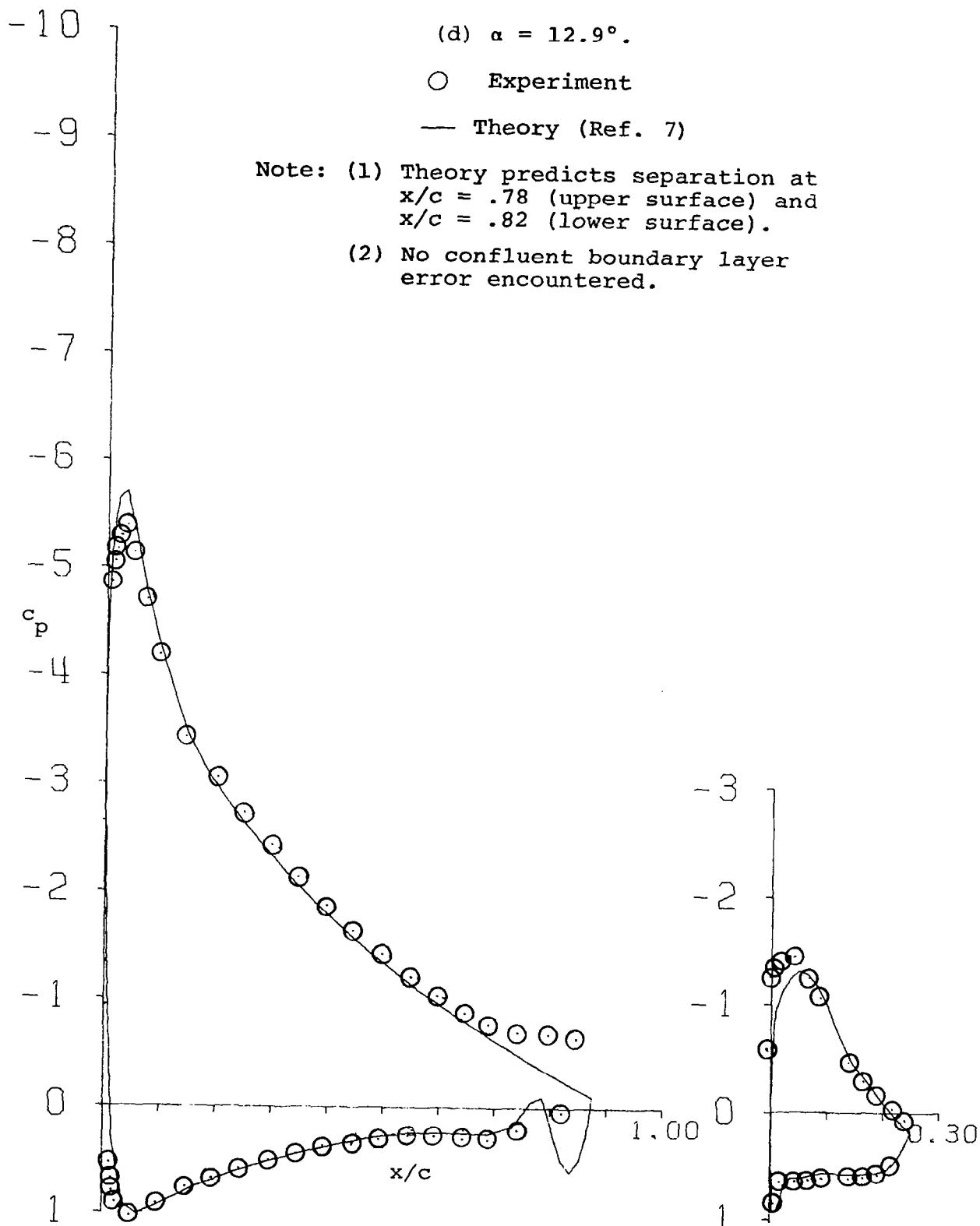


Figure 14 - Continued.

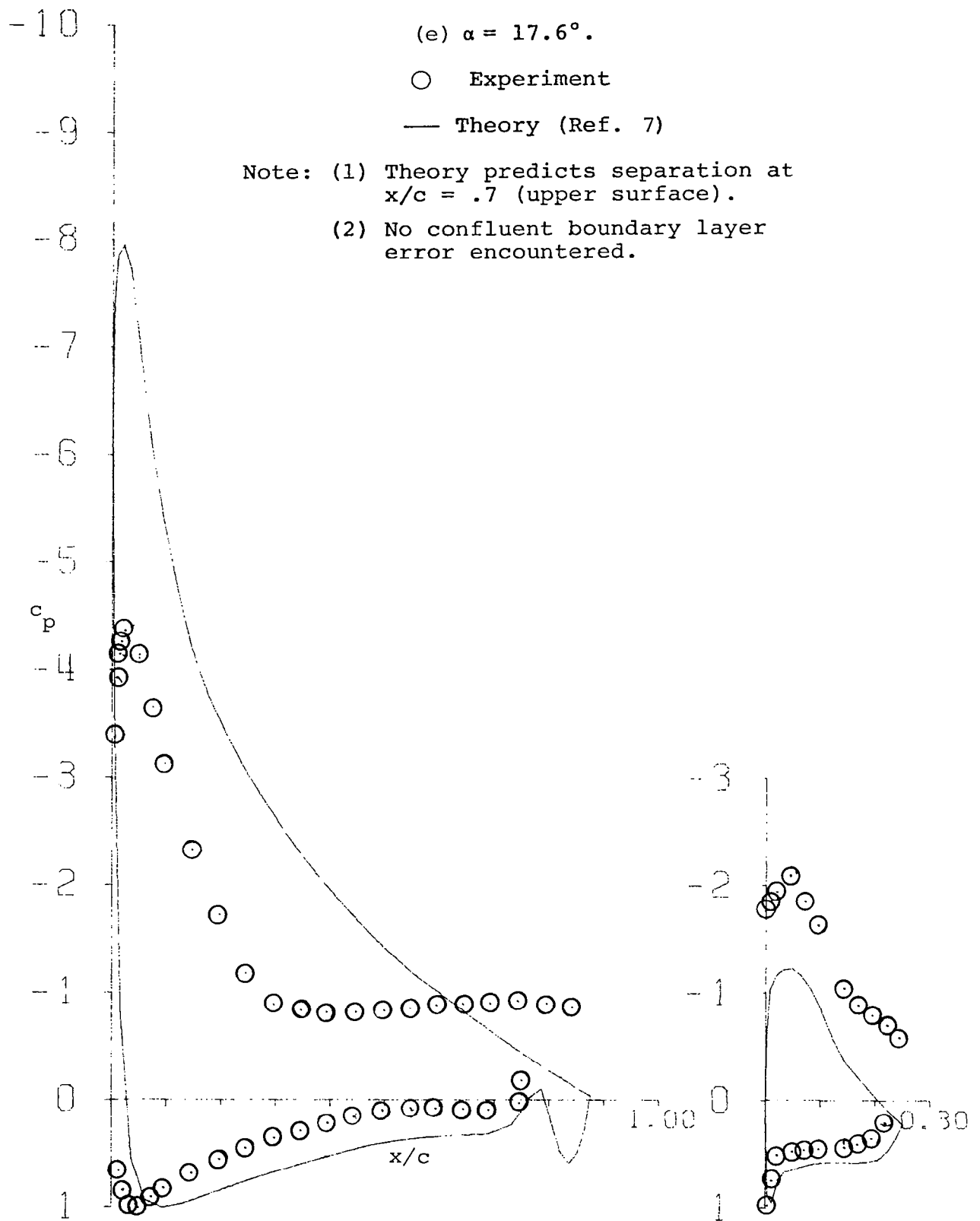


Figure 14 - Concluded.

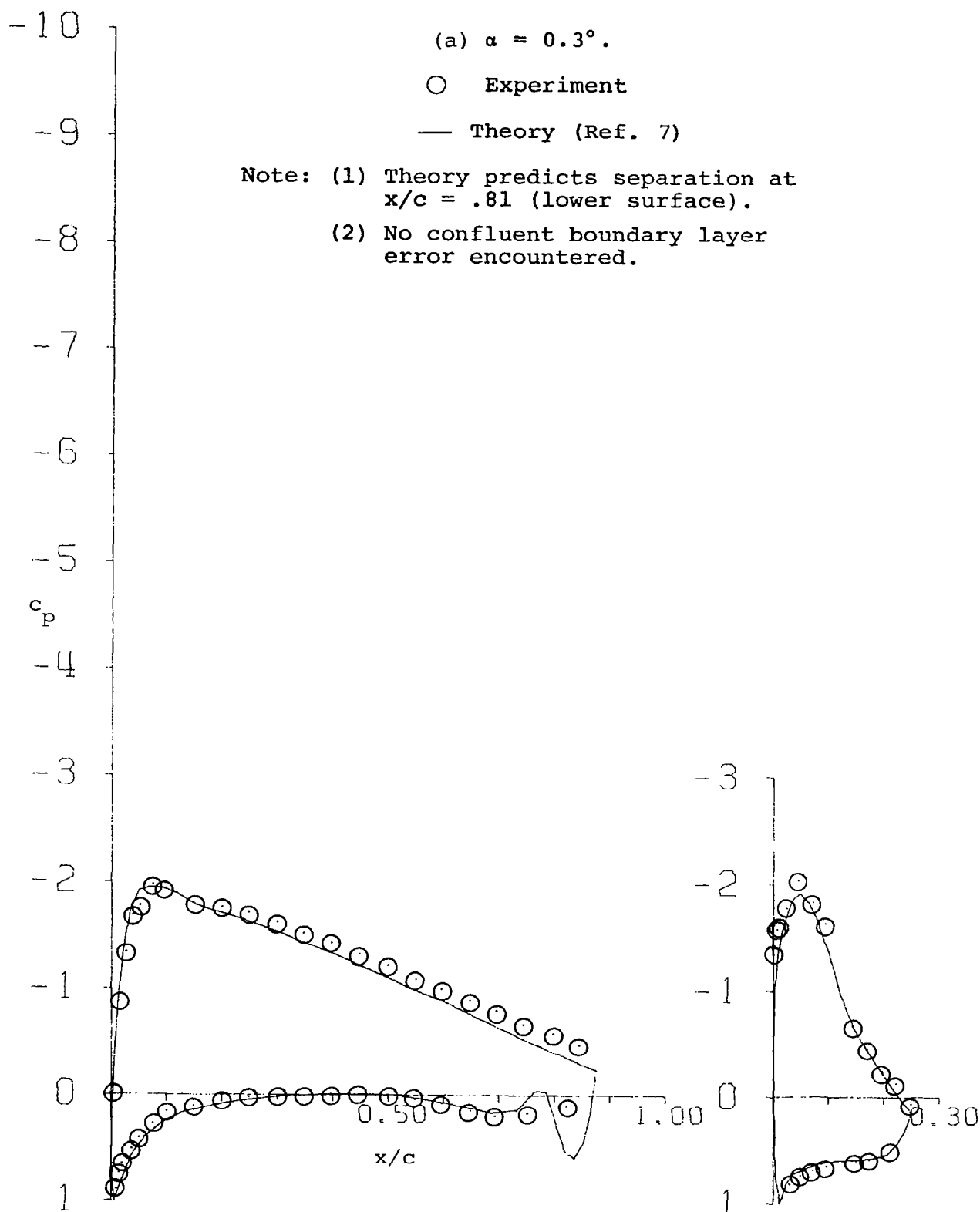


Figure 15 - Pressure Distributions with 25% Slotted Flap,
 20° Flap Deflection.

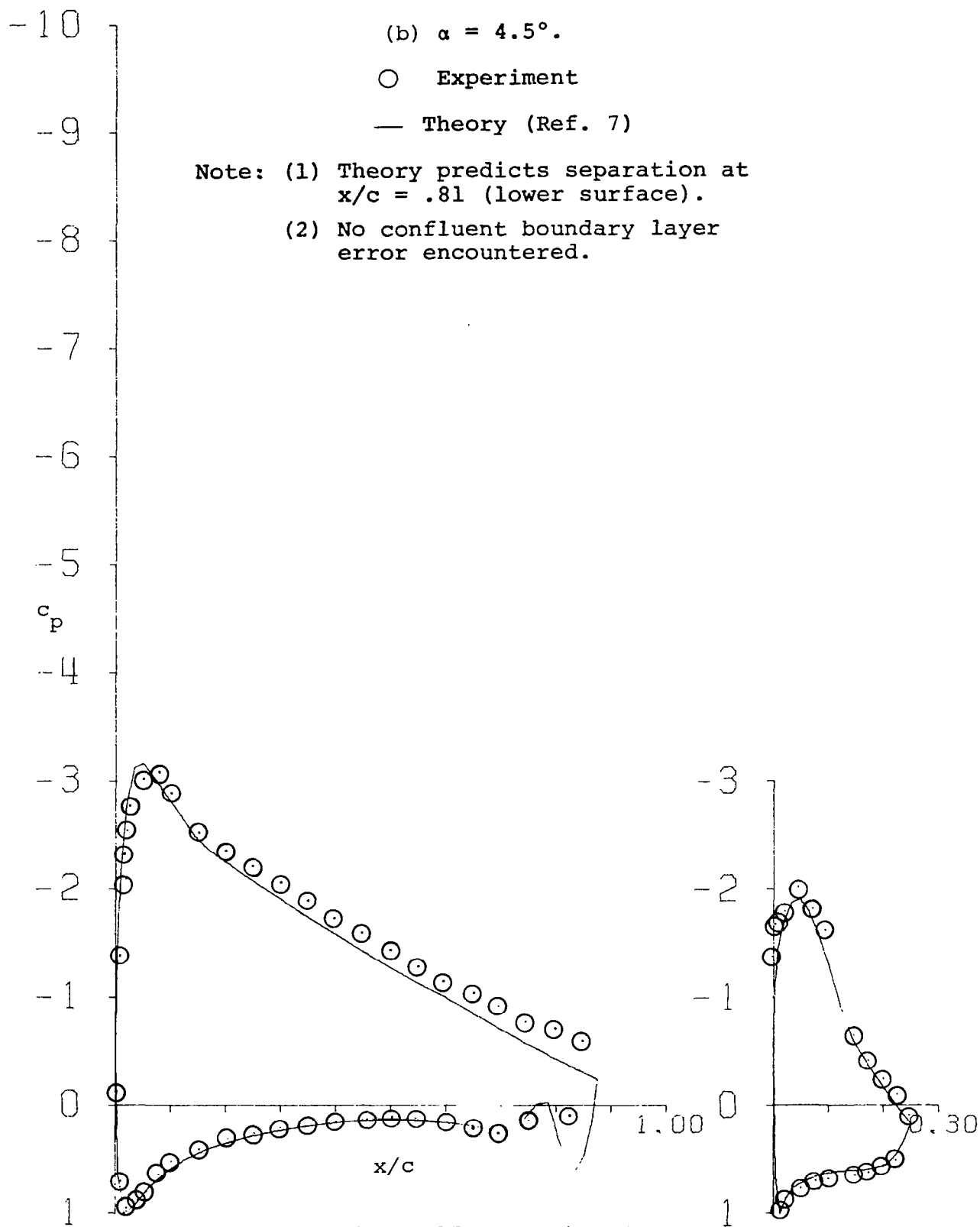


Figure 15 - Continued.

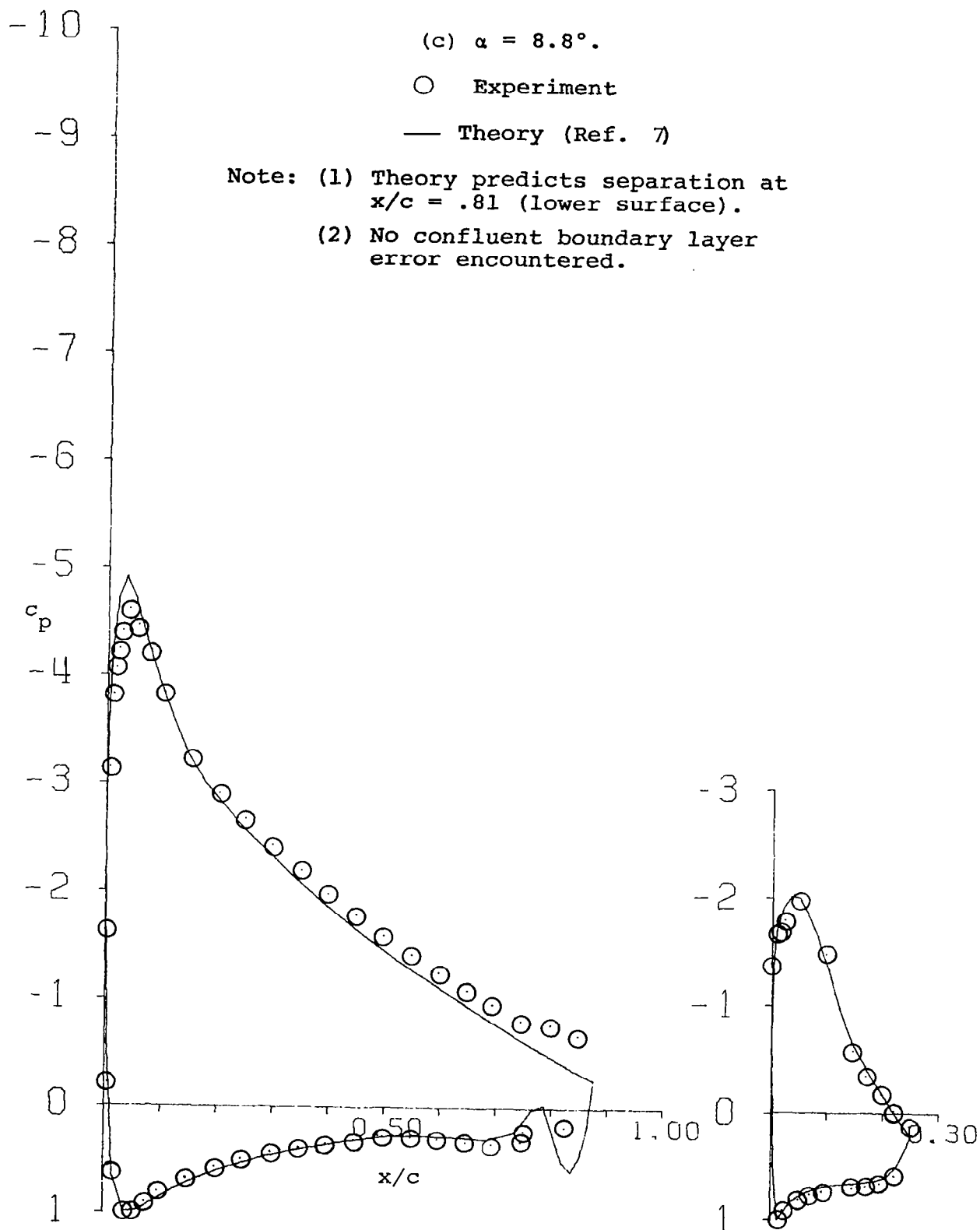


Figure 15 - Continued.

-10

(d) $\alpha = 13.2^\circ$.

○ Experiment

— Theory (Ref. 7)

Note: (1) Theory predicts separation at $x/c = .80$ (upper surface) and $x/c = .82$ (lower surface).

(2) No confluent boundary layer error encountered.

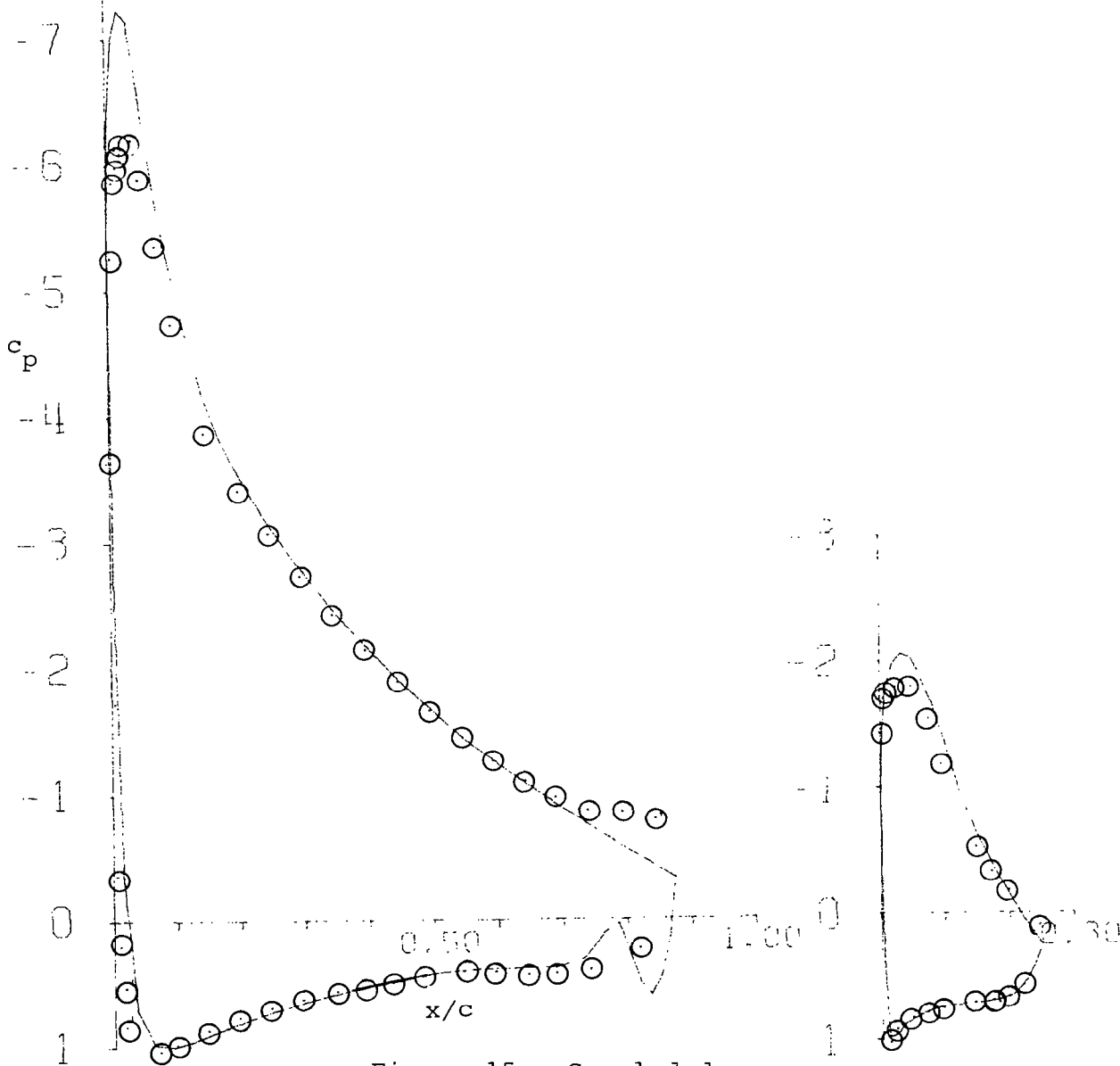


Figure 15 - Concluded.

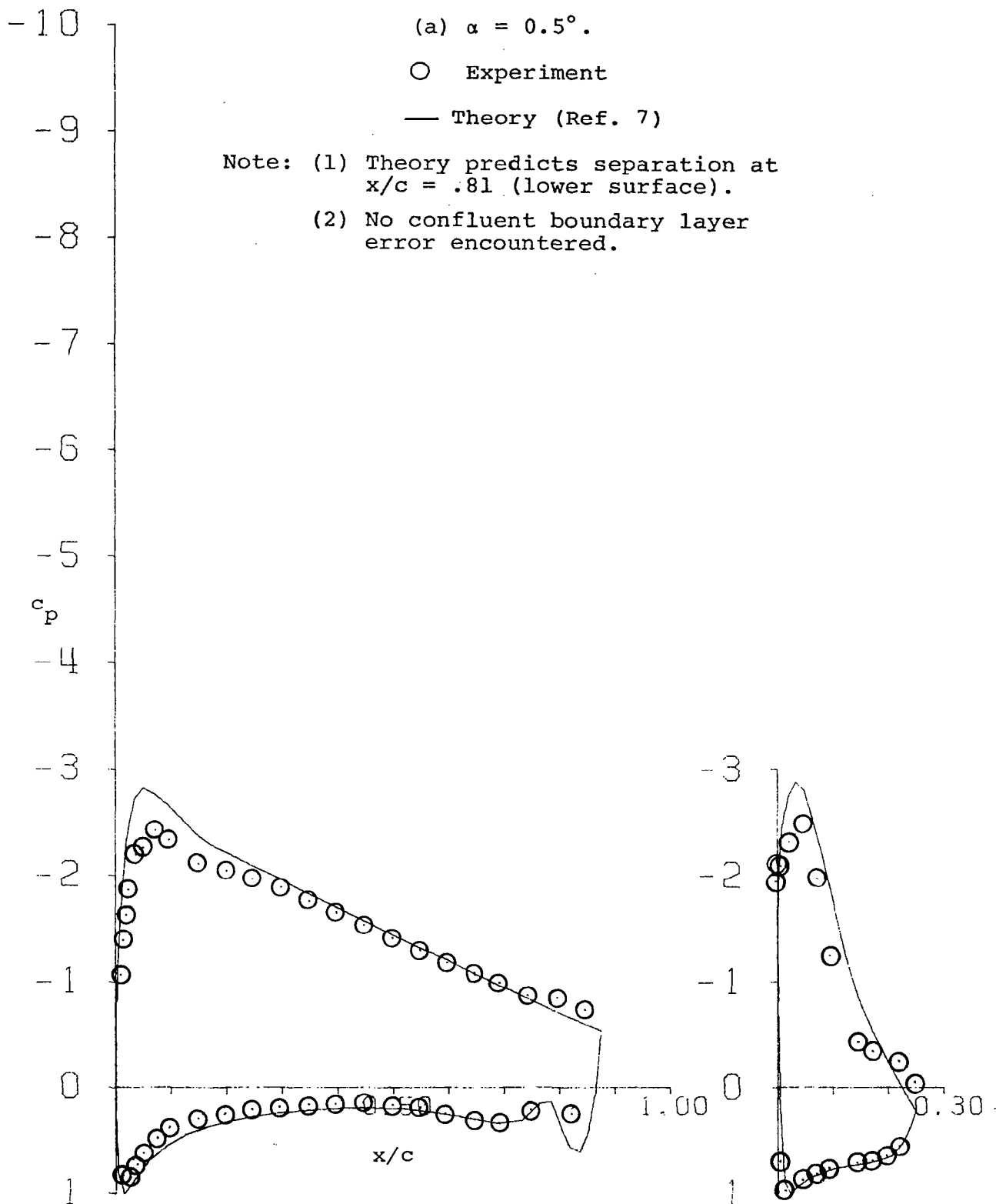


Figure 16 - Pressure Distributions with 25% Slotted Flap, 30° Flap Deflection.

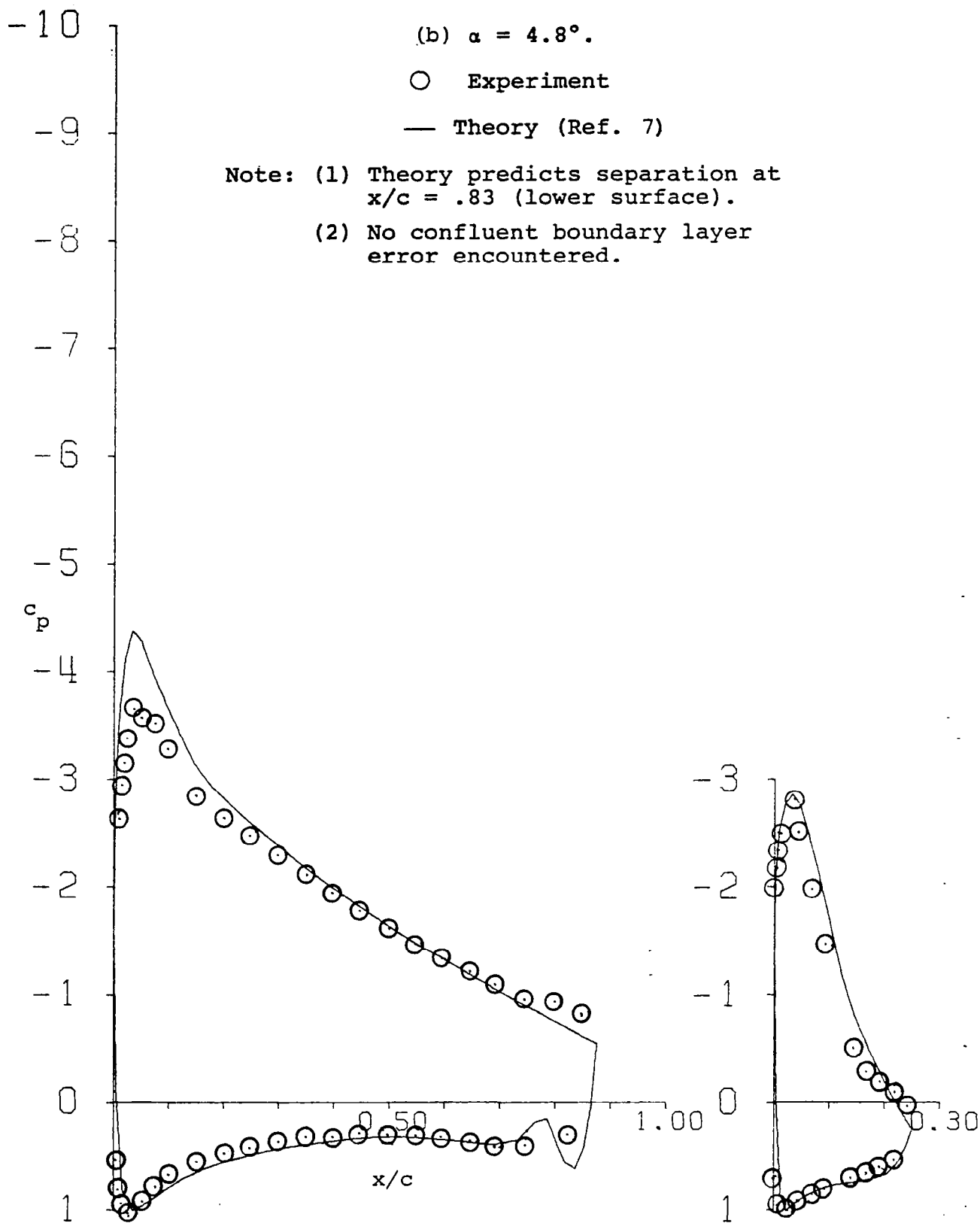


Figure 16 - Continued.

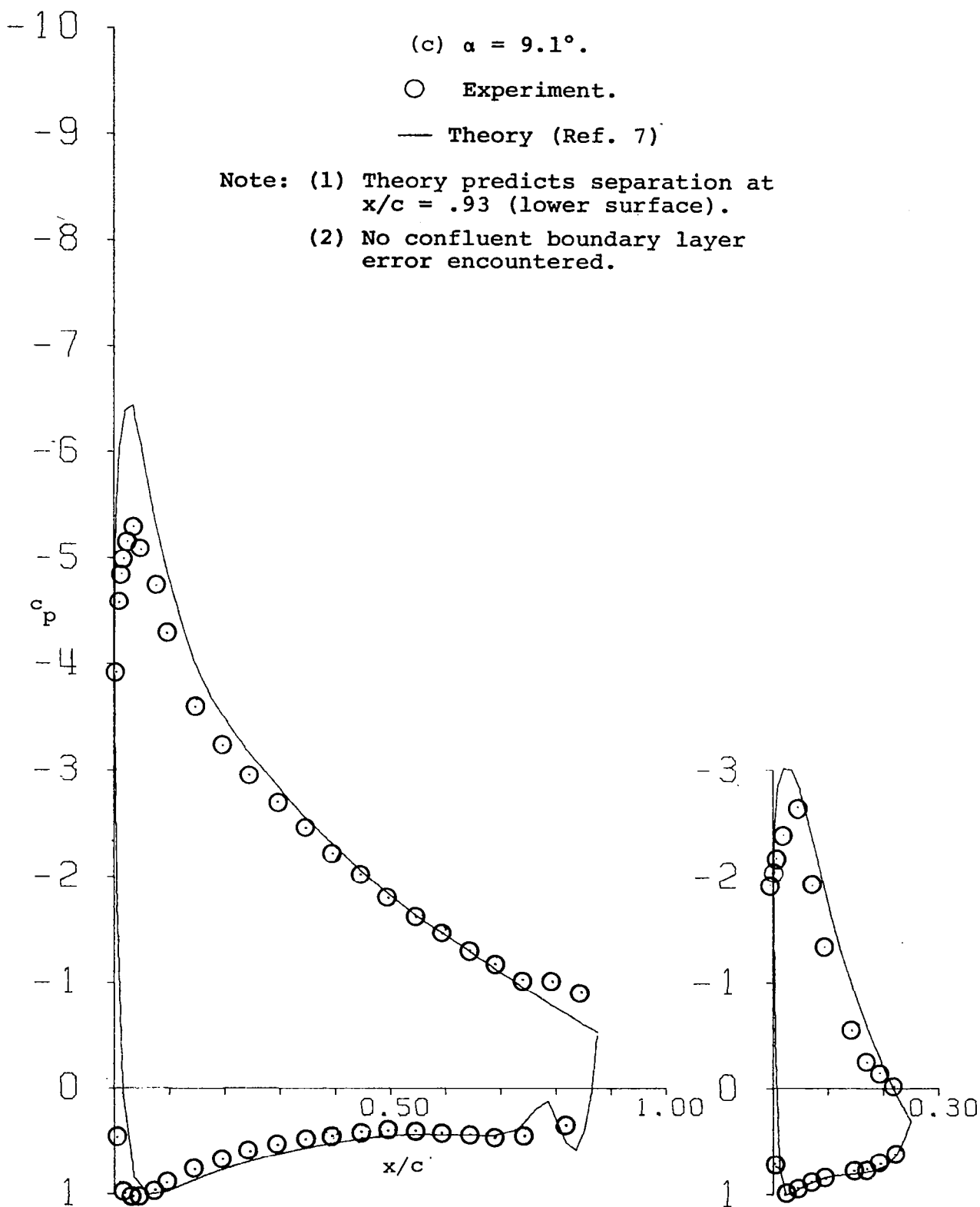


Figure 16 - Continued.

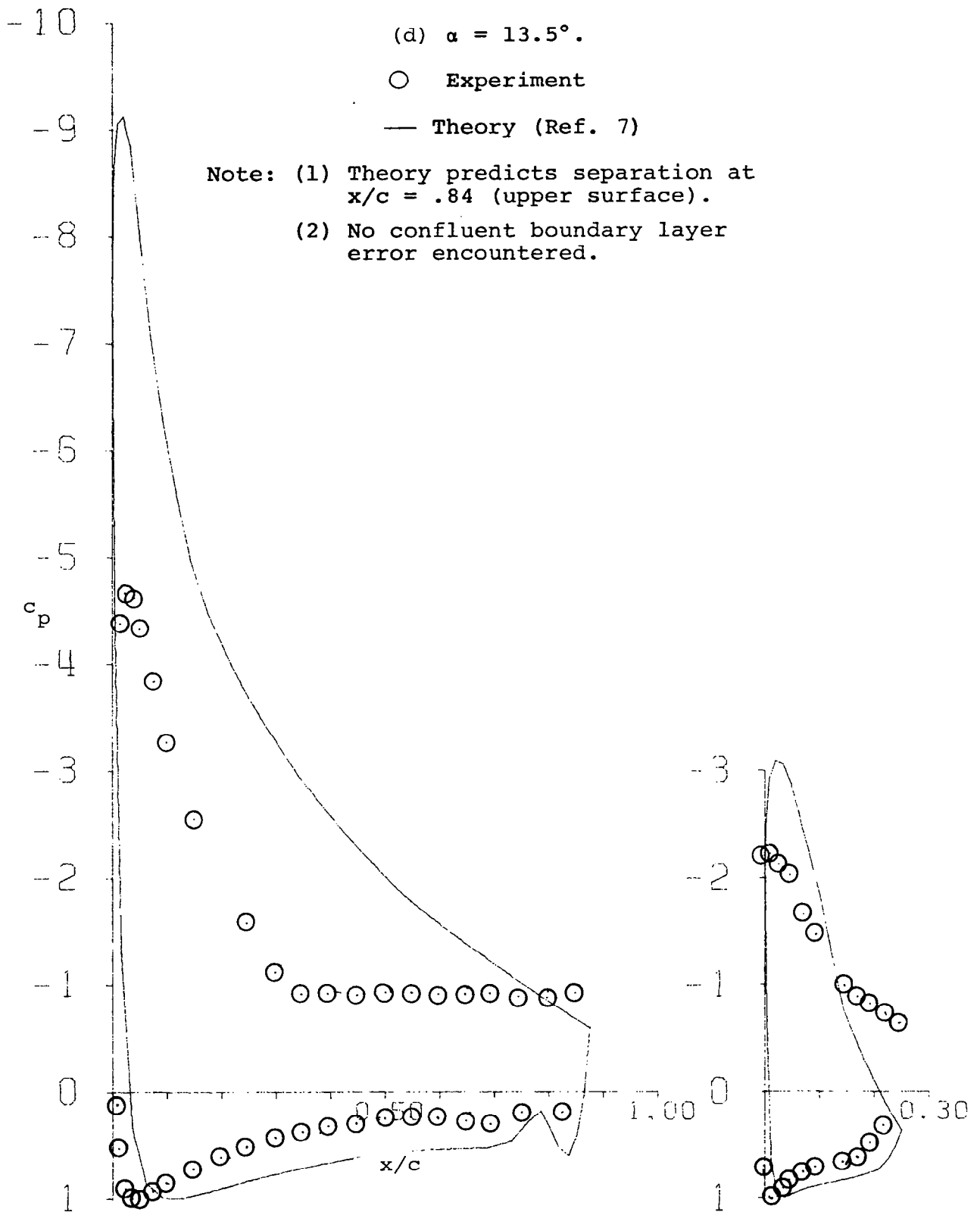


Figure 16 - Concluded.

-10

(a) $\alpha = 0.6^\circ$.

○ Experiment

— Theory (Ref. 7)

Note: (1) Theory predicts separation
at $x/c = .81$ (lower surface).

(2) No confluent boundary
layer error encountered.

-8

-7

-6

-5

c_p

-4

-3

-2

-1

0

1

x/c

-3

-2

-1

0

1

Figure 17 - Pressure Distributions with 25% Slotted Flap,
35° Flap Deflection.

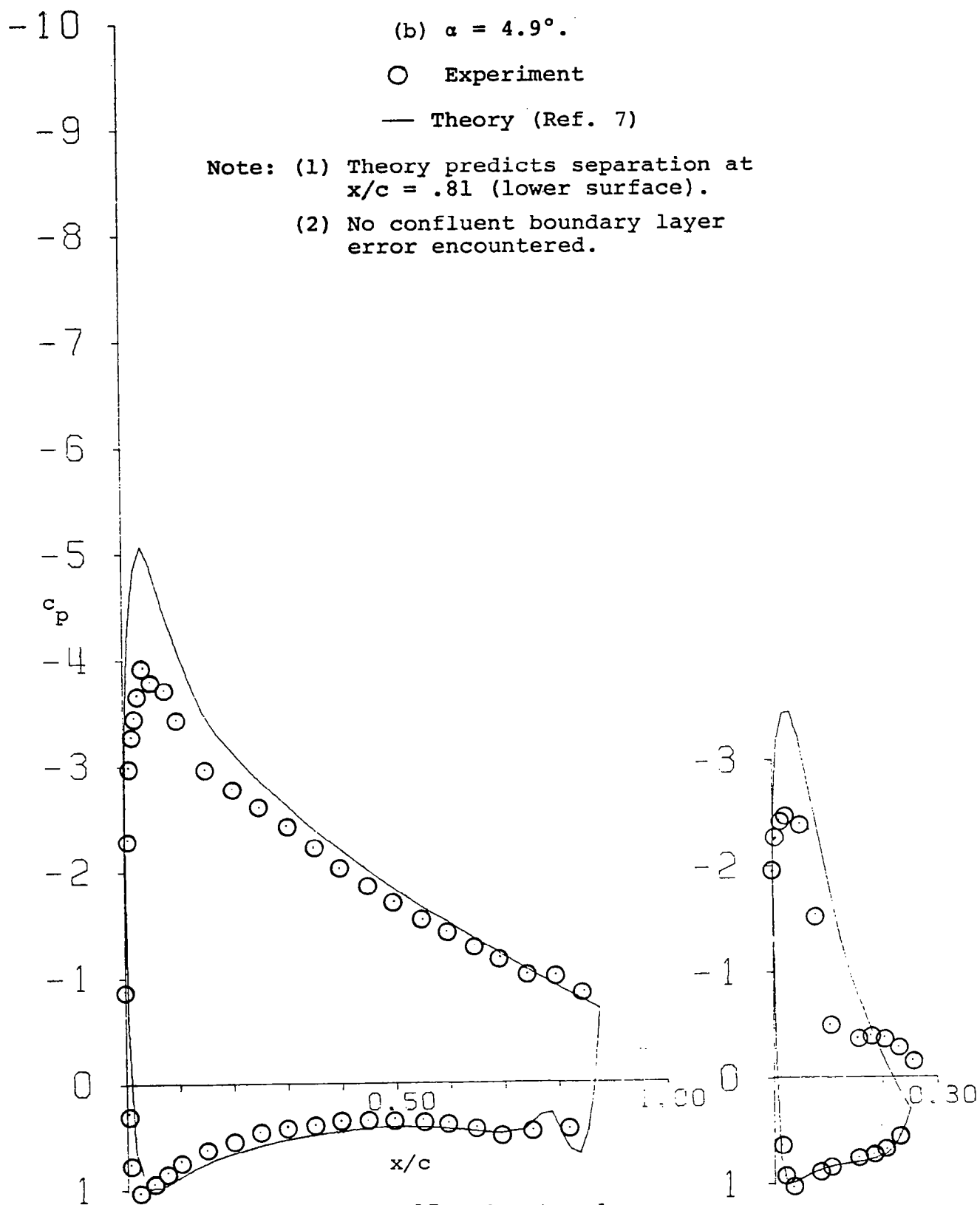


Figure 17 - Continued.

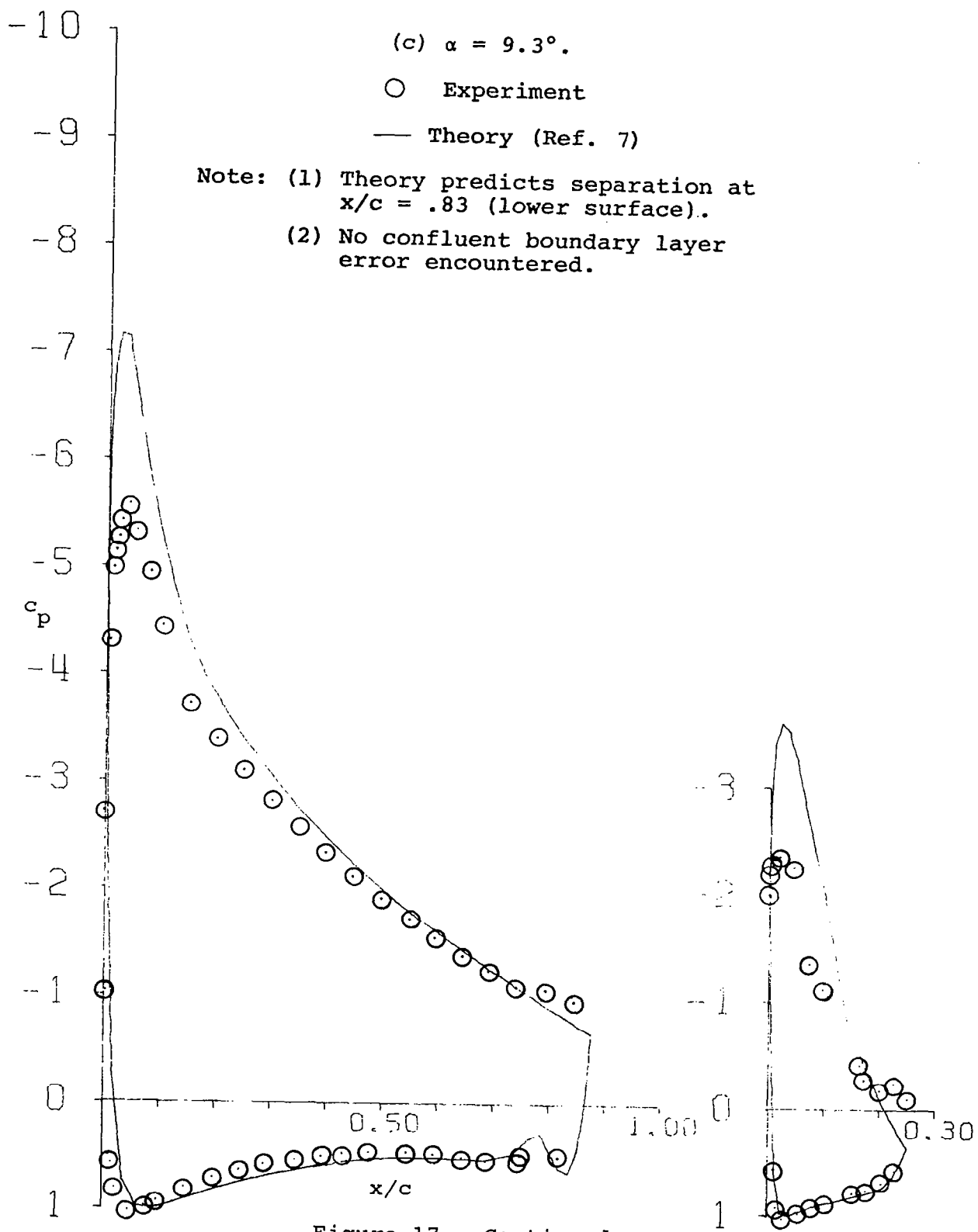


Figure 17 - Continued.

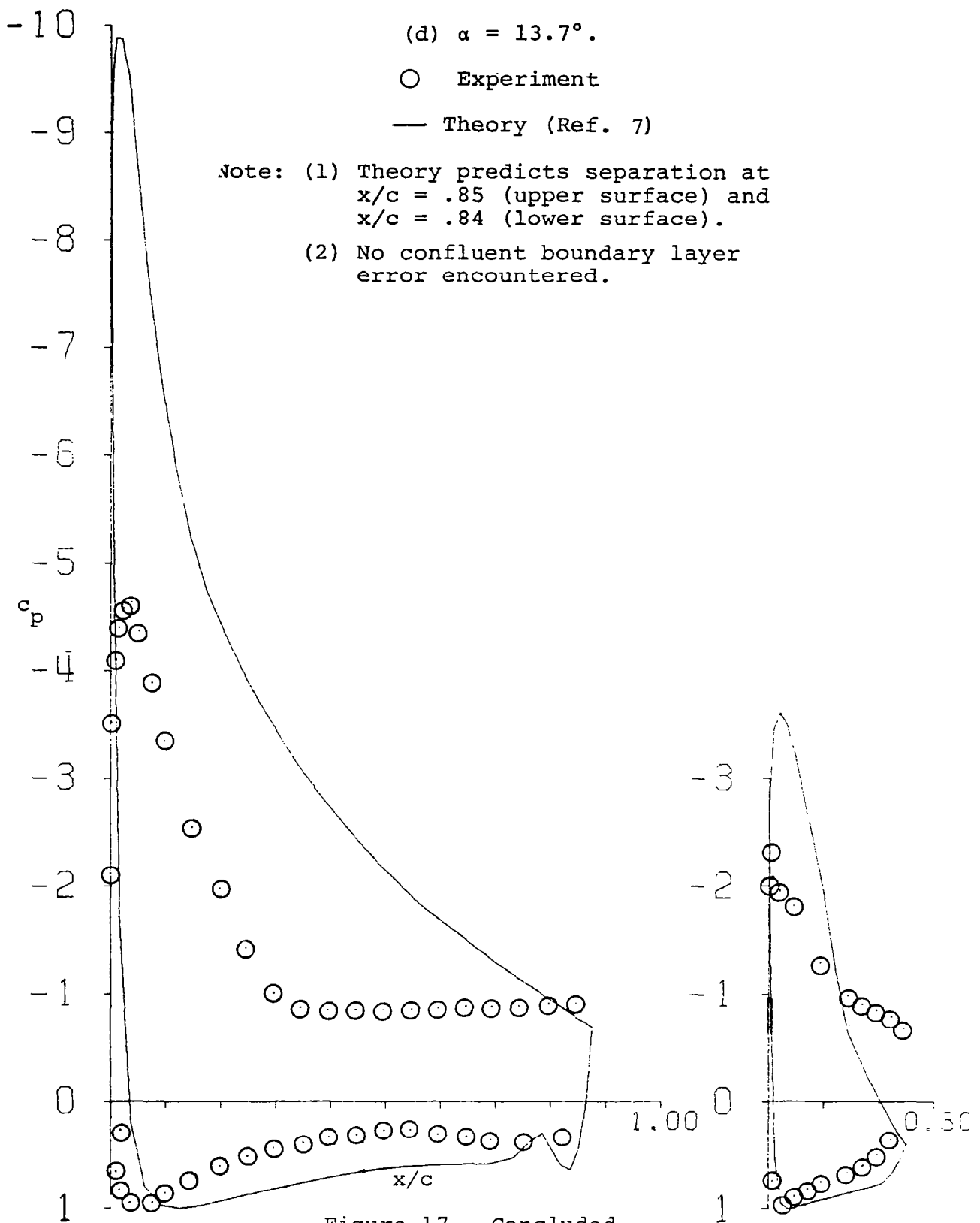
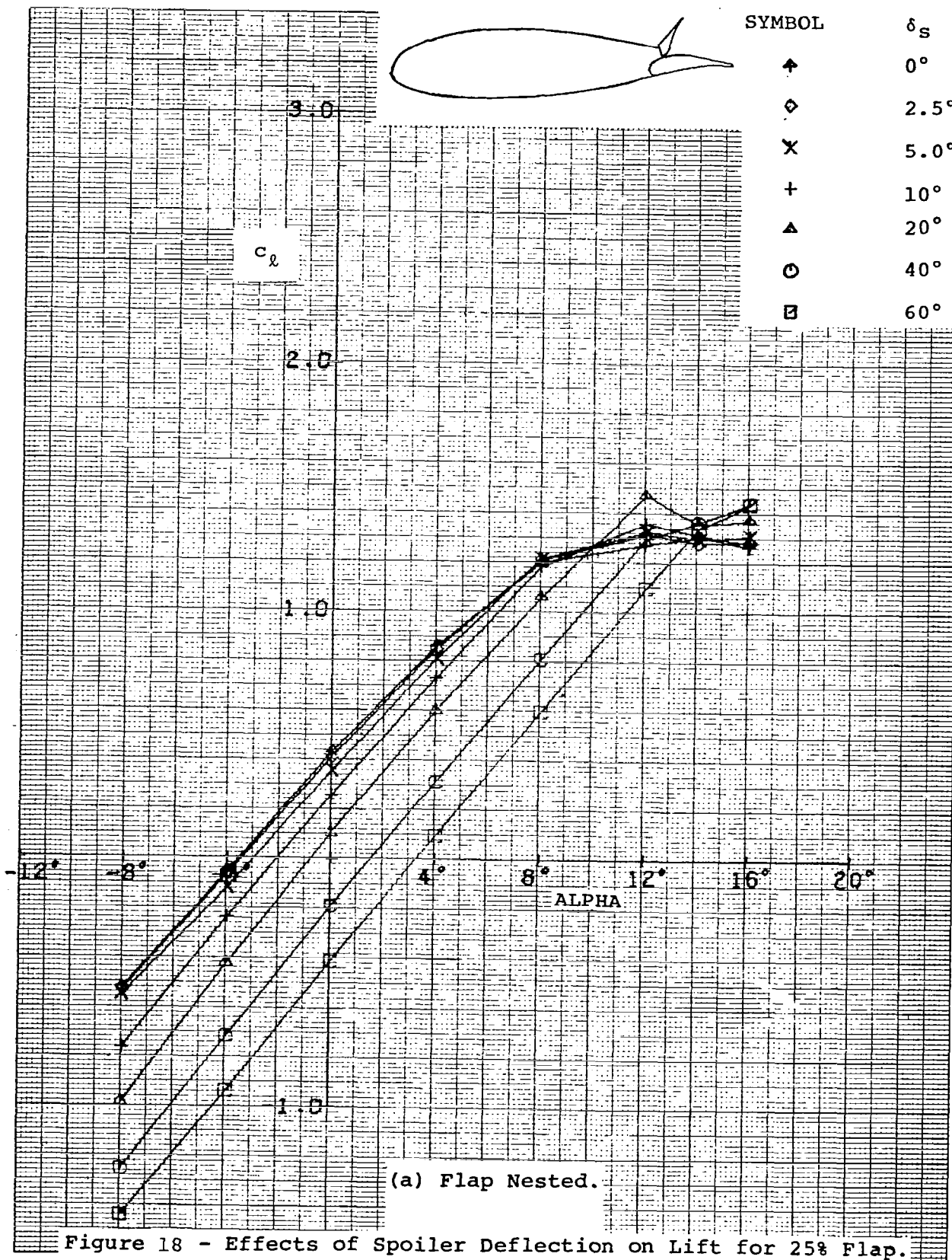
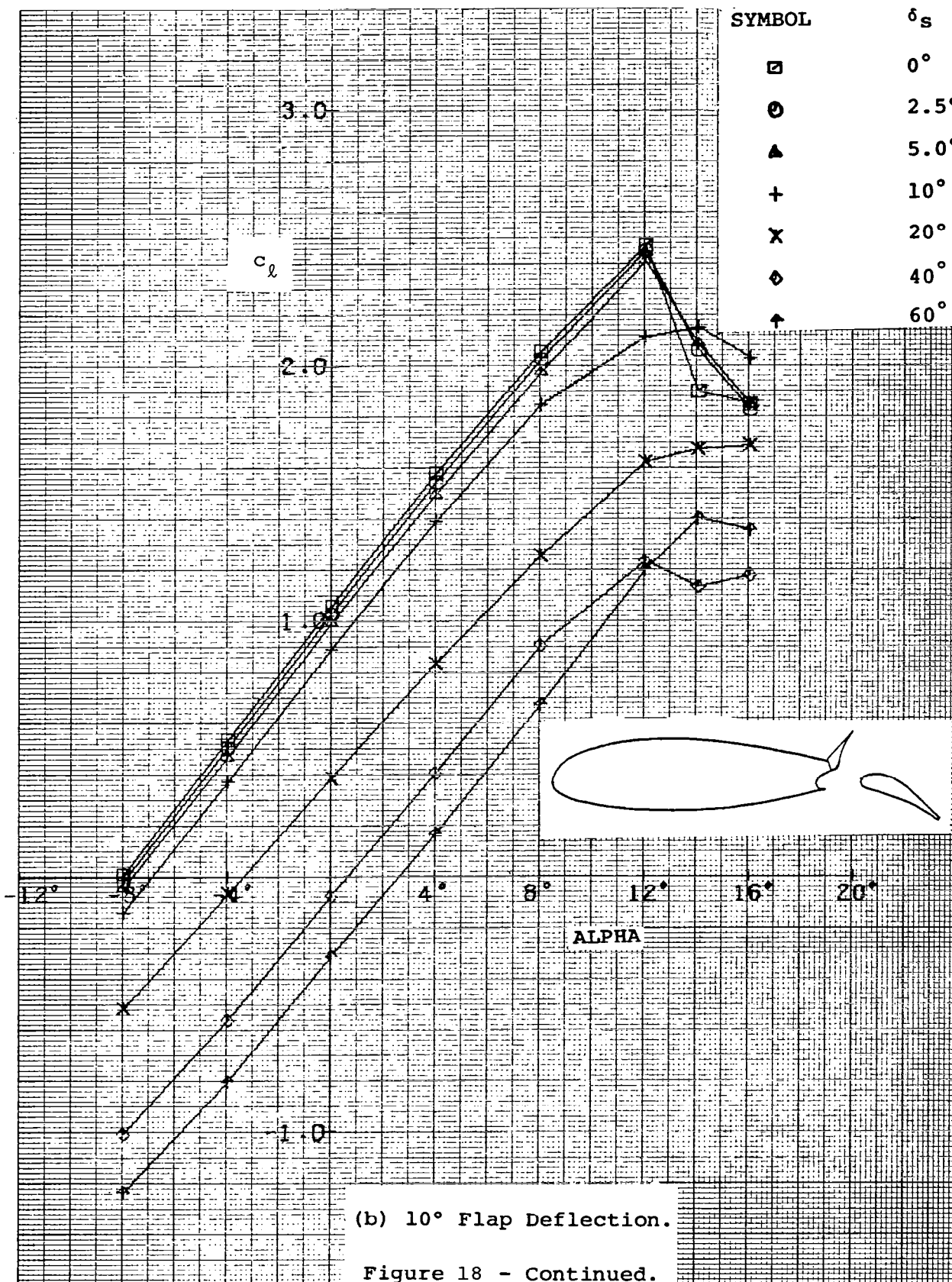
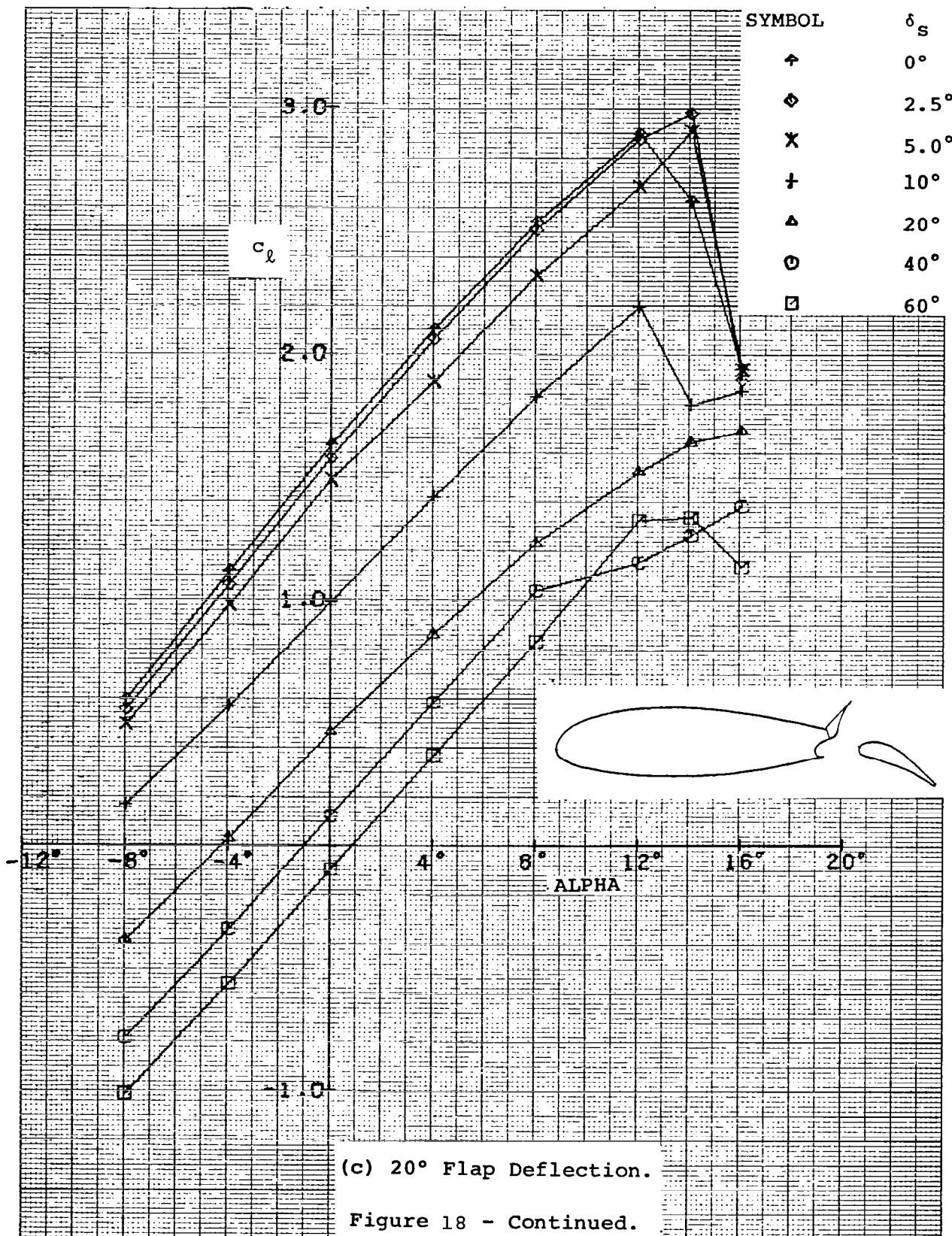
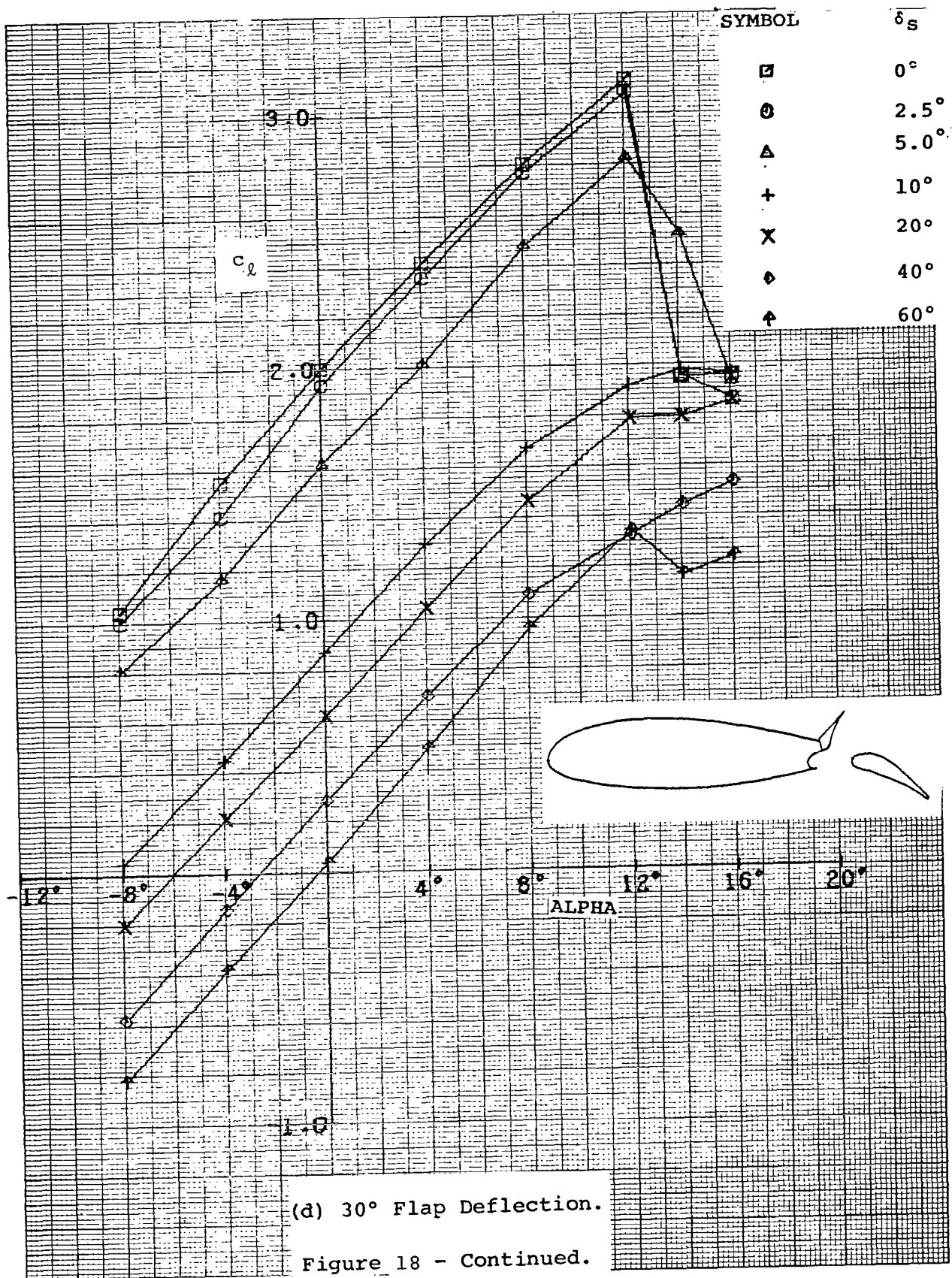


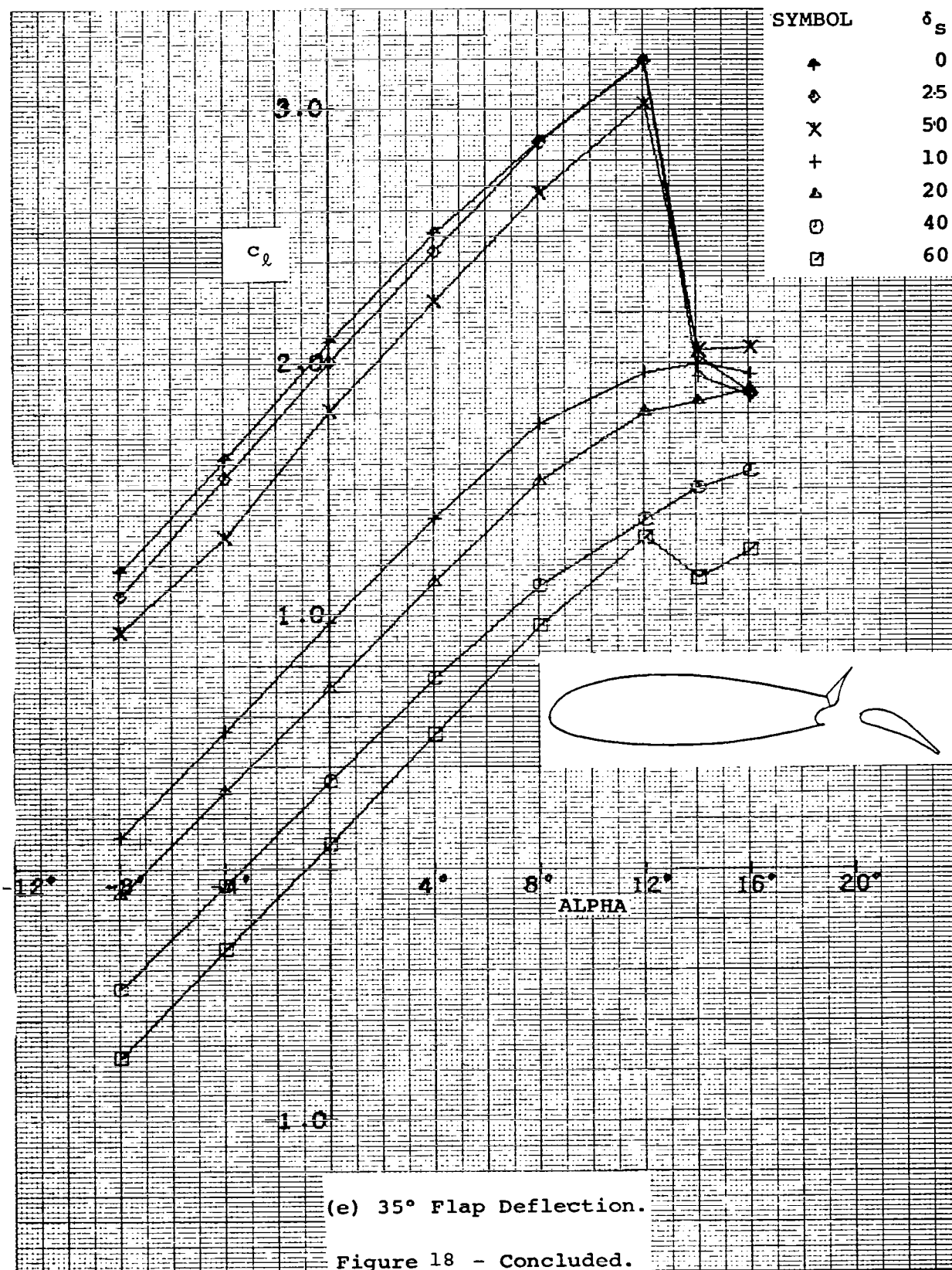
Figure 17 - Concluded.





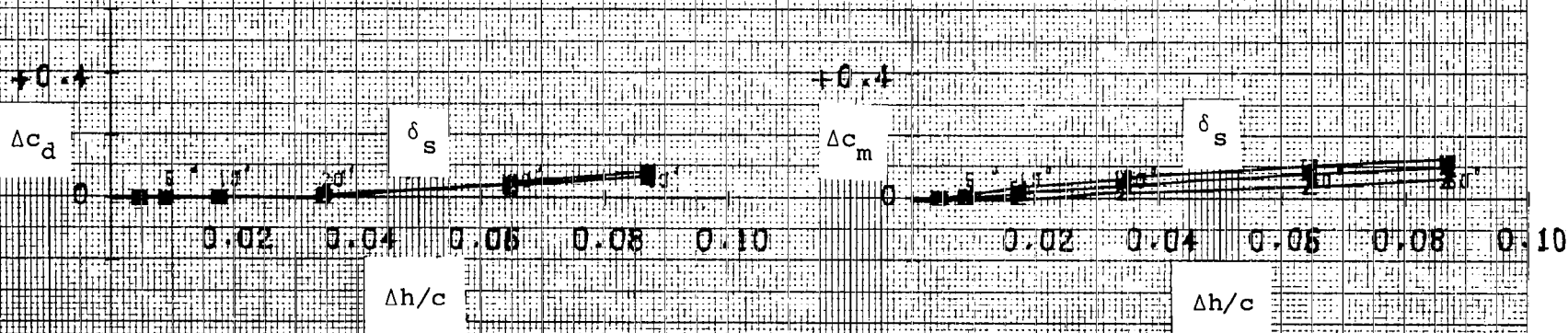


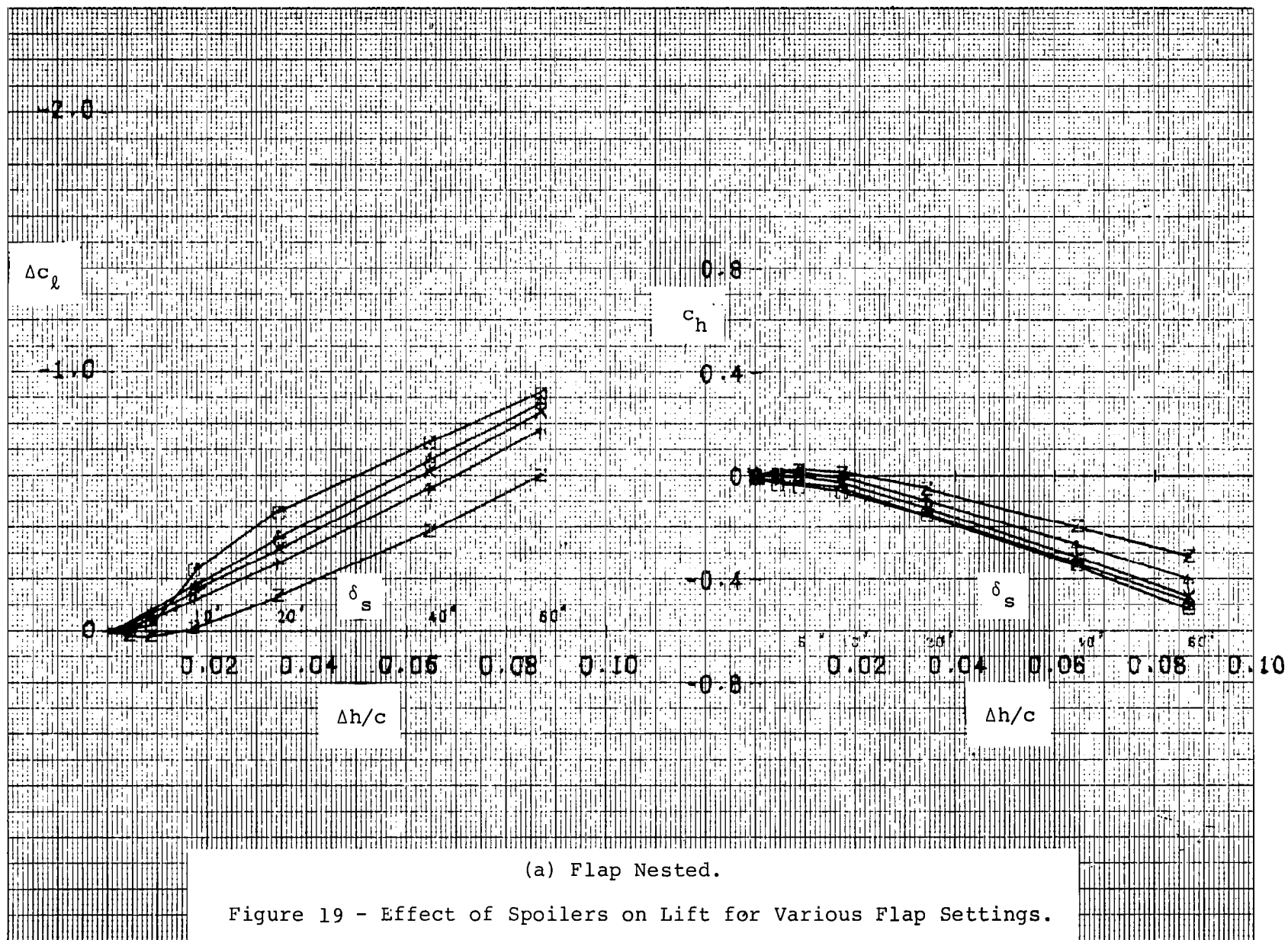






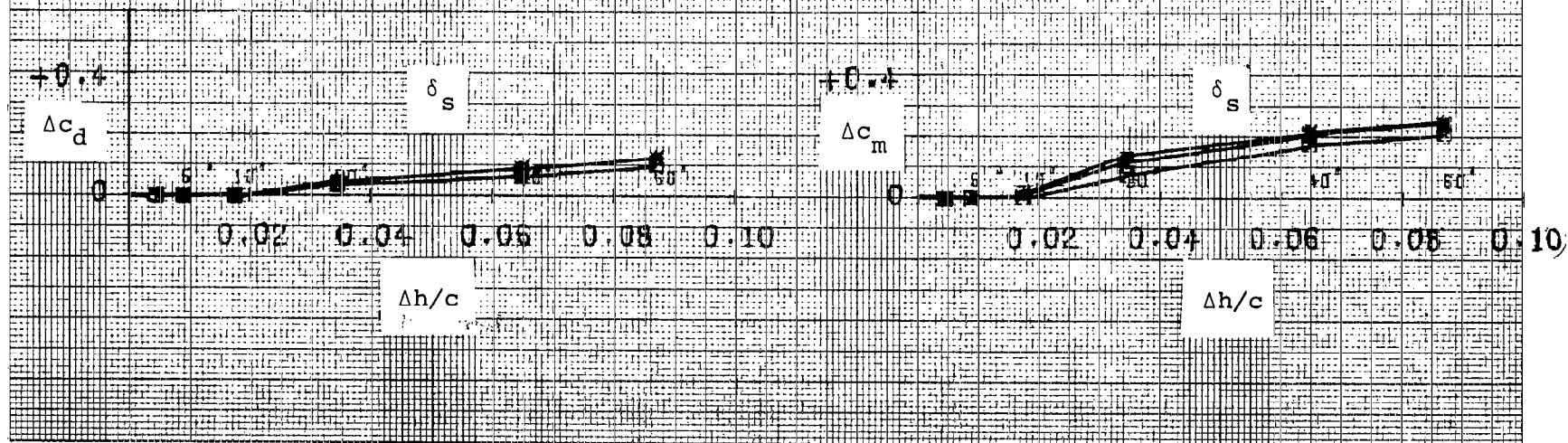
Symbol	Alpha
◻	-8°
△	-4°
×	0°
↑	4°
z	8°

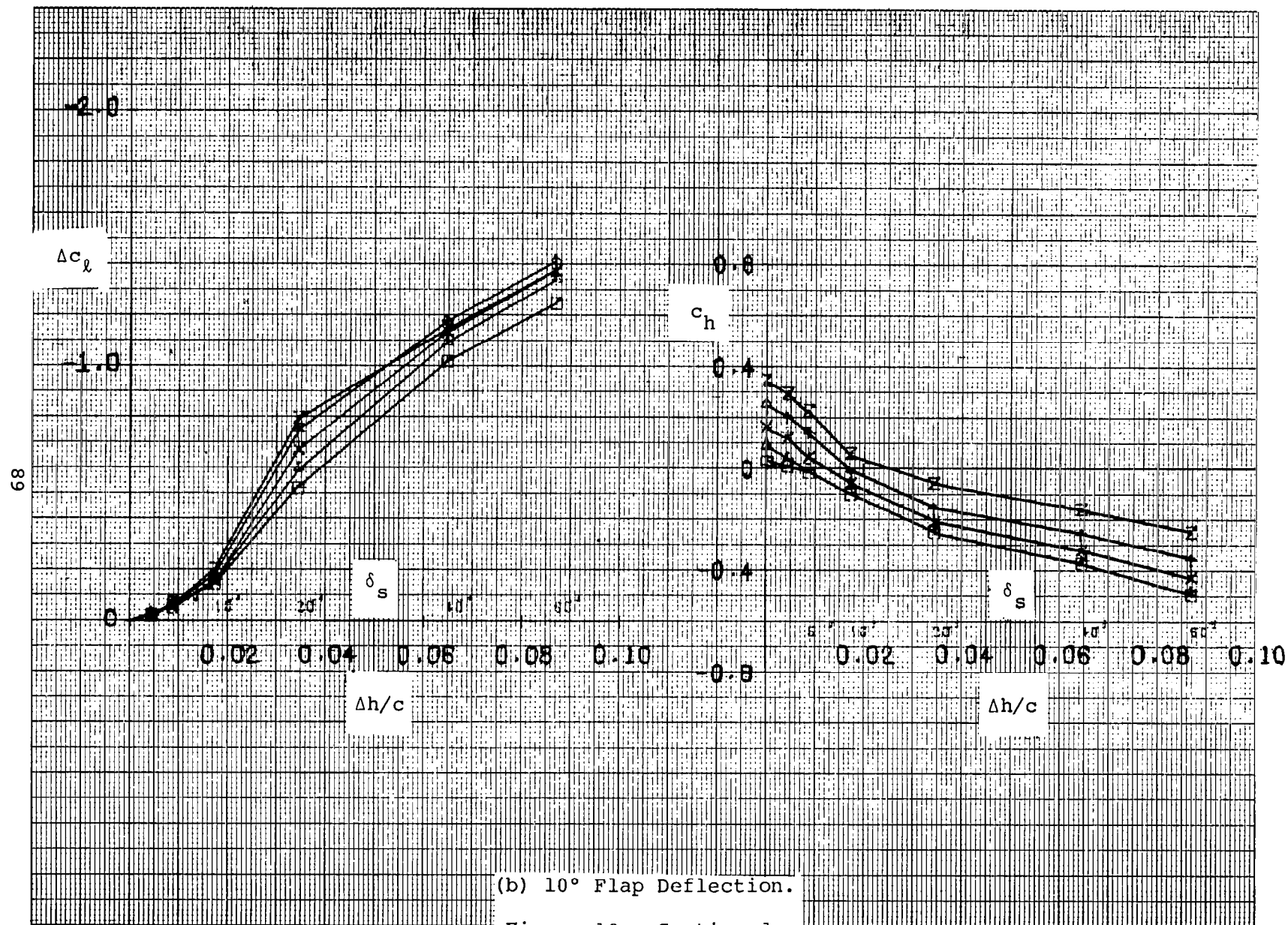


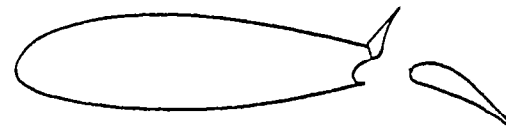




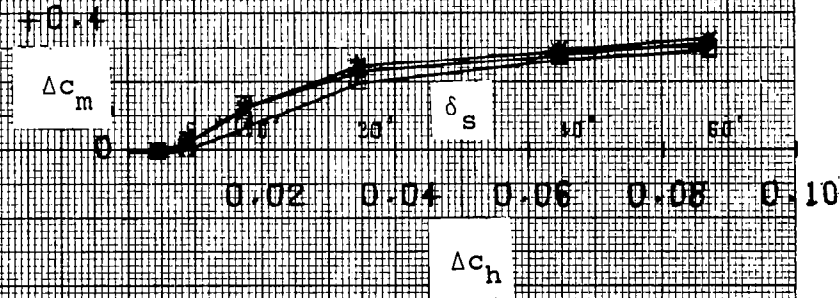
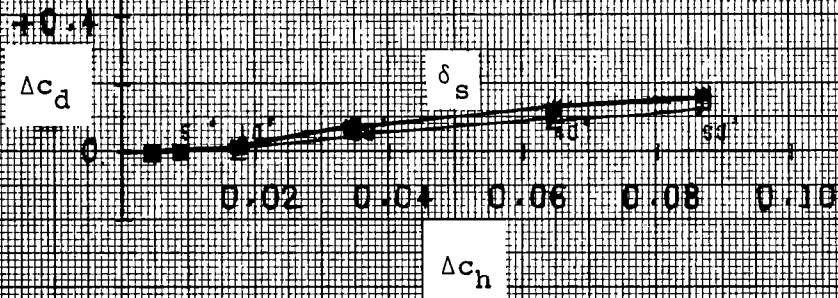
Symbol	Alpha
◻	-8°
△	-4°
×	0°
↑	4°
z	8°

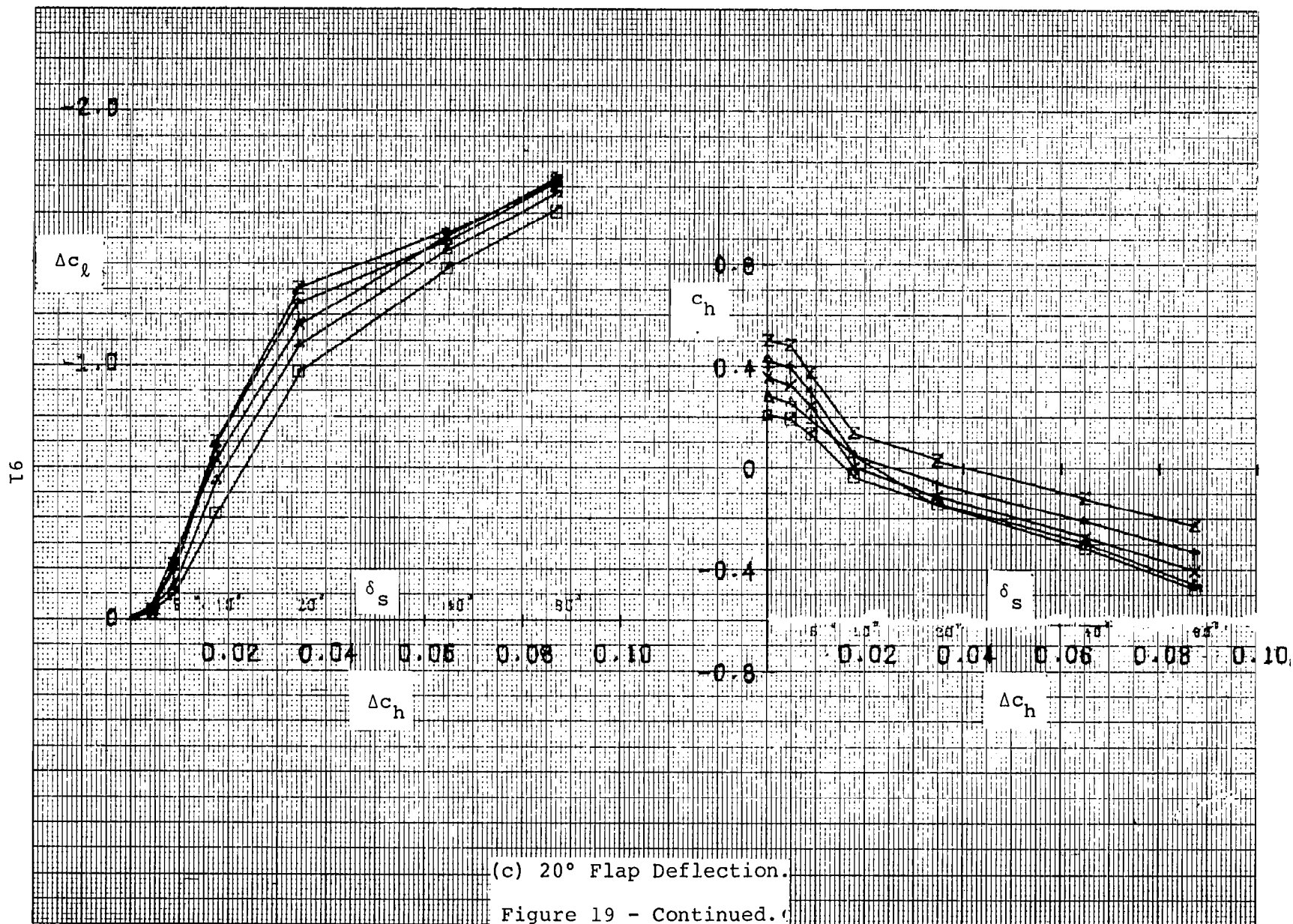






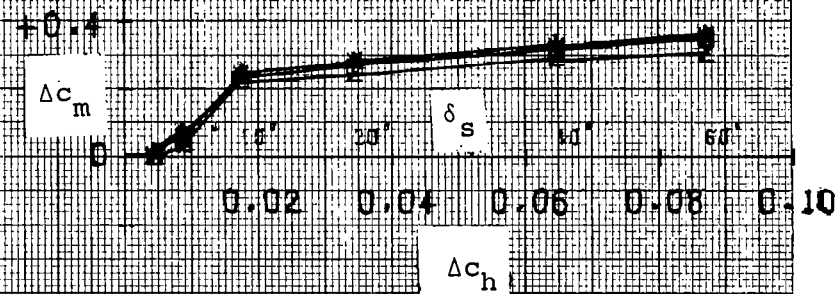
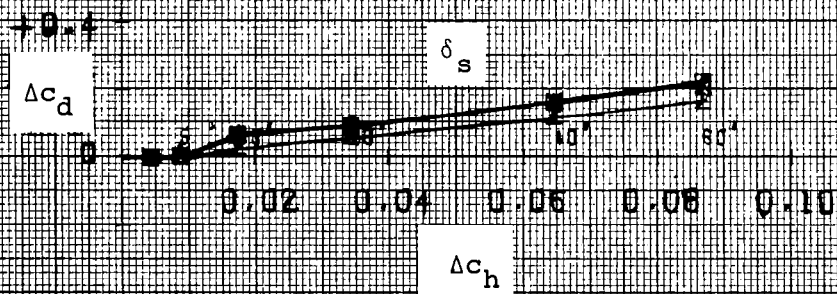
Symbol	Alpha
□	-8°
△	-4°
×	0°
↑	4°
z	8°

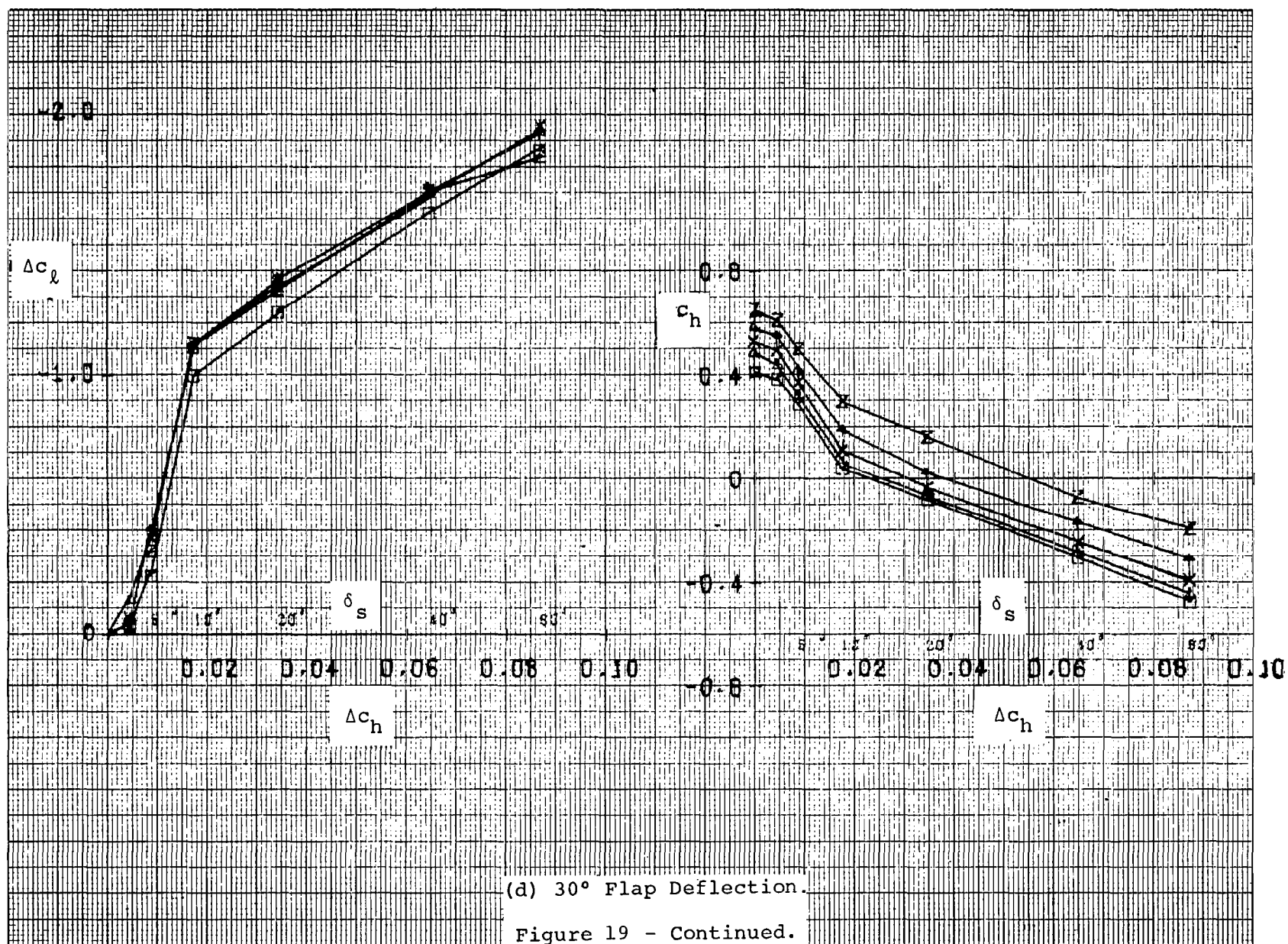






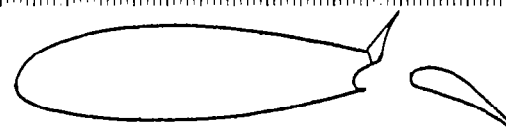
Symbol	Alpha
◻	-8°
▲	-4°
×	0°
↑	4°
z	8°



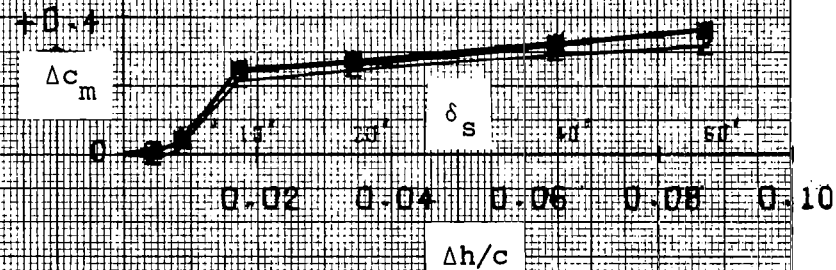
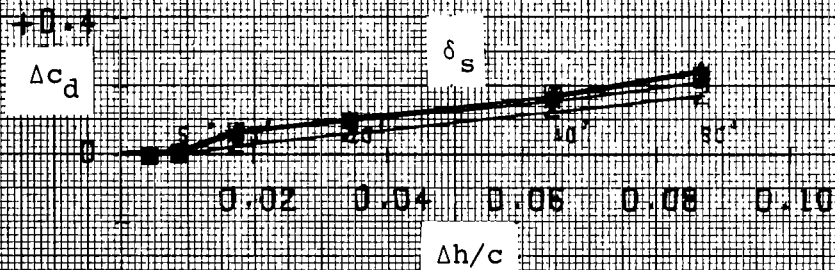


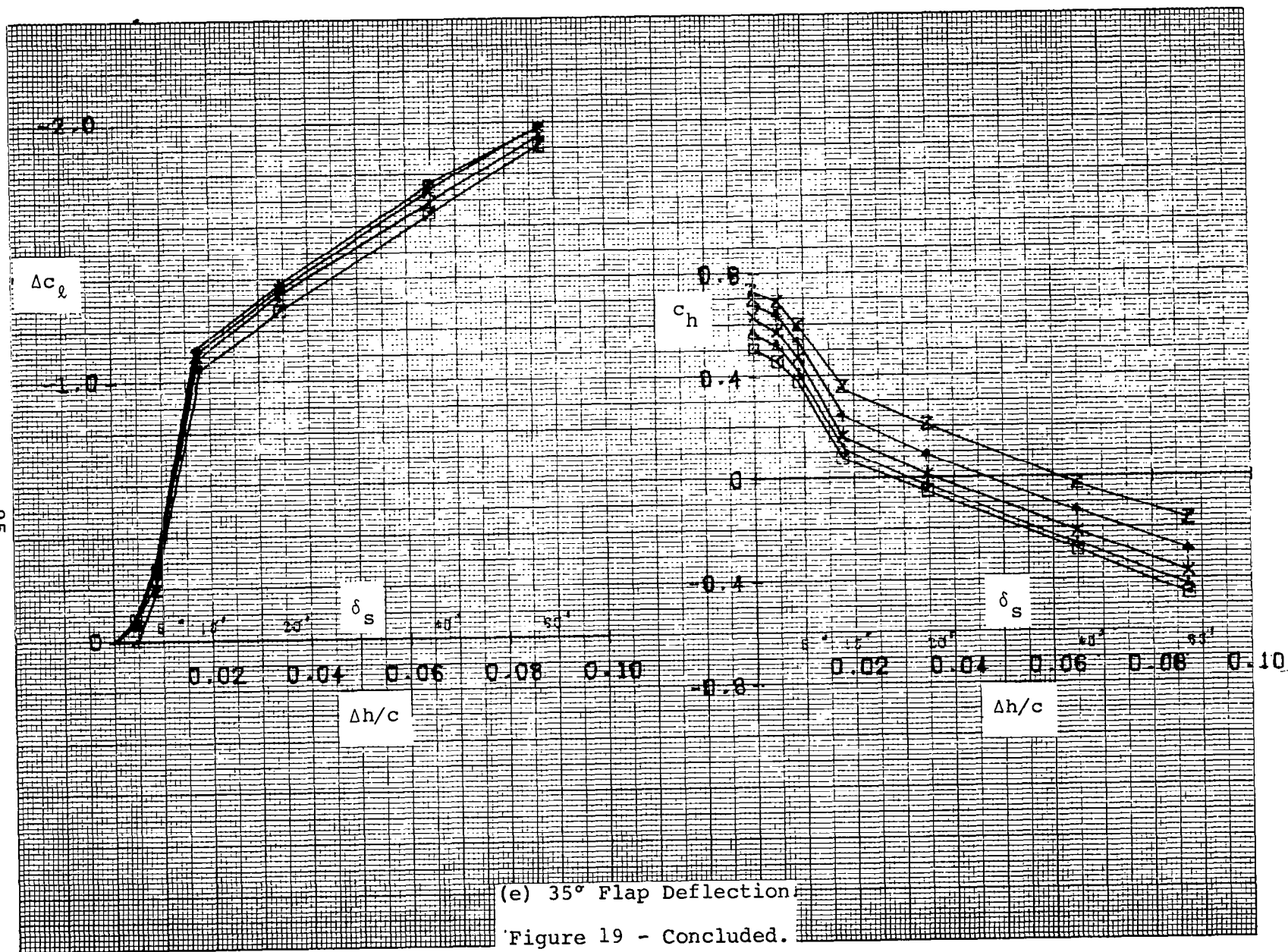
(d) 30° Flap Deflection.

Figure 19 - Continued.



Symbol	Alpha
□	-8°
△	-4°
×	0°
↑	4°
z	8°





APPENDIX A

End Plate Drag

End plate tare drag was evaluated as the difference between model plus end plate force measurements and model section drag from centerline wake surveys. Wake surveys were made using a scanning five-tube pressure probe described in reference A1. Since this probe provided the longitudinal component of velocity, drag was evaluated directly by means of the equation:

$$c_d = \frac{2}{c} \int_{-\infty}^{\infty} \frac{u_x}{u_{\infty}} \left(1 - \frac{u_x}{u_{\infty}}\right) dz \quad (A1)$$

from reference A2, where:

c_d = section drag coefficient

u_x = longitudinal velocity

u_{∞} = free stream velocity

z = vertical coordinate

c = section chord

At each angle of attack a preliminary scan was made to determine wake limits. These limits were determined by manual observation of the total pressure. Then a traverse was performed utilizing a step size selected to provide at least 20 readings within the wake. The probe was stopped for a few seconds at each measurement point to allow readings to stabilize.

The on-line mini-computer system calculated corrected pressures and velocities at each point, and recorded results in tabular form and on cassette tape. Integration to determine section drag coefficient was done later, with the wind tunnel fan-off. Limits of integration were determined manually from the tabulated output velocity data.

The finite difference form of the section drag coefficient equation as used in the computer program is:

$$c_d = \frac{2}{c} \sum_{i=1}^n \frac{u_x}{u_\infty} \left(1 - \frac{u_x}{u_\infty}\right) \Delta z \quad (A2)$$

where

i = the index of the data point

n = the index of the last data point

Δz = step size

Figure A1 shows the end plate drag obtained from the difference between the force measured drag and wake survey drag. Lift coefficients are determined from the force measurements. Since the end plate drag includes tare plus interference effects, it shows an increasing trend with lift coefficient.

Since the wake survey method cannot be applied to cases with flow separation, it is necessary to extrapolate the end plate drag curve to the high lift coefficient regime. Fortunately when separation occurs the airfoil section drag increases abruptly and end plate drag becomes a smaller proportion of the total measurement.

It is conservative to extrapolate the end plate drag coefficient as a constant for lift coefficients above separation. Figure A1 shows the extrapolation selected for the present case.

- A1. Seetharam, H.C., Wentz, W.H., and Walker, J.K.: Measurement of Post-Separated Flowfields on Airfoils, AIAA Journal of Aircraft note, vol. 14, No. 1, January 1977.
- A2. Pope, A. and Harper, J.J.: Low-Speed Wind Tunnel Testing. John Wiley, 1966.

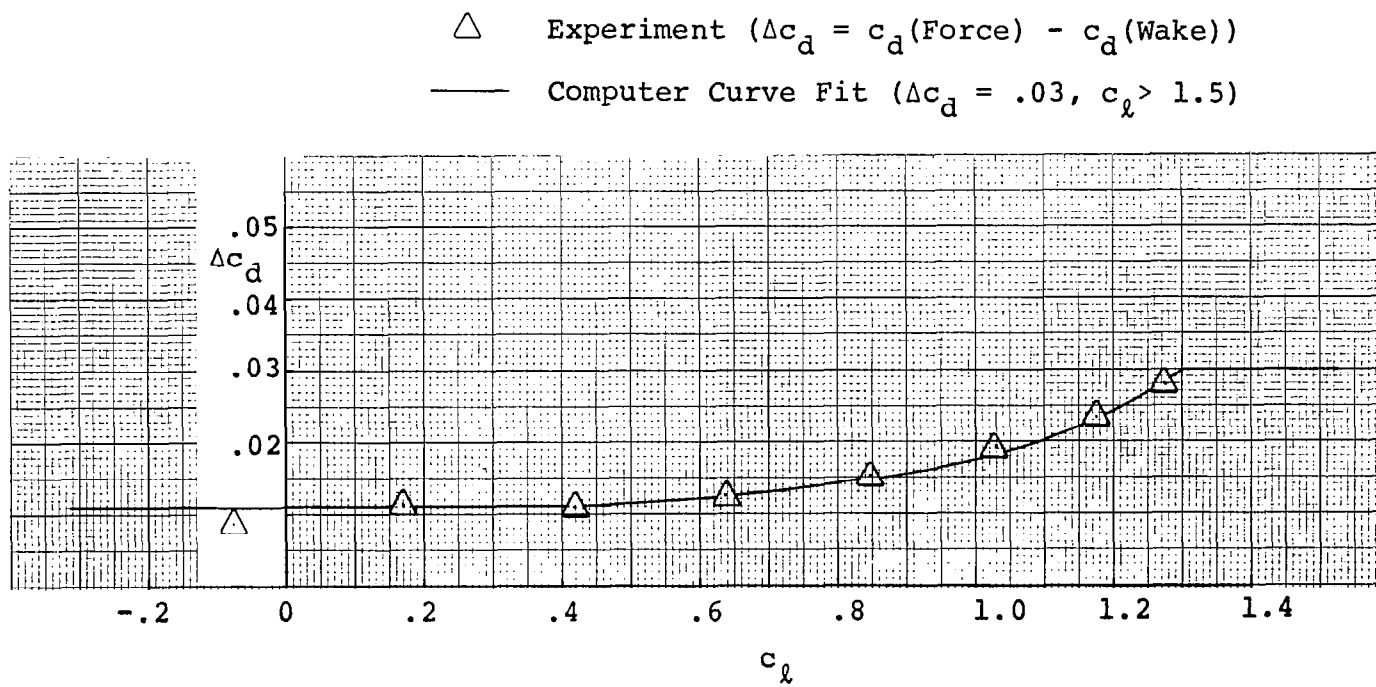


Figure A1 - End Plate Tare, LS(1)-0421 modified airfoil

APPENDIX B

Wind Tunnel Wall Corrections

INTRODUCTION

This appendix outlines the methods used to correct experimental force measurements for wind tunnel wall effects.

SYMBOLS

c	model reference chord
c_d	drag coefficient
c_l	lift coefficient
c_m	pitching moment coefficient
c_p	pressure coefficient
Q	dynamic pressure
h	test section height
Δh	vertical offset of static port
l_0	longitudinal offset of static port
l	distance from vortex to static port
α	angle of attack
α_u	tunnel upwash angle
ϵ	blockage factor, $\Delta V/V$
Γ	wing circulation
w	vortex induced velocity
V	free stream velocity
Λ	solid blockage model geometry factor
σ	solid blockage test section factor
Δ	increment

Subscripts:

B	buoyancy
cor	corrected

v vertical component

Corrections to force data:

The following corrections from ref. B1 have been applied to the force data measurements of the present report.

Tunnel upwash:

1. $\alpha = \alpha + \alpha_u$
($\alpha_u = +.18^\circ$ for WSU tunnel) (Ref. B2)

Solid blockage factor: $2. \Lambda = 1.75(t/c) + 1.875(t/c)^2$ (Ref. B1,
fig. 6:8)

Horizontal buoyancy: 3. $\Delta c_{dB} = -\frac{\pi}{8} * \Lambda * c * \frac{dc_p}{dl}$ (Ref. B1, eq. 6:7)

$$\left(\frac{dc_p}{dl} = -.0065/\text{ft for WSU tunnel} \right) \quad (\text{Ref. B2})$$

Solid blockage factor: 4. $\sigma = \frac{\pi^2}{48} \left(\frac{c}{h} \right)^2$ (Ref. Bl, eq. 6:8)

Solid blockage: 5. $\epsilon_{SB} = \Lambda\sigma$ (Ref. B1,
eq. 6:10)

Wake blockage: $6. \epsilon_{WB} = \left(\frac{c}{2h}\right) * c_{d_{un}}$ (Ref. B1,
eq. 6:12)

Total blockage: 7. $\epsilon = \epsilon_{SB} + \epsilon_{WB}$ (Ref. B1,
eq. 6:17)

Corrected lift: $C_L = C_{L_{un}} \frac{(1 - \sigma)}{(1 + \epsilon)^2}$ (Ref. B1, eq. 6:21)

$$\text{Corrected drag: } C_d = C_{dun} \frac{(1 - \Delta C_{dB})}{(1 + \epsilon)^2} \quad (\text{Ref. B1, eq. 6:23})$$

Corrected moment: $C_m = C_{m_{un}} (1 + \sigma C_l * .25) / (1 + \epsilon)^2$ (Ref. B1, eq. 6:22)

Corrected : $\alpha = \alpha + \frac{(57.3 * \sigma)}{2\pi} (C_l + 4C_m .25C)$ (Ref. B1, eq. 6:20)

The equations above have been modified to eliminate the restrictions to small ϵ imposed in the theoretical development given in reference B1.

Corrections to dynamic pressure measuring system:

The tunnel dynamic pressure measuring system is shown schematically in figure B1.

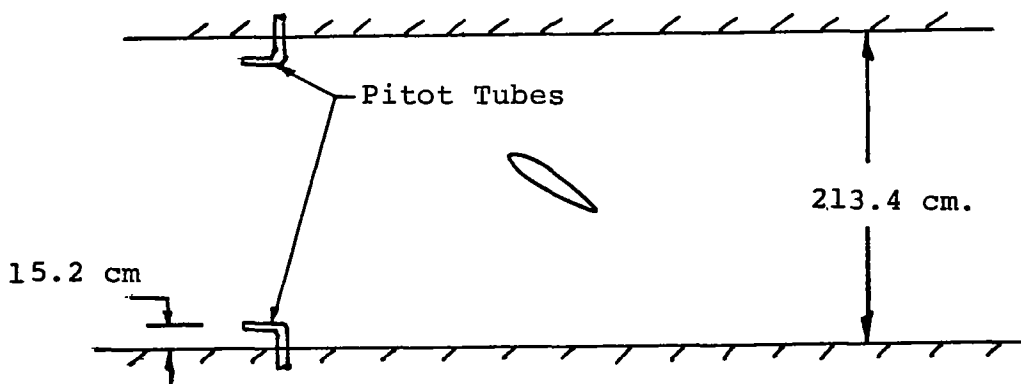


Figure B1 - Pitot Tube Locations.

It consists of two pitot tubes located 15.2 cm below the ceiling and 15.2 cm from the vertical walls. Calibrations have shown that stagnation pressure measurements at these locations are equal to tunnel centerline stagnation pressure, and this is as expected since sidewall and ceiling boundary layers are much thinner than the 15.2 cm instrument offset. Tunnel static pressure measurements for earlier research were obtained from these same locations, plus two similar pitot-static tubes located 15.2 cm above the tunnel floor. The four total pressures were manifolded to a single transducer, and the four static pressures were manifolded together for averaging purposes. At low C_l values this method is entirely satisfactory. At very high C_l values ($C_l \geq 3$),

Vertical Component of Induced Velocity:

The wing circulation is represented by a single vortex at the .25c location, and the first pair of an infinite set of image vortices are shown. The wing vortex induces an upwash at the static port, and the images induce a downwash (longitudinal components cancel).

From the notation in the sketch, the induced vertical velocities are:

Bound vortex term:

$$w_{0v} = \frac{\Gamma}{2\pi\ell} \quad (\text{upwash}) \quad (\text{B1})$$

First image:

$$w_{1v} = w_{2v} = -\frac{\Gamma}{2\pi r} \left(\frac{\ell}{r} \right) \quad (\text{downwash}) \quad (\text{B2})$$

From geometry:

$$r = \sqrt{\ell^2 + h^2} \quad (\text{B3})$$

From aerodynamic theory:

$$\Gamma = \frac{c_\ell V c}{2} \quad (\text{B4})$$

Substituting:

$$w_{0v} = \frac{c_\ell V}{4\pi(\ell/c)} \quad (\text{B5})$$

and

$$w_{1v} = -\frac{c_\ell V c}{4\pi} \left[\frac{\ell}{\ell^2 + h^2} \right] \quad (\text{B6})$$

Rearrange:

$$w_{1v} = -\frac{c_\ell V}{4\pi(\ell/c)} \left[\frac{1}{1 + \left(\frac{h}{\ell} \right)^2} \right] \quad (\text{B7})$$

For the next set of image vortices, equation (B7) will be modified by replacing h with $2h$, etc., and the velocity will be of opposite sign. Thus the total net upwash will become:

$$w_{net} v = \frac{c_l V}{4\pi(\ell/c)} \left[1 - \frac{2}{1 + \left(\frac{h}{\ell}\right)^2} + \frac{2}{1 + \left(\frac{2h}{\ell}\right)^2} - \dots \right] \quad (B8)$$

The "2" factor appearing in the second and subsequent terms accounts for the fact that the images appear in pairs. For the WSU wind tunnel geometry the following dimensions apply:

$$\begin{aligned} \ell &= 79.6 \text{ cm} \\ h &= 213.4 \text{ cm} \\ c &= 61.0 \text{ cm} \end{aligned}$$

Substituting these values into equation (B8) leads to the following result:

$$w_{net} v = .0494 * c_l V \quad (B9)$$

or

$$\boxed{\frac{w_{net} v}{V} = .0494 * c_l} \quad (B10)$$

This correction is applied to the measured dynamic pressure as follows:

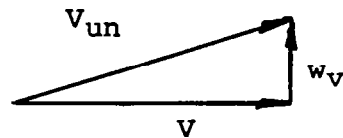


Figure B3 - Combined velocities.

$$V_{un}^2 = V^2 + w_v^2 \quad (B11)$$

$$\frac{V_{un}^2}{V^2} = 1 + \left(\frac{w_v}{V}\right)^2 \quad (B12)$$

Dynamic pressure correction:

$$\boxed{\frac{\Delta Q}{Q} = -\left(\frac{w_v}{V}\right)^2 = -.00244 * c_l^2} \quad (B13)$$

Longitudinal Component of Induced Velocity:

If the static port and the wing .25 chord do not lie on the same horizontal plane, a longitudinal component of velocity will be induced. For the present tests the static port was located above the tunnel centerline, and the model was pivoted about a point aft of the .25 chord. Image effects are neglected in this analysis. Since $c_{l_{\max}}$ with flap extended case occurs at about 12° angle of attack, the correction is calculated for the 12° case, and applied at all angles. Since the correction is relatively small, and is dependent upon c_l , this procedure will provide an appropriate correct at very large c_l values, and will not result in serious error at low α , lower c_l conditions. Figure B4 illustrates the geometry:

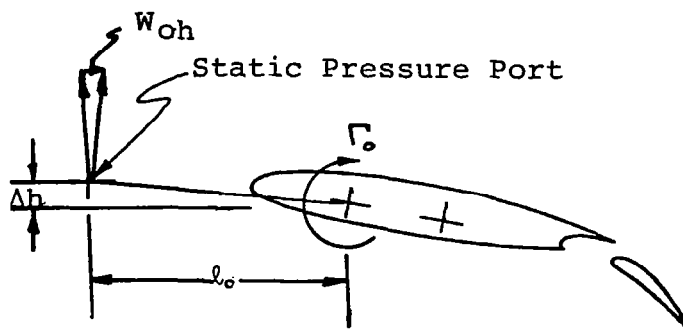


Figure B4 - Induced Longitudinal Velocity.

In this figure the dimensions are as follows:

Δh = vertical offset of static port = 1.91 cm

l_0 = longitudinal offset of static port = 79.6 cm

c = wing reference chord = 61.0 cm

The horizontal component of induced velocity is:

$$w_{0h} = \frac{\Gamma_0}{2\pi \sqrt{l_0^2 + \Delta h^2}} \frac{\Delta h}{\sqrt{l_0^2 + \Delta h^2}} \quad (B14)$$

Simplifying:

$$w_{0h} = \frac{\Gamma_0 \Delta h}{2\pi (l_0^2 + \Delta h^2)} \quad (B15)$$

Substituting from equation (B4):

$$w_{0h} = \frac{c_l V c \Delta h}{4\pi (l_0^2 + \Delta h^2)} \quad (B16)$$

Rearranging:

$$\frac{w_{0h}}{V} = \frac{1}{4\pi} \frac{c \Delta h}{(l_0^2 + \Delta h^2)} c_l \quad (B17)$$

Substituting all values given:

$$\boxed{\frac{w_{0h}}{V} = .00146 * c_l} \quad (B18)$$

Since this component is in the freestream direction, the corresponding dynamic pressure correction becomes:

$$\boxed{\frac{\Delta Q}{Q} = -2 \frac{w_{0h}}{V} = -.00292 * c_l} \quad (B19)$$

Combining this result with equation (B13), the total dynamic pressure correction becomes:

$$\frac{\Delta Q}{Q} = -0.00292 * C_l - .00244 * C_l^2 \quad (B20)$$

The negative signs indicate that corrected dynamic pressure is lower than indicated dynamic pressure. For an uncorrected C_l of 4.0, the first term is a 1.2% correction, and the second is a 3.9% correction. These corrections are much smaller at low C_l values.

REFERENCES

- B1. Pope, A. and Harper, J.J.: Low-Speed Wind Tunnel Testing. John Wiley, 1966.
- B2. Siew, R.: Calibration of a Two-Dimensional Insert for the WSU 7' x 10' Wind Tunnel. AR 73-2, Wichita State University, 1973.

APPENDIX C

Wake Blockage Corrections to Experimental c_p Data

INTRODUCTION

This appendix outlines the methods used to correct experimental pressure measurements for wind tunnel wall effects.

SYMBOLS

b	model span
C	test section
c	model reference chord
c_d	airfoil drag coefficient
c_l	airfoil lift coefficient
h	test section height
Q	dynamic pressure
S	model reference area
V	velocity
α	angle of attack
Δ	increment
ϵ	non-dimensional velocity increment, $\Delta V/V$

Subscripts:

cor	corrected
un	uncorrected
WB	wake blockage

Wake Blockage Corrections to Experimental C_p Data

Pope (ref. C1) quotes the following wake blockage correction to velocity, as developed by Maskell:

$$\epsilon_{WB} = \frac{S}{2C} C_d \quad (C-1)$$

(Ref. C1, p. 313)

For the WSU two-dimensional insert:

$$S = c \times b \quad (C-2)$$

$$C = h \times b \quad (C-3)$$

$$\epsilon_{WB} = \frac{c * b}{2 * h * b} * C_d \quad (C-4)$$

Simplifying,

$$\epsilon_{WB} = \frac{c}{2 * h} * C_d \quad (C-5)$$

For the present tests, $c/h = 2/7$.

Substituting:

$$\epsilon_{WB} = \frac{1}{7} * C_d \quad (C-6)$$

For small ϵ ,

$$Q_{cor} = Q_{un}(1 + 2\epsilon) \quad (C-7)$$

$$C_{p_{cor}} = C_{p_{un}}(1 - 2\epsilon) \quad (C-8)$$

$$\text{and } C_{l_{cor}} = C_{l_{un}}(1 - 2\epsilon) \quad (C-9)$$

Rather than adjusting all C_p values for the corrected static and dynamic pressures it is simpler to calculate an equivalent correction to angle of attack, as follows:

$$\frac{\Delta c_\ell}{c_\ell} = -2\epsilon \quad (C-10)$$

$$\Delta\alpha = \frac{-\Delta c_\ell}{(dc_\ell/d\alpha)} \quad (C-11)$$

(Note: An increase in α required is equivalent to a decrease in c_ℓ .)

Substituting:

$$\Delta\alpha = \frac{+2\epsilon c_\ell}{dc_\ell/d\alpha} \quad (C-12)$$

Substitute ϵ for the present case:

$$\Delta\alpha = \frac{2(\frac{1}{7} c_d) c_\ell}{(dc_\ell/d\alpha)} \quad (C-13)$$

For most cases $dc_\ell/d\alpha \approx 0.1/\text{degree}$.

Substituting this value:

$$\Delta\alpha = \frac{20}{7} * c_d * c_\ell (\text{deg.})$$

(C-14)

Using this relationship together with c_ℓ and c_d values from force measurements, corrected α values can be calculated for each flap setting and angle of attack. The theoretical computer runs were made at these corrected angles for comparison with the experimental c_p distributions.

References

- C-1. Pope, A. and Harper, J.J.: Low-Speed Wind Tunnel Testing. John Wiley and Sons, 1966.

1. Report No. NASA CR-3081		2. Government Accession No.		3. Recipient's Catalog No.	
4. Title and Subtitle Wind Tunnel Force and Pressure Tests of a 21% Thick General Aviation Airfoil With 20% Aileron, 25% Slotted Flap and 10% Slot-Lip Spoiler				5. Report Date June 1979	
				6. Performing Organization Code	
7. Author(s) W. H. Wentz, Jr., and K. A. Fisco				8. Performing Organization Report No. WSU AR 77-6	
				10. Work Unit No. 505-06-33-10	
9. Performing Organization Name and Address Wichita State University Wichita, KS 67208				11. Contract or Grant No. NSG-1165	
				13. Type of Report and Period Covered Contractor Report	
12. Sponsoring Agency Name and Address National Aeronautics and Space Administration Washington, DC 20546				14. Sponsoring Agency Code	
15. Supplementary Notes Langley Technical Monitor: Robert J. McGhee Topical Report					
16. Abstract Force and surface pressure distributions have been measured for the 21% LS(1)-0421 modified airfoil fitted with 20% aileron, 25% slotted flap and 10% slot-lip spoiler. All tests were conducted in the Walter Beech Memorial Wind Tunnel at Wichita State University at a Reynolds number of 2.2×10^6 and a Mach number of 0.13. Results include lift, drag, pitching moments, control surface normal force and hinge moments, and surface pressure distributions. The basic airfoil has a $c_{l_{max}}$ of 1.31 with nearly constant c_l beyond the stall at 2.2×10^6 Reynolds number. Incremental performance of flap and aileron are similar to that obtained on the GA(W)-2 airfoil. Spoiler control shows a slight reversal tendency at high α , low spoiler deflection angle conditions with flap nested. Flap extended spoiler control is non-linear but positive.					
17. Key Words (Suggested by Author(s)) Airfoil Flap Aileron Pressure distributions				18. Distribution Statement FEDD Distribution Subject Category 02	
19. Security Classif. (of this report) Unclassified		20. Security Classif. (of this page) Unclassified		21. No. of Pages 114	
22. Price*					

Available: NASA's Industrial Applications Centers

NASA-Langley, 1979